MICA (P) 105/02/2012

SNAMES

Society of Naval Architects and Marine Engineers Singapore

SNAMES 40th ANNIVERSARY

NEW FRONTIERS

34th Annual Journal 2012/2013

Society of Naval Architects and Marine Engineers Singapore

34th Annual Journal 2012/2013

SNAMES

Publication Committee
Ng Yi Han
Joan Chua

SNAMES Secretariat Address
205 Henderson Road
#02-01 Henderson Industrial Park
Singapore 159549
Tel: +65 6858 5846
Fax: +65 6725 8474
Email: admin@snames.org.sg
www.snames.org.sg

MICA (P) 105/02/2012

Design and Production
JMatrix Consulting Pte Ltd
Email I Web: info@jmatrix.co I jmatrix.co

Contents

ENGINEER **DESIGN** **MANAGE**

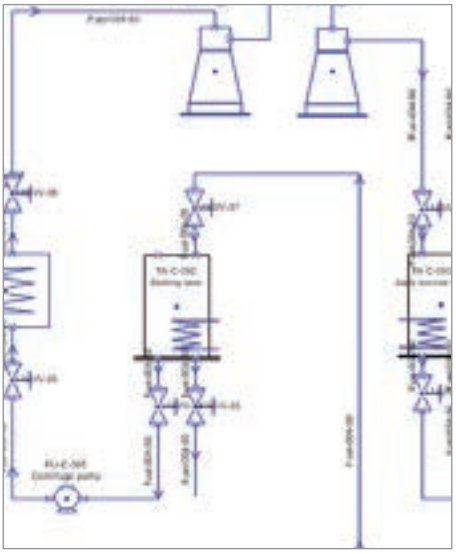

Information	yellow
OK	green
Accepted Difference	cyan
Check Required	limegreen
Warning	yellow
Minor Error	yellow
Member Attribute Diffe	orange
Attribute Difference	orange
Sequence Difference	orange
Connection Error	royalblue
Item Missing	yellow
Not Matched	brightred
Critical Error	brightred

AVEVA Marine
Building Reputations

Shipbuilding is complex and resource-intensive. Buyers want a competitive price from a shipyard with a solid reputation for rapid, on-time delivery and high-quality workmanship.

AVEVA Marine is a powerful software suite for the design and construction of every type of vessel and offshore project. Through an Integrated Engineering & Design approach offering multi-site collaboration, reduced design man-hours, minimised material waste and eliminated production rework, a new level of efficiency delivers demonstrable savings of up to 30% compared to alternative solutions.

With a proven track record, it is the solution of choice of the world's most competitive shipbuilders. Discover how AVEVA Marine can help to build your reputation.

The leader in design, engineering and information management software for the process plant, power and marine industries, AVEVA invests in our customers' success through a global sales and support network in more than 40 countries.

To find out more, contact us at: **Marketing.Malaysia@aveva.com**

AVEVA – building solid reputations for 45 years

www.aveva.com/marine

AVEVA™
CONTINUAL PROGRESSION

President's Message

Dear Members

This year, the Society of Naval Architects and Marine Engineers Singapore (SNAMES), celebrates our 40th Anniversary. It's a cause for celebration, and a time for reflection and bold thinking.

Much has changed over the last four decades at SNAMES, and mirroring it to a larger extent, Singapore's marine and offshore industry. There have been rough as well as calm seas, and through it all, we have weathered well and become stronger than ever. Today, SNAMES is widely regarded as a leading and responsible society with distinguished professionals as our members and partners in the maritime industry of Singapore. As an industry, Singapore now stands shoulder-to-shoulder with global leaders in the marine and offshore industry. We are currently the largest designer and constructor of jack-up rigs and commands 70% of the world market. We also have 70% of the global market share for the conversion of Floating Production Storage and Offloading (FPSO) vessels. In ship repair, we have 20% of the global market share. The output from the marine and offshore industry stood at a notable S$16 billion in 2012.

Going forward, there is much to hope for, and to dream on. That is why the SNAMES Council has chosen the theme "New Frontiers" for our 34th Annual Journal. The theme embodies a new exciting phase of leading-edge exploration, research and development, and ventures in the marine and offshore industry. The global marine & offshore industry has grown and expanded into both deeper waters as well as into subsea. We should seize exciting opportunities in these frontiers by stepping up resources and push to ride on this wave. Another ongoing important frontier is the preservation of the earth – through employing green technology – amid the growing needs for energy and developments around the world. Our industry has a vital role to play in this regard – to combat global warming and to reduce emissions from various sources, such as ships, offshore support vessels and oil rigs. A sustainable maritime industry that cares

"The global marine & offshore industry has grown and expanded into both deeper waters as well as into subsea. We should seize exciting opportunities in these frontiers by stepping up resources and push to ride on this wave."

for the environment is in everyone's interest and responsibility. Whether you are a marine scientist, naval architect, vessel operator, or ship owner, it is important to work together to pursue this quintessential vision for a greener maritime industry.

SNAMES had a busy year in 2012, with many events organised for our members and the maritime industry at large. We held professional and technical talks at least once a month, as well as social networking events. The Society has supported the Ngee Ann Polytechnic organized Primer Courses in Offshore Drilling Technology, Offshore Safety & Management Systems, and Production/Topside Processing Systems, to enhance the professional development of our members. Affiliation agreements were signed with maritime societies to collaborate on issues of mutual interests, share knowledge and experiences and provide opportunities for our members to network internationally.

We continue to organise our Annual Dinner and Annual Golf Tournament, and co-organise the Annual Chua Chor Teck Memorial Lecture. And as part of SNAMES' 40th Anniversary celebrations, we also organised the SNAMES Family Day at Maritime Experiential Museum on 27 Oct 2012.

On the industry front, SNAMES members are serving in eight industrial committees, including the Technical Committee for Bunkering under Spring Singapore; the Work, Safety and Health Committee (Marine Industry) under the Work, Safety and Health Council; and the Singapore MaritimeONE Working Group under the Singapore Maritime Foundation. I am also pleased to report that the inaugural issue of SNAMES eNewsletter "Thrusters" was launched on 22 Dec 2012. It aims to provide SNAMES members and partners timely update of new developments in the industry and the Society, as well as events being organised.

On behalf of the Council, I would like to sincerely thank all our members and industry partners for the unreserved support given to the Society over the years. Our role as a Society is to continue to nurture talents and advance the maritime profession, through good or challenging times. I believe the best is yet to come for SNAMES, and I hope you will continue to join me to support the growth of our Society and industry at large.

Happy 40th Anniversary SNAMES!

With best wishes

Professor Choo Yoo Sang
President
SNAMES Council 2012/2013

Council Members 2012/2013

Prof Choo Yoo Sang
President

Ang Ee Beng
Vice-President

Foo Nan Cho
Honorary Treasurer

Ng Chun Wee
Honorary Secretary

Justin Wee
Asst. Honorary Secretary

Nigel Koh
Chairman
Technology Committee

Nicky Loh
Chairman
Membership Committee

Koh Shu Yong
Co-Chairman
Membership Committee

Ng Yi Han
Chairman
Publication Committee

Cong Yu Jie
Chairman
Website Committee

Yeo Teck Chye
Council Member
Social Committee

Prakash Balasubramaniam
Council Member
Technology Committee

Cheah Aun Aun
Council Member
Membership Committee

Edwin Wee Cheng Chua
Council Member
Social Committee

Md Shafiqzzaman
Council Member
Website Committee

Ham Wan Ling
Council Member
Social Committee

Lu Shang Yuan
Council Member
Technology Committee

Lee Ee Win
Council Member
Membership Committee

Joan Chua
Executive Secretary
Secretariat

Past Presidents of SONAS/SNAMES 1973-2012

SOCIETY OF NAVAL ARCHITECTS SINGAPORE (SONAS)

Year	President	Vice-President
1973/1974	Mr Tan Kim Chuang	Mr Keki R Vesuna
1974/1975	Mr Tan Kim Chuang	Mr Ho Ming Yeh
	Mr Ho Ming Yeh	Mr Keki R Vesuna
1975/1976	Mr Chua Chor Teck	Mr Alan Bragassam
1976/1977	Mr Chua Chor Teck	Mr Kalman E Nagy
1977/1978	Mr Chua Chor Teck	Mr Alan Bragassam
1978/1979	Mr Chua Chor Teck	Mr Alan Bragassam
1979/1980	Mr Chua Chor Teck	Mr Tan Kim Chuang
1980/1981	Mr Chung Chee Kit	Mr Lim Boon Heng

SOCIETY OF NAVAL ARCHITECTS AND MARINE ENGINEERS SINGAPORE (SNAMES)

Year	President	Vice-President
1981/1982	Mr Cheng Huang Leng	Mr Choo Chiau Beng
1982/1983	Mr Cheng Huang Leng	Mr Choo Chiau Beng
1983/1984	Mr Choo Chiau Beng	Mr Ronald M Pereira
1984/1985	Mr Ronald M Pereira	Mr Tay Kim Hock
1985/1986	Mr Choo Chiau Beng	Mr Charlie Foo
1986/1987	Mr Choo Chiau Beng	Mr Charlie Foo
1987/1988	Mr Charlie Foo	Mr Toh Ho Tay
1988/1989	Mr Toh Ho Tay	Mr Teh Kong Leong
1989/1990	Mr Teh Kong Leong	Mr Loke Ho Yong
1990/1991	Mr Loke Ho Yong	Mr Dennis Oei
1991/1992	Mr Dennis Oei	Mr Goh Choon Chiang
	Mr Goh Choon Chiang	Mr Wong Kin Hoong
1992/1993	Mr Tan Kim Pong	Mr Zafrul Alam
1993/1994	Mr Zafrul Alam	Mr Ng Thiam Poh
1994/1995	Mr Ng Thiam Poh	Mr Dennis Oei
1995/1996	Mr Dennis Oei	Mr Kan Seng Chut
1996/1997	Mr Kan Seng Chut	Mr James Tan
1997/1998	Mr James Tan	Mr Phua Cheng Tar
1998/1999	Mr Phua Cheng Tar	Mr Leslie Low
1999/2000	Mr Leslie Low	Mr Wong Kin Hoong
2000/2001	Mr Wong Kin Hoong	Mr Leow Ban Tat
2001/2002	Mr Leow Ban Tat	Mr Ying Hing Leong
2002/2003	Mr Ying Hing Leong	Mr Tan Chor Hiong
2003/2004	Mr Tan Chor Hiong	Mr Dennis Chua
2004/2005	Mr Dennis Chua	Mr Ernest Wee
2005/2006	Mr Ernest Wee	Mr Fabian Chew
2006/2007	Mr Fabian Chew	Mr Goh Boon Guan
2007/2008	Mr Goh Boon Guan	Mr Chen Chin Kwang
2008/2009	Mr Chen Chin Kwang	Mr Simon Kuik
2009/2010	Mr Ronald M Pereira	Mr Kenneth Kee
	Mr Kenneth Kee	Mr David Kinrade
2010/2011	Mr Kenneth Kee	Mr Simon Kuik
2011/2012	Mr Kenneth Kee	Prof Choo Yoo Sang

SNAMES Annual Report

SNAMES Annual Report

Based on the Council Report year ended 2012 presented at the 41st SNAMES Annual General Meeting (AGM), this Report highlights the Society's vision and general approach to achieving growth, its major developments, programmes and activities that took place in 2011/2012.

SNAMES VISION

The vision underpinning the Society of Naval Architects and Marine Engineers Singapore (SNAMES) is to "be the most admired respected and responsible society of people in the maritime industry of Singapore".

SNAMES APPROACH

SNAMES adopts a multi-prong approach as its core general strategy for growth. They are:

1. Create an active and growing SNAMES membership and council
2. Manage SNAMES assets and operating costs effectively
3. Promote inclusive networking events, e.g. Annual Dinner and Annual Golf Tournament
4. Publish quality SNAMES Annual Journal and other relevant publications
5. Organise leading-edge technical talks for its members and affiliates
6. Encourage students' participation in SNAMES' selected events
7. Conduct the annual Chua Chor Teck Memorial Lecture
8. Pursue and strengthen relationships with Singapore and overseas-based organisations
9. Participate in joint activities with other organisations with maritime visits and dialogues
10. Better communications through SNAMES website

SNAMES' STEADY GROWTH

SNAMES' steady growth over the years can be attributed to an array of factors, namely:

1. Active database membership
2. Extension of junior membership
3. Provision of technical leadership
4. Active social interaction
5. Exciting and relevant public forums
6. Proactive communications
7. Close working relationship with tertiary institutions
8. Good relationships with individual and corporate sponsors and supporters
9. New programmes developed to cater to emerging trends and needs of members
10. Effective management of fees

SNAMES COUNCIL MEMBERS 2012/2013

The Executive Committee Members in the SNAMES Council are:

President	Prof Choo Yoo Sang
Vice President	Ang Ee Beng
Honorary Treasurer	Foo Nan Cho
Honorary Secretary	Ng Chun Wee

SNAMES would like to recognise and appreciate the Executive Committee Members who served in the SNAMES Council year ended 2012:

President	Kenneth Kee
Vice President	Prof Choo Yoo Sang
Honorary Treasurer	Ang Ee Beng
Honorary Secretary	Ng Chun Wee

SNAMES current Council Members, among them the respective Committee Chairmen, are:

Technology Chairman	Nigel Koh
Membership Chairman	Nicky Loh & Koh Shu Yong
Publication Chairman	Ng Yi Han
Social Chairman	–
Website Chairman	Cong Yu Jie
Council Member	Yeo Teck Chye
Council Member	Prakash Balasubramaniam
Council Member	Cheah Aun Aun
Council Member	Edwin Wee Cheng Chua
Council Member	Md Shafiqzzaman
Council Member	Ham Wan Ling
Council Member	Lu Shang Yuan
Council Member	Lee Ee Win
Secretariat	Joan Chua

EVENTS IN SUMMARY 2012

Technical Talks

	Date	Titles	Speakers
1	16 Mar 2012	MAN Diesel & Turbo Industry Nite	Mr. Lars Bryndum Mr. Stig Baungaard Jakobsen Mr. Christian Ludwig
2	18 Apr 2012	SyncroliftR - Ship-lift and Transfer Systems	Mr. Dean Reeves
3	20 Apr 2012	Sizing, Selection and Installation of Cables on Ships and Offshore Installations	Mr. James Teng
4	2 May 2012	An Introduction to Metocean Matters	Mr. Chris Nielsen
5	16 May 2012	An Introduction to the Design, Construction & Commissioning of Modern Rigs	ER Seow Tiang Keng
6	13 Jun 2012	Brief Guide of Patenting Process for Engineers	Dr. Freeman Yu
7	5 Jul 2012	Capacity of Grouted Connections in Offshore Structures	Dr. Inge Lotsberg
8	18 Jul 2012	Concrete for Offshore & Floating Structure	Dr. Kong Decheng
9	15 Aug 2012	LNG as the Next Generation Marine Fuel: Challenges and opportunities	Dr. Lorenzo Casarosa
10	12 Sep 2012	The Brave New World of Shipping – Regulatory Emissions Challenges Facing Shipping	Mr. Douglas Raitt
11	3 Oct 2012	Fibre Reinforced Plastic (FRP) Composite Materials for Marine Structures	Professor R Ajit Shenoi
12	17 Oct 2012	Mitigating the Airborne Emissions from Shipping	Dr. Alan J Murphy
13	25 Oct 2012	Present Research and Challenges in Computational Methods for Naval and Offshore Engineering	Dr. Julio García-Espinosa
14	14 Nov 2012	Industry Nite by SeaTech Solutions	Mr. Donald MacPherson
15	22 Nov 2012	Industry Nite by Pruftechnik S.E.A	Mr. Randal Ong
16	11 Dec 2012	Technology Challenges and Opportunities for 2013 and beyond	Mr. Todd W. Grove

Primer Courses

	Date	Titles	Speakers	Venue	Co-Sponsors
1	8 Mar – 9 Mar 2012	Primer Course in Subsea Production Systems	Dr. John Preedy	Ngee Ann Polytechnic	Ngee Ann Polytechnic Mechanical Engineering Division & AZUR Offshore, UK
2	12 Mar – 13 Mar 2012	Primer Course in Offshore Gas Production & Floating Liquefied Natural Gas	Dr. John Preedy	Ngee Ann Polytechnic	Ngee Ann Polytechnic Mechanical Engineering Division & AZUR Offshore, UK
3	15 Mar – 16 Mar 2012	Primer Course in Installation & Commissioning of Offshore Activities	Dr. John Preedy	Ngee Ann Polytechnic	Ngee Ann Polytechnic Mechanical Engineering Division & AZUR Offshore, UK
4	10 Sep - 11 Sep 2012	Primer Course in Offshore Drilling Technology	Dr. John Preedy	Ngee Ann Polytechnic	Ngee Ann Polytechnic Centre of Innovation – Marine & Offshore Technology & AZUR Offshore, UK
5	13 Sep - 14 Sep 2012	Primer Course in Offshore Production / Topside Processing Systems	Dr. John Preedy	Ngee Ann Polytechnic	Ngee Ann Polytechnic Mechanical Engineering Division & AZUR Offshore, UK
6	17 Sep - 18 Sep 2012	Primer Course in Offshore Safety & Management Systems	Dr. John Preedy	Ngee Ann Polytechnic	Ngee Ann Polytechnic Mechanical Engineering Division & AZUR Offshore, UK

Industry Nite

	Date	Titles	Speakers	Venue
1	16 Mar 2012	SNAMES – MAN DIESEL & TURBO Industry Nite	Mr. Lars Bryndum Mr. Stig Baungaard Jakobsen & Mr. Christian Ludwig	The St. Regis Singapore
2	14 Nov 2012	SNAMES - SeaTech Solutions Industry Nite	Mr. Donald MacPherson	Ngee Ann Polytechnic
3	22 Nov 2012	SNAMES – Pruftechnik Industry Nite	Mr. Randal Ong	Ngee Ann Polytechnic

Events

Date	Events	Guest-of-Honour	Venue
2 Mar 2012	SNAMES Annual Dinner	Choo Chiau Beng CEO of Keppel Corporation Ltd	Sheraton Towers
20 Mar 2012	40th SNAMES Annual General Meeting	–	Singapore Polytechnic
20 Jul 2012	Mariner's Nite	–	Marina Bay Sands
27 Oct 2012	SNAMES Family Day	–	Maritime Experiential Museum
2 Nov 2012	SNAMES Golf Tournament 2012	–	Raffles Country Club

TECHNOLOGY COMMITTEE

The Technology Committee rolled out a series of high-level as well as quality conferences and seminars in 2011/2012. It organised, co-organised with or had the support of our partners: Joint Branch of RINA-IMarEST, CORE, Keppel O&M, Singapore Maritime Academy (SMA), Ngee Ann Polytechnic (NP), Intergraph and MAN Diesel and Turbo. Please see table above for details.

MEMBERSHIP COMMITTEE

The highlights for Membership are:

- Membership drive at "YES Gathering" held at Singapore Maritime Foundation (SMF)
- Recruitment of 83 new SNAMES members since last AGM, a 93% increase from 2011
- Fellowship upgrade (17 members upgraded)
- Conferment of Honorary Membership to Mr. Choo Chiau Beng
- Roll out of personalised membership card and three-year membership scheme

SOCIAL COMMITTEE

The Social Committee successfully organised:

- The Annual Dinner at the Sheraton Towers on 2 March 2012
  - Graced by Guest-of-Honour and Distinguished Member Mr. Choo Chiau Beng, CEO of Keppel Corporation Ltd. Mr. Choo was also conferred the Honorary Membership.
  - Over 390 guests attended
  - Supported by 27 companies/organisations from across the maritime industry
- Mariner's Nite on 20 July 2012 at IDarts Senso
  - Attended by 60 members
- The Annual Golf Tournament on 2 November 2012 at Raffles Country Club
  - Attended by 116 members with 29 flights
- SNAMES Family Day on 27 Oct 2012 at Maritime Experiential Museum
  - Attended by 60 members

PUBLICATION COMMITTEE

The Publication Committee achieved the following:

- Published the SNAMES Annual Journal (33rd Edition) in Mar 2012
- Journal Theme: "Innovations and Green Technology: Marine & Offshore Industry"
- Copies of the Journal were distributed to individual and corporate members, supporting organisations and partners
- Over 9 strategic and technical papers covering strategic maritime developments, technical innovations and green technology were submitted and vetted by professionals, and published in the Journal
- Inaugural issue of Bi-annual newsletter 'Thrusters' released in Dec 2012
  - 8 pages of information to update members on recent events
  - Distribution - Members

WEBSITE COMMITTEE

The Website Committee successfully implemented the following:

- Update of all sections of the website by its council members, saving on 3rd-party costs
- Creation of banner spaces for sponsors and supporters of SNAMES, and advertisers
- Interface of SNAMES Membership Database program
- Making source codes available for future enhancements
- Platform for "Memories of Mariners" project
- A more dynamic and user-friendly SNAMES website
- A more content-rich website that provides details of all events, conferences and seminars

SPECIAL MENTION

SNAMES would like to single out a few individuals who have been outstanding in their contribution to the advancement of SNAMES' objectives.

- Immediate Past President Mr. Kenneth Kee
- SNAMES' Secretariat Ms Joan Chua

SNAMES Activities for Year 2012

Annual Dinner 2012

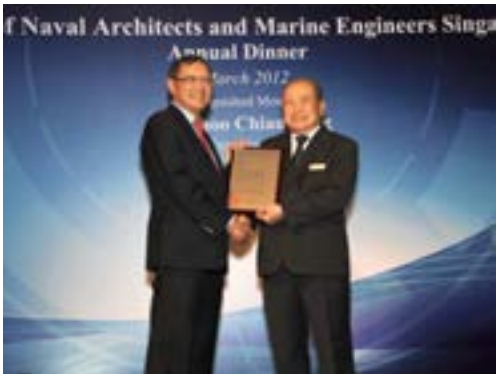


ociety of Naval Architects and Marine Engineers Singapore
Annual Dinner

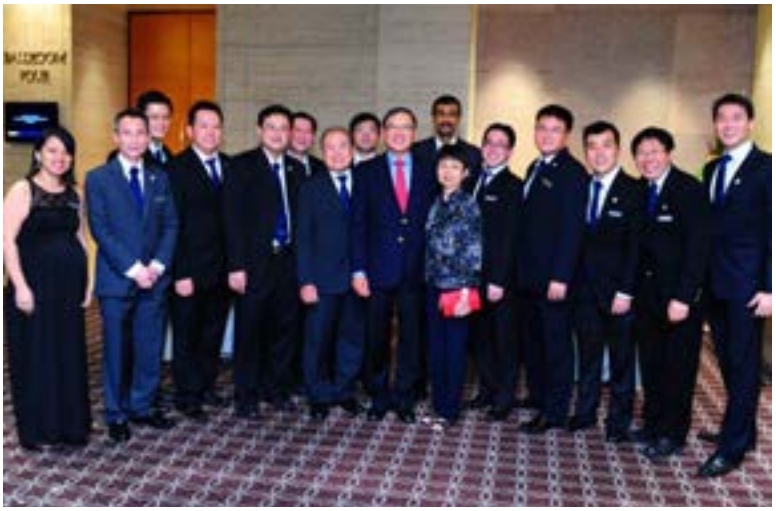

27th Chua Chor Teck Memorial Lecture


SINGAPORE
POLYTECHNIC

Technical Talks

Involvement in Industry Committee and Technical Group & Industry Nite

Annual Golf Tournament 2012

Annual Golf Tournament 2012

Technical Papers

Julio García-Espinosa, Borja Serván, Daniel Di Capua, Pere-Andreu Ubach and Eugenio Oñate
Centre Internacional de Mètodes Numèrics en Enginyeria (CIMNE)

Advances in the Development of a FEM Model for Evaluation of a Surface-Effect Ship (SES) Including Skirt Dynamics

ABSTRACT

This paper shows the recent work of the authors in the development of a time-domain FEM model for evaluation of a SES including skirt dynamics. In this work, a potential flow approach along with a stream-line integration of the free surface is used. The paper focuses on the fluid-structure algorithm that has been developed to allow the simulation of the complex and highly dynamic behavior of the seals in the interface between the air cushion, and the water. The algorithm is based, on one side, on a staggered explicit algorithm, using a TCP/IP sockets link, able to communicate pressure forces and displacements of the seals at memory level and, on the other side, on an innovative wetting and drying scheme able to predict the water action on the seals. Several cases of the XR-1B T-Craft model have been studied to demonstrate the developed algorithm.

Keywords: seakeeping; surface effect ship; finite element; fluid structure interaction.

1. INTRODUCTION

The Innovative Naval Prototype Transformable Craft (T-Craft) is a novel United States Navy concept for a seabase-to-shore connector, operative in multiple modes. It can self deploy from an intermediate support base to the sea base and then be used as a high speed connector from the sea base to the shore, transporting wheeled and tracked vehicles and other heavy equipment and cargo through the surf zone and onto the beach, where it can discharge its cargo without the need for a port.

T-Craft has been conceived as a surface-effect ship (SES) with a fan-activated air cushion between two rigid hulls, allowing the vessel to operate in modes of full displacement, partial air-cushion support, and full aircushion support.

Predicting the overall performance of a SES is of paramount importance to support the design phase, as the motion of the ship can be affected by the interaction between the air, the cushion, the ship structure, the seals, the sea waves and the sea bottom in the shallow water region. Different approaches with different types of complexity and accuracy have been taken to cope with this type of analyses.

In the last decade, there have been extensive applications of Navier-Stokes models to naval hydrodynamics problems. For example, Oñate and García-Espinosa [1] presented a stabilized FEM for fluid structure interaction with free surface. In [2] Löhner et al. developed a FEM capable of tracking violent free surface flows interacting with objects. Also García-Espinosa et al. [3] developed a new technique to track complex free surface shapes. More recently, in [4], an application for the calculation of the flow about a SES in still water, using a commercial Volume of Fluid model, has been presented. While, in [5], Mousaviraad et al. uses an URANS solver for evaluating the manoeuvring performance of the XR-1B SES. While the outcome

of the analyses is outstanding, the CPU-time reported in this paper, makes this model quite unaffordable for being used during design stages.

Actually, it is a common consensus that solvers based on the Navier-Stokes equations are too expensive computationally speaking when it comes to simulate unsteady naval hydrodynamics problems. These sorts of problems can be more efficiently calculated using potential flow theory. This approach, jointly with the Stokes perturbation approximation, is widely used for analysis of seakeeping problems [6]. In [7], Connell et al., uses a boundary-element time-domain potential flow solver to calculate the multi-body seakeeping behaviour of a T-Craft SES and a LMSR in different scenarios. While, in [8], the same computational solver is adapted to calculate the maneuver of a SES.

Despite the complexity of the above referred SES computational models, none of them takes into account the skirt dynamics, or the effect of sea-skirt interaction. However, it is well known the relevance of this interaction in the unsteady dynamics of a SES [9][10]. The complexity of this phenomenon makes impossible to develop a theoretical background, and prompts many design parameters to be traditionally decided by empirical formulas [9]. Actually, only limited theoretical and computational models have been developed to analyze skirt dynamics [11][12] [13].

This paper shows the recent work of the authors in the development of a time-domain FEM model for evaluation of a SES including skirt dynamics. In this work, a potential flow approach along with a stream-line integration of the free surface is used. While this approximation is much simpler than using RANS computations, significant outcomes can be obtained as well, allowing to significantly reducing computational time by 2 or 3 orders of magnitude even when computing on a regular desktop or laptop. Despite of starting off with lesser computational requirements, special attention has been paid to reducing computational time, including the use of parallel computing based on GPU cards.

This paper will focus in the fluid-structure algorithm that has been developed to allow the simulation of the complex and highly dynamic behavior of the seals in the interface between the air cushion, and the water [14]. The algorithm is based, on one side, on a staggered explicit algorithm, using a TCP/IP sockets link, able to communicate pressure forces and displacements of the seals at memory level and, on the other side, on an innovative wetting and drying scheme able to predict the water action on the seals.

The developed model is applied to the study of the T-Craft XR-1B.

2. HYDRODYNAMIC SOLVER

2.1 Governing equations

We consider the first order diffraction-radiation problem of a ship moving on the horizontal plane. The two dimensional movement of the ship is identified by $\mathbf{v}_b(\mathbf{x}) = \mathbf{T}_b + \mathbf{W}_b \times (\mathbf{x} - \mathbf{x}_G)$, where $\mathbf{T}_b$ and $\mathbf{W}_b$ are the linear and angular velocity of the ship. We assume that the flow is incompressible and irrotational, so that the velocity field $\mathbf{v}$, is derived from a potential function φ as: $\mathbf{v} = \nabla\varphi$. The following assumptions are made on the order of magnitude of the velocity components and free surface elevation ζ :

$$\begin{aligned} &V_b \sim O(1); \quad \varphi_x \sim O(1); \quad \varphi_y \sim O(1); \\ &\varphi_z \sim O(\varepsilon); \quad \varphi_{\alpha\beta} \sim O(\varepsilon); \quad \zeta_x \sim O(1); \qquad \zeta_y \sim O(1); \end{aligned} \tag{1}$$

Based on the previous assumption, the governing equations for the first order diffraction-radiation wave problem are:

$$\begin{aligned} &\nabla^2\varphi = 0 && in\ \Omega \\ &\partial_t\varphi + \mathbf{u}\cdot\nabla_h\varphi + \tfrac{1}{2}\nabla_h\varphi\cdot\nabla_h\varphi + P/\rho + g\zeta = 0 && in\ z = 0 \\ &\partial_t\zeta + (\mathbf{u} + \nabla_h\varphi)\cdot\nabla_h\zeta - \varphi_z = 0 && in\ z = 0 \\ &\left(\mathbf{u} + \nabla\varphi\right)\cdot\mathbf{n}_b = \mathbf{v}_b\cdot\mathbf{n}_b && in\ \Gamma_b \\ &\varphi_z = 0 && in\ z = -H \end{aligned} \tag{2}$$

where $\nabla_h = (\partial_x, \partial_y)$ is the gradient in the horizontal plane, Ω is the fluid domain, Γ_b represents the wetted surface of the ship, $\boldsymbol{H}$ is the water depth, $\mathbf{v}_b$

is the local ship velocity of a point over the wetted surface, $\mathbf{n}_b$ is the normal of the ship wetted surface pointing outwards the ship, **u** is the water current, and ***P*** is the free surface pressure.

In order to solve the governing equations provided in Eq., a velocity potential decomposition is introduced. Let φ and ζ be such that;

$$\begin{aligned} \varphi &= \phi + \psi \\ \zeta &= \eta + \xi \end{aligned} \tag{3}$$

Then, we can split the governing equations into the following sets of equations:

Set 1:

$$\begin{aligned} &\nabla^2\psi = 0 && in\ \Omega \\ &\partial_t\psi + \mathbf{u}\cdot\nabla_h\psi + g\xi = 0 && in\ z = 0 \\ &\partial_t\zeta + \mathbf{u}\cdot\nabla_h\xi - \psi_z = 0 && in\ z = 0 \\ &\psi_z = 0 && in\ z = -H \end{aligned} \tag{4}$$

Set 2:

$$\begin{aligned} &\nabla^2\phi = 0 && in\ \Omega \\ &\partial_t\phi + \mathbf{u}\cdot\nabla_h\phi + \tfrac{1}{2}\nabla_h\phi\cdot\nabla_h\phi + \nabla_h\psi\cdot\nabla_h\phi + \tfrac{1}{2}\nabla_h\psi\cdot\nabla_h\psi + P/\rho + g\eta = 0 && in\ z = 0 \\ &\partial_t\eta + (\mathbf{u} + \nabla_h\phi + \nabla_h\psi)\cdot\nabla_h\eta + (\nabla_h\phi + \nabla_h\psi)\cdot\nabla_h\xi - \phi_z = 0 && in\ z = 0 \\ &\nabla\phi\cdot\mathbf{n}_b = (\mathbf{v}_b - \nabla\psi - \mathbf{u})\cdot\mathbf{n}_b && in\ \Gamma_b \\ &\phi_z = 0 && in\ z = -H \end{aligned} \tag{5}$$

The finite element method, FEM, is adopted in this work to solve above system of equations. Further details on the FEM solver can be found in [14].

2.2 Body dynamics

The ship dynamics consist of using Newton's laws to obtain the ship movements once external loads acting on it are known. In this work, it is assume that the ship trajectory is fixed in the horizontal plane, constraining the surge, sway and yaw movements. On the other hand, heave, roll, and pitch will be free.

$$\overline{\overline{\mathbf{M}}}\ddot{\mathbf{x}} + \overline{\overline{\mathbf{K}}}\mathbf{x} = \sum \mathbf{F} \tag{6}$$

where $\overline{\overline{\mathbf{M}}}$ is the mass matrix, $\overline{\overline{\mathbf{K}}}$ is the restoring matrix, and **F** represents all kind of external forces and moments. Above equations of motion are solved using the well known Newmark´s scheme.

2.3 Free surface boundary condition

Solving the free surface boundary condition efficiently is the key point when dealing with water waves problem. The free surface conditions can be rewritten as:

$$\begin{aligned} &\partial_t\eta + \underbrace{\mathbf{U}\cdot\nabla_h\eta}_{Convective\ term} + \nabla_h\phi\cdot\nabla_h\xi - \phi_z = 0 \\ &\partial_t\phi + \underbrace{\mathbf{U}\cdot\nabla_h\phi}_{Convective\ term} - \tfrac{1}{2}\nabla_h\phi\cdot\nabla_h\phi + \nabla_h\psi\cdot\nabla_h\phi + P/\rho + g\eta = 0 \end{aligned} \tag{7}$$

where $\mathbf{U} = (\mathbf{V}_b + \nabla_h\phi)$ is the base flow. In this work no linearization is assumed since it is considered that $\nabla_h\phi \sim O(1)$.

The numerical schemes adopted for solving the kinematic-dynamic free surface boundary conditions are based on Adams-Bashforth-Moulton schemes, using an explicit scheme for the kinematic condition, and implicit one for the dynamic condition. Then ϕ^{n+1} can be imposed as a Dirichlet Boundary condition. The schemes read as follows:

$$\begin{aligned} \eta^{n+1} &= \eta^n - \Delta t\left(\mathbf{U}\cdot\nabla_h\eta\right)^n - \Delta t\nabla_h\phi^n\cdot\nabla_h\xi^n + \Delta t\phi_z^n \\ \phi^{n+1} &= \phi^n - \Delta t\left(\mathbf{U}\cdot\nabla_h\phi\right)^{n+1/2} + \Delta t\tfrac{1}{2}\left(\nabla_h\phi\cdot\nabla_h\phi\right)^n - \Delta t\nabla_h\psi^n\cdot\nabla_h\phi^n - \Delta t\left(P^{n+1}/\rho + g\eta^{n+1}\right) \end{aligned} \tag{8}$$

In this work, the convective term is obtained by differentiating along streamlines. The streamline derivatives are estimated using a two points upstream and one point downstream differential operator inspired by the quickest scheme [15].

This formulation has been developed to be used in conjunction with unstructured meshes. The use of unstructured meshes enhances geometry flexibility and speed ups the initial modelling time. Furthermore it helps to reduce the number of elements by refining only in those areas of interest.

2.4 RAOS evaluation of the XR-1B Surface Effect Ship

A set of numerical tests were run to analyse the seakeeping characteristics of the XR-1B T-Craft, using the aircushion model presented above. Figure 1 shows the geometry of the ship, and Table 1 provides information regarding its particulars, as well as of the design conditions.

Figure 1: XR-1B geometry

Length overall (m)	76.35
Length waterline on cushion (m)	67.52
Draft on cushion (m)	1.33
Beam max. (m)	22.25
Cushion width (m)	16.50
Cushion length (m)	67.14
Displacement (tonnes)	1560
LCG from wet deck transom (m)	33.75
TCG from starboard of centreline (m)	0
VCG above water line (m)	2.35
Pitch gyradius (m)	21.6
Roll gyradius (m)	8.01
Aircushion average pressure (KPa)	11
Water depth (m)	10

Table 1: Particulars for the XR-1B

For the different cases analysed, the aircushion is modelled as a pressure distribution. This pressure distribution is given by the following analytical model [16]:

$$P^{ac}(\mathbf{x},t) = P_{ave} \cdot 0.25 \cdot \left[\tanh\left(50\left(\frac{\text{x-37}}{65}+0.5\right)\right)-\tanh\left(100\left(\frac{\text{x-37}}{60}-0.5\right)\right)\right] \cdot \left[\tanh\left(10\left(\frac{\text{y}}{16}+0.5\right)\right)-\tanh\left(10\left(\frac{\text{y}}{16}-0.5\right)\right)\right] \quad (9)$$

The above pressure distribution accounts for a smooth pressure drop in the areas of the seals as well as when getting closer to the hull. Evaluations of this pressure field on specific locations are straightforward introduced in Eq.(8).

The predictions of the computational model are compared to experimental results performed with a scale model by NSWC CD [17]. Figure 2 and Figure 3 show the zero-speed heave and pitch response of the vessel in monochromatic head seas, compared with experimental results. The computational results have been obtained for an infinite depth condition and for an equivalent experimental depth.

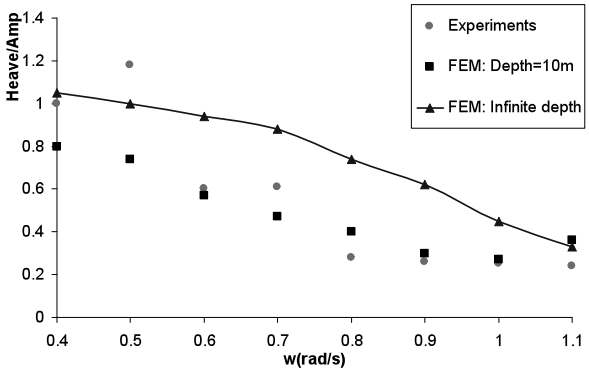

Figure 2. Zero-speed T-Craft heave RAO from model test and computational predictions.

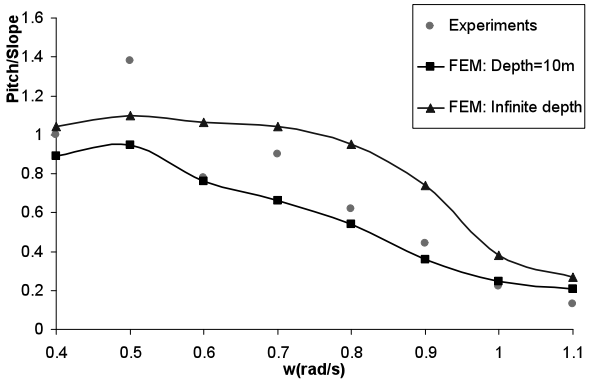

Figure 3. Zero-speed T-Craft pitch RAO from model test and computational predictions.

The computational model captures fairly well the zero-speed response of the craft. However, substantial differences are found in the lower frequency range. Similar behaviour is justified in [7], due to the limitations of the model regarding air flow and skirt dynamics.

Some limited experimental data were also available for the response of the T-Craft scale model in head seas at a speed of 30kt (full scale). Equivalent simulations were performed using the presented computational model. Figure 4 shows the heave response of the model, compared with experimental results, showing a good agreement overall.

Finally, a set of numerical tests for a range of wave periods and wave directions have been carried out for Fr=1.6 and forward speed. The aim of these tests is to estimate response amplitude operators (RAOs) in heave, roll and pitch, so that complicated navigating conditions could be anticipated. The wave direction is measured respect to the OX axis and positive clockwise. That is to say, a direction of 180º means head seas, while 0º means following seas.

Figure 5 provides the roll results from the computational tests. It can be observed that stern quartering waves with wave periods around 9s-10s are the most dangerous ones out of the range analyzed. Strong resonance effect might appear leading to an unstable behaviour of the ship. Unfortunately, no experimental results are available to confirm these results.

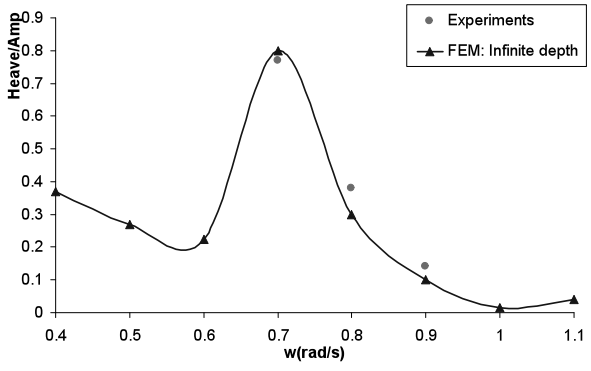

Figure 4. 30kt forward speed T-Craft heave RAO from model test and computational prediction.

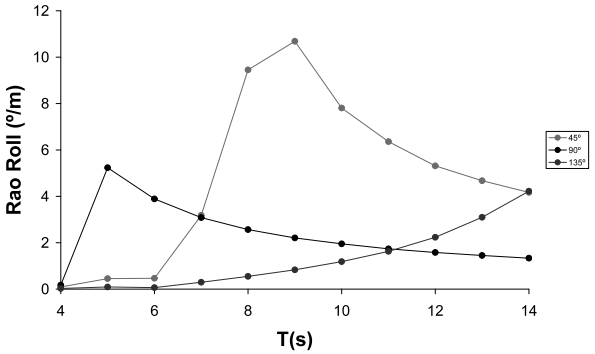

Figure 5: Response amplitude operator in roll for XR-1B in waves at Fr=1.6

3. FLUID-STRUCTURE INTERACTION SOLVER

3.1 Free surface-seal interaction

Modelling the behaviour of the seals of aircushion vehicles is not a trivial issue, due to the complex interaction of the seals with free surface. In this work, a new algorithm for handling the free surface-seal interaction problem is formulated. It is based on finding an equivalent pressure field to be applied over the free surface such that the elevation of this one is limited by the location of the seal. That is to say, the seal act as an upper limit for the free surface elevation.

The free surface boundary conditions are applied in different ways depending on whether the free surface is in contact with the seal or not. Actually, the free surface node where the algorithm is to be applied is dry if the seal is not in contact with the free surface at that location, and wet if it is. Figure 6 illustrates the wet and dry concepts.

The main challenge for an algorithm like this is to be capable of capturing when a node goes from dry to wet and vice versa, as well as estimating the pressure field on the wet nodes. For a dry node, the implementation of both, the kinetic and dynamic boundary condition is the same as for any other node not interacting with the seal. However, for wet nodes, the free surface boundary condition is applied by imposing that the free surface elevation matches the seal elevation, and ensuring that there

is no flow across the seal. These two conditions are represented by the following equations:

$$\eta_{wet}^{n+1} + \xi^{n+1} = H_{SEAL}^{n} \rightarrow \eta_{wet}^{n+1} = H_{SEAL}{}^{n+1} - \xi^{n+1} \quad (10)$$

$$\phi_z^{n+1} = \mathbf{U}^{n+1/2} \cdot \nabla_h H_{SEAL}{}^{n+1} + \nabla_h \phi^n \nabla_h \xi^{n+1} + \tfrac{1}{\Delta t}(H_{SEAL}{}^{n+1} - H_{SEAL}{}^{n}) \quad (11)$$

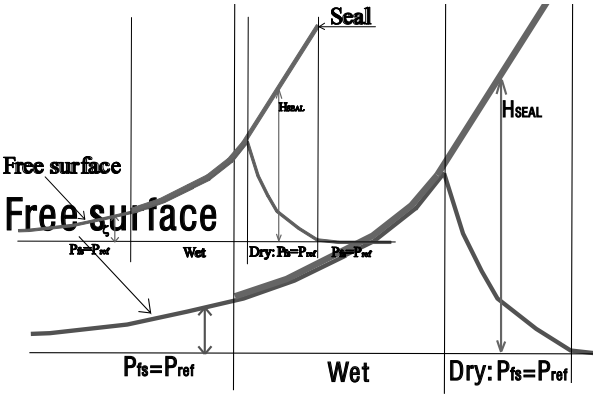

Figure 6: Wet and dry seal regions for free surface boundary condition implementations.

The change from being a dry node to become a wet node is identified via the kinematic BC though the condition $\eta^n + \xi^n > H_{SEAL}^n$.

3.2 Structural solver

The flexible seals have been modelled using a FEM formulation for a 3-noded membrane triangle. After different tests, the membrane element has finally been selected, as it is expected that the seals are mostly subjected to tension state stress. The membrane solver uses a total Lagrangian formulation with an implicit time integration scheme, and assumes a linear-elastic behaviour of the material [18]. The kinematic description is formulated in large displacements and large deformations, making use of the right Cauchy-Green deformation tensor.

The loads on the membrane are of two types. First, the loads imposed by the air cushion system considered. The air cushion system acts differently on the bow skirt and the stern seal. Second, the loads applied by the water on the seals. The interaction algorithm developed for this purpose will be presented in the next section. The structural solver has been modified in order to consider the loads applied by the liquid as follower loads.

3.3 Free surface-flexible seals coupling algorithm

The fluid-structure coupling is performed by an explicit staggered interaction algorithm. This way, the pressure field computed in the hydrodynamic solver is sent to the structural solver to compute the seals deformation. The resulting displacements are used to compute the new pressure field for the following time step.

Since the hydrodynamics and structural solvers used in this work are independent, the strategy developed to communicate both solvers is based on the interchange of information at memory level by means of TCP-IP sockets. For this purpose, a C++ library has been developed, and integrated with the already available TCL programming interface of both solvers. Furthermore, this library has been extended to be able to interpolate data from one mesh to another mesh.

The communication protocol developed for the library is quite simple. Actually, it just requires sending and receiving functions for vectorial fields (including an implicit waiting instruction in the receiving function for synchronization purposes) plus specific support to read and process mesh data. This way, only minor adaptations of the solvers were required.

3.4 Analysis of the XR-1B in still water with flexible bow seals

In this section, the towing test of the craft is analysed, including flexible seals, using the fluid-structure coupling algorithm proposed. Three velocities were run, Froude numbers 0.4, 0.8 and 1.2, until a quasi-static distant wave pattern is obtained. These cases were run including only bow seals (fingers) and both bow and stern seals.

Figure 7 shows the bow seal deformation and wave patter for the case Fr = 0.8. It can be seen how the

seals interaction creates an unstable free surface deformation pattern in the cushion. This happens for the higher Froude numbers, while the solution is quite steady for the smaller figures. In this latter case, the deformation of the seals is very small, since the dynamic pressure acting on the seals is quite similar to the cushion pressure.

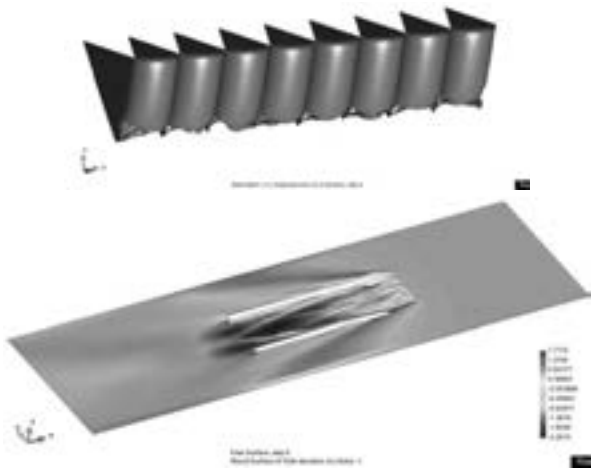

Figure 7. Bow seals deformation (top) and wave pattern (bottom) for Fr=0.8 and t=6 s.

In figures 10-12, the deformed bow and stern seals, wave pattern and cushion free surface deformation are shown. The results show how the bow seals create an unstable free surface deformation pattern in the cushion area, while the stern seal is deformed until it is adapted to a configuration in which it almost slides on the water.

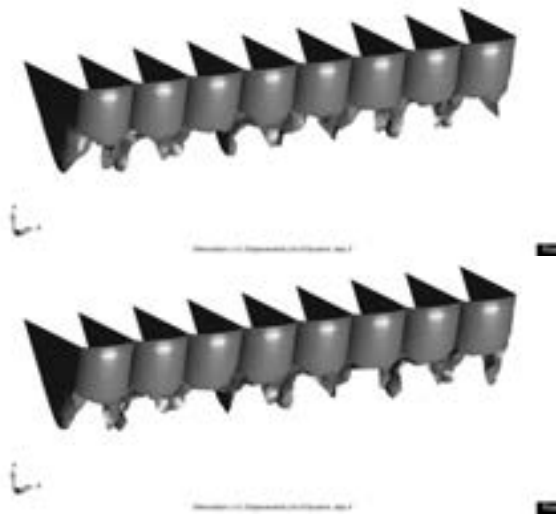

Figure 8. Bow seals deformation for t=2, 4 s (Fr=1.2).

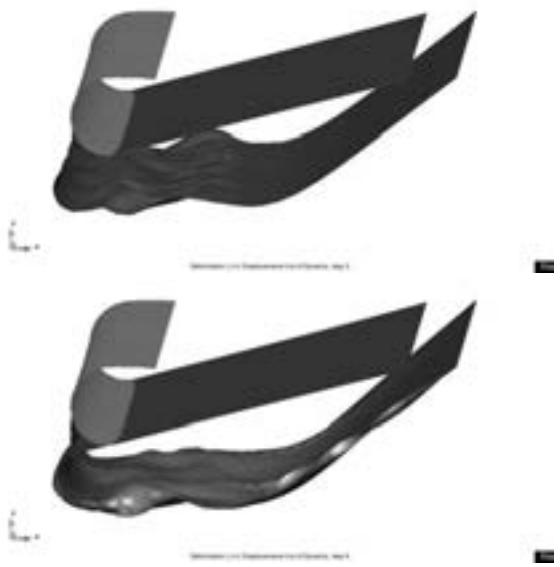

Figure 9. Stern seals deformation for t=2, 4 s (Fr=1.2).

Figure 10. Wave pattern and cushion free surface deformation for t=4 s (Fr=1.2).

The bow seals deformation obtained in these analyses qualitatively agrees with the experimental information available in reference [9]. In fact, the deformation mode obtained in the computational model is quite similar to that found experimentally. Unfortunately, no quantitative data exists to further validate these results.

4. CONCLUSIONS

This paper reports the advances in the development of a time-domain FEM model for evaluation of a SES including skirt dynamics. The developed fluid-structure interaction algorithm is based, on one side, on a staggered explicit algorithm, using a TCP/IP sockets link, able to communicate pressure forces and displacements of the seals at memory level

and, on the other side, on an innovative wetting and drying scheme able to predict the water action on the seals. The flow solver uses a potential flow approach along with a stream-line integration of the free surface, while the skirt dynamics are solved using a Lagrangian FEM formulation for a 3-noded membrane triangle.

Different validation and demonstration cases, including different analyses of a XR-1B SES model have confirmed the validity of the approach to study the complex and highly dynamic behavior of the seals in the interface between the air cushion, and the water.

5. ACKNOWLEDGEMENTS

This research is sponsored by the Office of Naval Research under Grant N62909-10-1-7053 administered by Ms. Kelly Cooper.

6. REFERENCES

[1] Oñate E. & García-Espinosa, J., A finite element method for fluid-structure interaction with surface waves using a finite calculus formulation, *Comp. Methods Appl. Mech. and Eng.* 2001; 191: 635-660.

[2] Löhner, R., Yang, C. & Oñate, E., On the simulation of flows with violent free surface motion and moving objects using unstructured meshes, *Comp. Methods Appl. Mech. Engng.* 2007; 53: 1315-1338.

[3] García-Espinosa, J., Valls A., & Oñate, E., ODDLS: A new unstructured mesh finite element method for the analysis of free surface flow problems, *Int. J. Numer. Meth. Fluids* 2008; 76 (9): 1297-1327.

[4] Donnelly D. J., and Neu W. L., Numerical Simulation of Flow About a Surface-Effect Ship, 11th International Conference on Fast Sea Transportation FAST 2011, Honolulu, Hawai. September 2001.

[5] Mousaviraad, S. M., Bhushan, S., and Stern, F. CFD Prediction of Free-Running SES/ACV Deep and Shallow Water Maneuvering in Calm Water and Waves. MARSIM 2012. Singapore, April 23-27, 2012.

[6] Camas, B. and García-Espinosa, J., Advances in the development of a time-domain unstructured finite element method for the analysis of waves and floating structures interaction, IV International Conference on Computational Methods in Engineering MARINE 2011, Lisbon, 2011

[7] Connell, B. S. H., Milewski, W. M., Goldman, B., & Kring, D. C. Single and Multi-Body Surface Effect Ship Simulation for T-Craft Design Evaluation, 11th International Conference on Fast Sea Transportation FAST 2011, Honolulu, Hawai. September 2001.

[8] Kring, D. C., Parish, M. K., Milewski, W. M., and Connell, B. S. H. Simulation of Maneuvering in Waves for a High-Speed Surface Effect Ship, 11th International Conference on Fast Sea Transportation FAST 2011, Honolulu, Hawai. September 2001.

[9] Yun, L. and Bliault, A.Theory & Design of Air Cushion Craft, Elsevier, Oxford, 2005.

[10] Hirata N., and Faltinsen O. M., 2000, Computation of Cobblestone effect with unsteady viscous flow under a stern seal bag of a SES, *Journal of Fluids and Structures*, 2000: 14, 1053–1069.

[11] Doctors, L. J., Nonlinear motion of an air-cushion vehicle over waves. *Journal of Hydronautics* 1975: 9 (2), 44–57.

[12] Sullivan, P. A., Charest, P. A., Ma, T.. Heave stiffness of an air cushion vehicle bag and finger skirt. *Journal of Ship Research* 1994: 38 (4), 302–307.

[13] Yang, Q., Jones, V., and McCue, L.. Investigation of Skirt Dynamics of Air Cushion Vehicles under Non-linear Wave Impact Using a SPH-FEM Model, 11th International Conference on Fast Sea Transportation FAST 2011, Honolulu, Hawai. September 2001.

[14] Evaluating Manoeuvering and Seakeeping Performance of a Surface Effect Ship. Technical Report, CIMNE IT-630, October 2012.

[15] Leonard, B. P. A stable and accurate convective modelling procedure based on quadratic upstream interpolation. *Comp. Meth. Appl. Mech. Eng.* 19 (1979) 59-98.

[16] [Maki, K. J., Broglia, R., Doctors, L. J., and Mascio, A. Nonlinear wave resistance of a two-dimensional pressure patch moving on a free surface. *Ocean Engineering*. 39 (2012) 62–71

[17] Bishop, R. C., Silver, A. L., Tahmasian, D., Lee, S. S., Park, J. L., Snyder, L. A. and Kim, J., "T-Craft Seabase Seakeeping Model Test Data Report Update", Naval Surface Warfare Center Carderock Division, Technical Report, NSWCCD-50-TR–2010/062, 2010

[18] R.L. Taylor, E.Oñate and P.-A. Ubach, Finite element analysis of membrane structures. Textile composites and inflatable structures. Springer (2005) 47-68.

Centre Internacional de Mètodes Numèrics en Enginyeria (CIMNE)
Gran Capitán s/n, 08034 Barcelona, Spain
e-mail: julio@cimne.upc.edu,
web page: http://www.cimne.upc.edu

Julio García-Espinosa

Pere-Andreu Ubach

Borja Serván

Eugenio Oñate

Daniel Di Capua

Stefan Harries, Fabian Tillig, Marc Wilken and George Zaraphonitis

THE PAPER HAD PREVIOUSLY BEEN PUBLISHED AT COMPIT 2011

An Integrated Approach for Simulation in the Early Ship Design of a Tanker

ABSTRACT

An integrated approach is presented that combines the simulation of key measures of merit in the early phase of ship design. The approach was applied to an Aframax tanker for which payload, steel weight, strength, oil outflow, stability and hydrodynamics were considered simultaneously. Required freight rates, Energy Efficiency Design Index and maximum speed for given engine output were determined so as to rank design variants. Formal exploration and exploitation strategies were utilized to investigate the design space and, subsequently, advance competing design proposals into certain directions such as maximum energy efficiency, attainable speed and environmental protection in case of accidents. The paper focuses on integration and optimization, utilizing the tanker as an elaborated design example to illustrate the holistic view.

1. INTRODUCTION

Ship design is often considered a sequential process that is classically pictured as a design spiral, Fig.1. Even though this represents an idealization, the traditional work flow is to study one issue at a time and to advance a design step by step, undertaking modifications and establishing refinements iteratively. Particularly when looking at a complex system with many relationships and dependencies, it is beyond any single individual's capacity to bear in mind all options and consequences. However, an integrated approach can be taken, Fig.1, that brings together key aspects of a design task at the same time. A synthesis model of Computer Aided Engineering (CAE) allows investigating the design space to a greater extent, leading to new insights and promising new options.

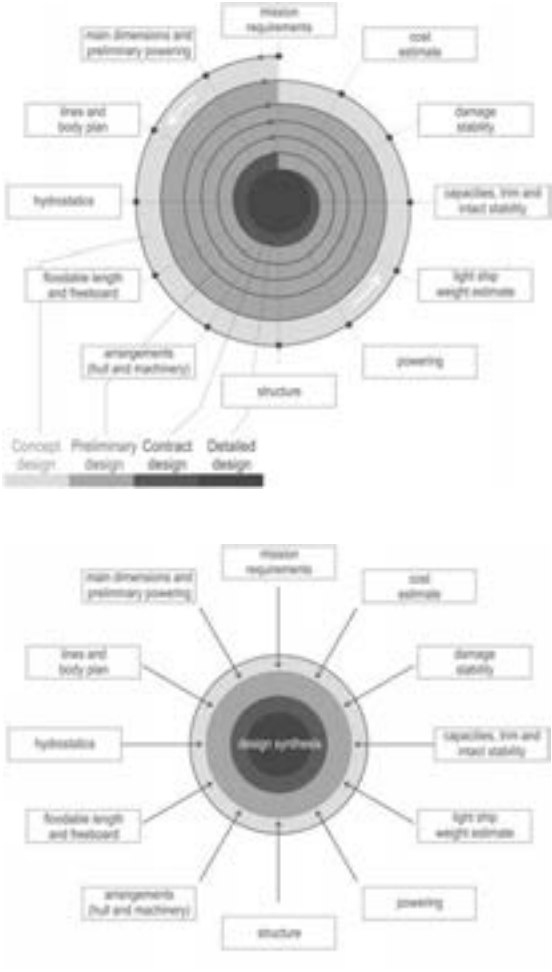

Fig.1: Traditional design spiral (top) vs. integrated approach (bottom)

Looking at an Aframax tanker for Caribbean trade, a CAE environment was established to examine key measures of merit for a considerable number of variants simultaneously: Payload, steel weight, strength, oil outflow, stability and hydrodynamics were computed by means of sophisticated simulation codes. Required freight rates (RFR), Energy Efficiency Design Index (EEDI) and maximum attainable speed for given engine output were determined so as to judge and rank variants.

2. OVERVIEW

Shipping's major ecological impact stems from energy consumption and associated green-house gas emissions in standard fleet operations. The introduction of the EEDI as put forward by the *MEPC (2009)* raises both awareness and efforts for higher energy efficiency while high bunker prices continue to excite economic pressure on the operators. A recent study for large oil tankers showed that potential loss of cargo is dominated by grounding and collision along with fire and explosions, *MEPC (2008)*. Enlarged double hull width and double bottom height consequently lead to better environmental protection as elaborated by *Papanikolaou et al. (2010)*.

An analysis using Lloyd's Register Fairplay WSE Database revealed that one fifth of the existing Aframax tonnage would be older than 15 years by 2012. Even though current tanker capacity appears to outweigh anticipated demand of oil transport, the fleet's ageing is likely to trigger replacements.

It is therefore safe to assume that new tanker designs will be sought in the near future. However, it is not obvious what will be the main driving forces:

- Safer shipping by containing oil outflow in case of an accident,
- Greener operations by reducing emissions per ton-mile of cargo,
- Smarter business by increasing returns (higher cargo capacity and lower fuel consumption).

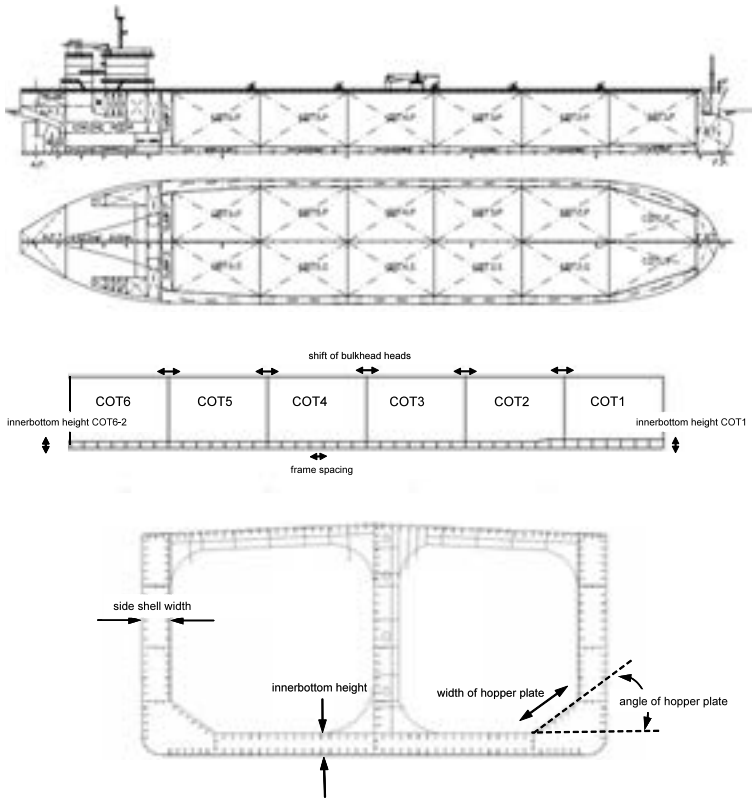

Fig.2: General arrangement along with layout of tanks and selected free variables

A reasonable combination is likely to be favored over an extreme, depending on the specific situation and preference of the stake holders. The more high-quality design data are available the easier it is to understand opposing influences, come to a sound judgment and choose the best compromise.

2.1 Design task

So as to have a focused design task Aframax tanker trades in the Caribbean Sea between St. Eustacius (transshipment), Aruba and Maracaibo (source) and the US Gulf region (sink) were selected for elaboration. This not only allowed to create and prove an integrated CAE approach but also to propose interesting novel designs for a ship type of imminent commercial interest. Restrictions of the prevailing shipping lanes, the main US port facilities and the US Emission Control Area (ECA) established important constraints, most notably limits on maximum length, beam and draft and an additional demand for tanks to carry marine gas oil (MGO). Requests from ship operators active in the trade were taken into account. A prominent call was to attain relatively high speeds. Furthermore, major structural modifications that would lead to deviating from recognized Aframax design principles - like cargo tanks without hopper plates - were to be avoided. A conventional 6x2 layout for the tanks was used, Fig. 2. The challenge was to identify designs that would not deviate too much from conventional practice but still yield significant improvements.

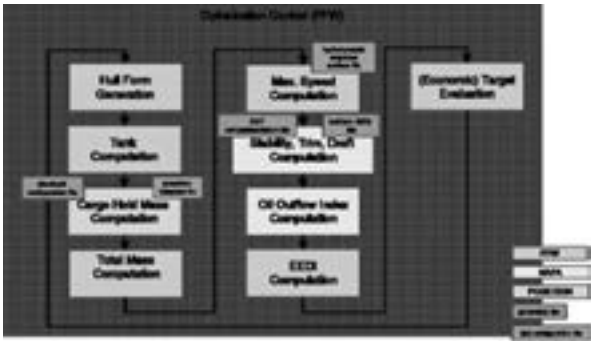

Fig.3: Flow chart of integrated approach

2.2 Design approach

The process was set up in the FRIENDSHIP-Framework (FFW), combining POSEIDON, NAPA and SHIPFLOW simulations. The following key measures were computed:

- Cargo tank capacity in full load and design load conditions,
- Steel weight of the cargo tank area,
- Maximum ship speed at design, ballast and scantling drafts,
- Probability of oil spill in case of accidents measured by IMO's oil outflow index (OOI).

A general flow chart is presented in Fig.3. For each variant a hull form is generated within FFW along with optimal tank shapes. The ship structure in the cargo tank area is then determined with POSEIDON in accordance to the prescriptive part of the Common Structural Rules (CSR) for Double Hull Oil Tankers. The hydrodynamic performance is computed via a response surface model (RSM) built from a priori flow simulations using SHIPFLOW with potential flow (XPAN) and viscous (CHAPMAN) analyses. This is followed by a batch mode execution of NAPA to get intact stability and trim characteristics plus the probability of oil outflow on the basis of the current tank shapes and hull form. The process is complemented by several additional features within the FRIENDSHIP-Framework to gather and combine the various outputs from all external simulations.

From cargo tank capacity, steel weight and ship speed two combined performance measures for ecology and economics were derived:

- Operational impact measured by the energy efficiency design index (EEDI), combining engine power, deadweight and ship speed according to IMO,
- Financial attractiveness measured in terms of required freight rate (RFR), combining the annual cost of transport via capital, fuel and other operating costs with the number of roundtrips times cargo mass per year.

Free variables of the overall investigations were parameters that controlled the hull form (outer shell), the tank layout and geometry as well as the inner structure, Table I. Starboard (S) and port (P) parameters were assumed to be the same. As a use case tankers optimized in terms of RFR (cost of transport) were created by variation of the hull form and selected structural parameters, Fig. 2.

Having established the most favorable main particulars, cargo holds and scantlings, in a global optimization, the ship's aftbody was subsequently fine-tuned with regard to wake quality and total resistance. In addition, systematic changes were undertaken to study the dependencies of selected measures of merit on specific parameters, e.g. the change of oil outflow probability by further stepping the bottom of the foremost tanks.

3. PARAMETRIC MODELS

3.1 Hull form

A fully parametric hull model was developed within FFW for typical tanker hull forms, Fig. 4. The model is divided into forebody, parallel midbody and aftbody. While the forebody and the aftbody are created using meta-surfaces, the parallel midbody is a simple ruled surface for connection.

Basic curves for points, tangents and integral values are employed to define the shape of the hull surfaces. The basic curves depend on global variables, e.g. length between perpendicular (LPP), and local variables which influence only small regions. The shapes of the basic curves are controlled by specifying the tangents at their start and end positions, respectively, as well as specific areas between the curve and an axis of reference. In special cases, for example the waterlines in the aftbody, additional points in the middle are utilized along with associated tangent information.

The forebody is realized using one single meta-surface with rotating sections, with the center of rotation at the intersection of the aft end of the forebody, the midship plane and the flat of bottom. In the aftbody region several surface patches are combined, using sections (x constant) as input to the meta-surfaces except for the aft bulb which features a surface built on waterlines (z constant) to ensure tangent continuity at the transition to the adjacent surface.

Free variable	Lower bound	Upper bound	Primary influence
Length over all (LOA)	242 m	250 m	Hull form
Beam	42 m	44 m	Hull form
Shift of longitudinal center of buoyancy	-0.008 LPP	0.008 LPP	Hull form
Block coefficient	0.8	0.885	Hull form
Depth	20.5 m	23 m	Tank geometry
Inner bottom height of cargo oil tanks 2 to 6 (S+P)	2.0 m	2.7 m	Tank geometry
Lifting of inner bottom of cargo oil tank 1 (S+P)	0 m	1.5 m	Tank geometry
Side shell width	2.0 m	2.7 m	Tank geometry
Angle of hopper plate	30°	60°	Tank geometry
Width of hopper plate	4.8 m	5.8 m	Tank geometry
Shift of the intermediate bulkheads (frame spacing *a*)	-1 *a*	+1 *a*	Inner structure
Number of frames per tank	7	8	Inner structure

Table I: Free variables and their bounds for the global optimization

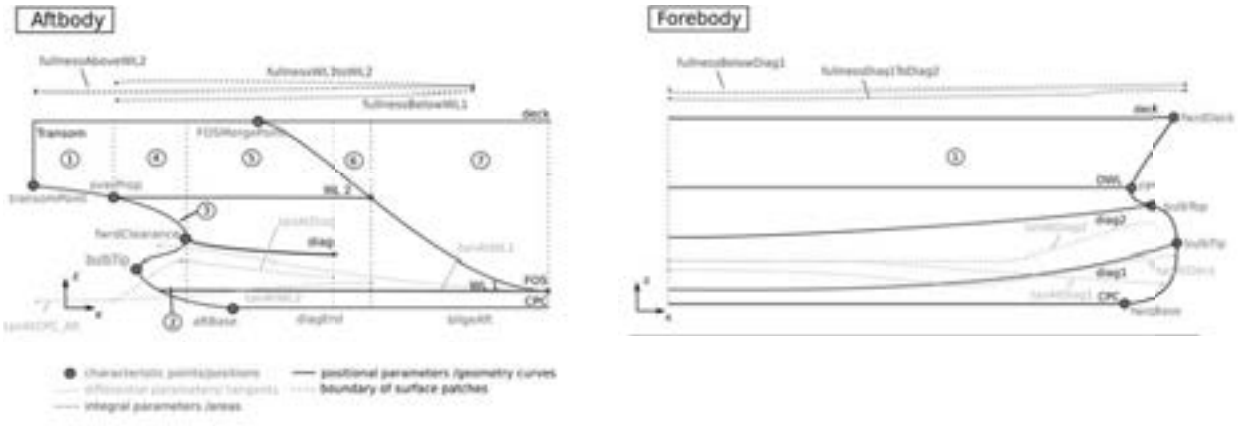

Fig.4: Fully parametric hull model for a tanker

For hydrodynamic analyses, see section 4.2, the length, beam, longitudinal position of the center of buoyancy (XCB) and displacement volume were changed systematically. While length and beam of the hull form are global parameters of the fully parametric model, the variations of XCB and displacement were realized by means of a Generalized Lackenby for partially parametric modifications, *Abt and Harries (2007)*. Local parameters defining the shape of the aftbody's basic curves were changed during the hydrodynamic fine tuning. In this phase 12 local parameters were varied, for instance the fullness of the diagonal starting in the forward clearance point, the forward clearance of the propeller and the fullness of the aft bulb curve in the midship plane.

An existing geometry following previous studies by *Papanikolaou et al. (2010)* was taken as a good starting point for the design task. The parametric model was adjusted to closely resemble the existing hull form. Realizing a new variant then simply meant changing the selected set of parameters.

3.2 Tank arrangement

The cargo tanks were generated within the FFW using feature technology, e.g. *Brenner (2009)*. The tanks are computed such that maximum cargo volume is realized while ensuring a minimum distance to the hull form, e.g. 2 m. The feature takes the hull form, the minimum distance of the inner structure to the hull (outer shell) and the longitudinal position of the engine room's bulkhead as inputs. The collision bulkhead's position is computed according to IMO rules.

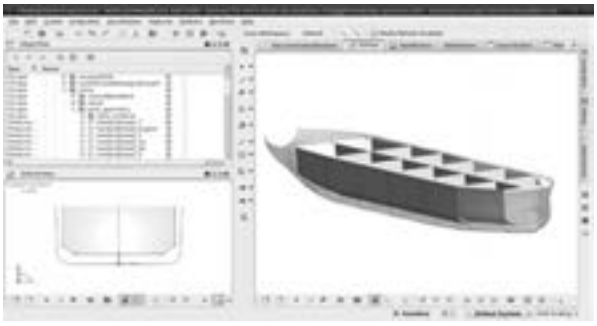

Fig.5: 6x2 tanks generated within the FRIENDSHIP-Framework (FFW)

During the global optimization the side shell width at deck height, the double bottom height at amidships, the angle and width of the hopper plate and the step in the double bottom towards the foremost tank were changed. The bulkhead positions were moved discretely according to the frame positions. The total number of frames was controlled by specifying the number of frames per tank. The first tanks (COT1) and the last tanks (COT6) were flexible in length by allowing shifts of the bulkhead positions by one frame distance forward or aft, Fig. 2. The tanks associated with a specific design variant were represented as an assembly of planar surfaces within the FFW, Fig. 5, and transferred to NAPA by means of the edge points for the bulkheads and hopper plates.

3.3 Structural model

For strength assessments a computational model containing all CSR relevant structural information was needed. The model had to include information about the main particulars of the vessel, plate distribution and stiffener arrangement of primary and secondary members, tank arrangement and load definitions.

For the design process at hand it was decided that only those elements should be addressed that would influence the key measures significantly. Therefore, there was no need to make all strength relevant data readily accessible for the actual design task which tangibly reduced data management. Nonetheless, the structural information had to be prescribed for all strength assessments. This was done by providing the principle steel design externally as a POSEIDON template database that could be transformed into a complete structural design by insertion of the current set of free variables. This template database specified the steel structure of the cargo tank area of an Aframax tanker with 6x2 layout and a plate arrangement and stiffener distribution complying with a conventional design, Fig. 6:

- Vertically stiffened flat transverse bulkheads with transverse girders,
- Longitudinally stiffened main deck, hopper plate, inner hull, inner bottom, stringer decks, longitudinal girders,
- Longitudinal bulkhead stiffened with transverse girders,
- Regularly positioned web and floor plates,
- Main deck supporting transverse girders.

Using a *Python* interface to POSEIDON's database, the template model could be modified according to the current design instance. An ASCII file was provided by the FFW which included an adaptation of the hull form in POSEIDON's specific offset format, the actual tank compartmentation and the free variables for the inner structure like the number of frames per cargo tank.

Fig.6: Hull structure modeled within POSEIDON (main deck removed to show inner structure)

4. ANALYSES AND SIMULATIONS

4.1 Structure and strength

For the design task the Common Structural Rules for Double Hull Oil Tankers had to be applied with their different levels of assessment. CSR start with prescriptive rules based on beam theory which are followed by Finite Element Analyses (FEA) of primary and secondary members and then finish with detailed FEA for fatigue assessment of structural details in a hot spot approach.

Here, only the prescriptive part of the CSR was applied to determine the strength of the structure. In this sense the proposed integrated approach yields a "pre-dimensioned" tanker design that needs to be approved - and slightly adapted - in a subsequent step to comply fully with the CSR. The reason behind this is that model generation for FEA is a rather sophisticated undertaking in its own right and that corresponding simulations need considerable resources. It was therefore decided to utilize the prescriptive part to rank variants according to their overall properties within the optimization process.

Each design variant was measured in terms of the steel mass necessary to fulfill the strength requirements. The steel mass computation was performed by POSEIDON's automatic plate sizing capability at given cross sections of the vessel. Characteristic frame cross sections like the main frame or transverse bulkheads, Fig. 7, were chosen to obtain the steel mass of the total cargo region.

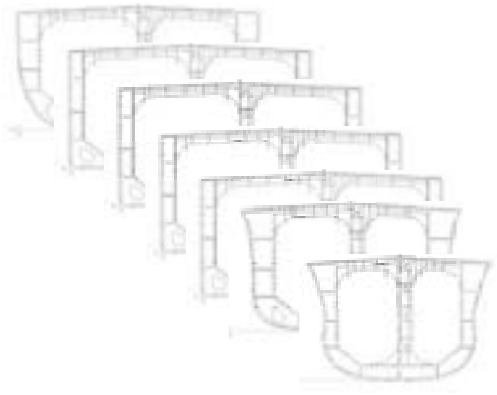

Fig.7: Cross sections of a generated design

4.2 Hydrodynamics

Since the Computational Fluid Dynamics (CFD) simulations are the most resource intensive of all analyses within the design task, response surface models (RSM) were utilized to capture resistance and propulsion characteristics for different speeds and drafts. In other words: Rather than to include a very time-consuming full CFD simulation for each variant during the overall optimization the hydrodynamics was pre-computed and then replaced by suitable meta-models.

Four free variables were chosen, namely length over all (LOA), maximum beam, a relative change in the position of the longitudinal center of buoyancy (Delta XCB) and the displacement volume. As summarized in Table II these variables were allowed to vary within meaningful bounds that stemmed from general constraints (like relevant harbor facilities in the Gulf of Mexico), pure hydrodynamic considerations and estimates for expected total displacement.

Hydrodynamic performance was considered at design draft (13.7 m on even keel at rest), scantling draft (14.8 m on even keel) and ballast draft (6 m at FP and 8 m at AP) in parallel. The fully parametric hull model, Fig. 4, was utilized to vary the free variables globally.

Free variable	Lower bound	Lower bound
Length over all	242 m	250 m
Beam	42 m	44 m
Delta XCB	-0.90%	0.90%
Displacement volume	126 075 m³	136 325 m³

Table II: Free variables and bounds for hydrodynamic RSM

Both potential flow and viscous computations were performed using the zonal approach offered within the flow solver SHIPFLOW. A sequence of computations was undertaken: A potential flow computation without free surface for the entire hull (XPAN), a subsequent thin boundary layer computation for the forebody (XBOUND) and, finally,

a RANSE computation for the aftbody (CHAPMAN). The propeller was modeled as a force actuator disk, idealizing an active propeller for all computations. All viscous computations were performed at full-scale Reynolds number with the model free to sink and trim. For each valid variant, the viscous flow computations provided the frictional and viscous pressure resistance as well as the wake field in the propeller plane. Additional potential flow computations including nonlinear boundary conditions at the free surface were carried out to obtain the wave pattern resistance, Fig. 13.

In all computations - be it for building the response surfaces or for the final aftbody refinement - the same panel meshes and volume grids were employed. For the potential flow analysis, a body mesh with 1150 panels and a free surface mesh with 7175 panels were used. The volume mesh for viscous simulations featured 1.7 million cells with a longitudinal stretch toward smaller cells in the skeg region. An impression of panels and grids can be gotten from Fig. 8.

In order to achieve convergence, 3000 iterations were done for the RANSE solutions of globally changed variants and also for the baseline of the succeeding fine-tuning. One of these computations including potential and viscous flow simulations took about 8 h on a quad core 4x3.0 GHz AMD workstation. Subsequent computations for only locally changed variants, as created during the hydrodynamic optimization, were restarted from the baseline solution with some additional 800 iterations. The restarted computations then only took about 2.5 h each.

For the response surfaces, a total of 486 variants were investigated via an ensemble investigation, i.e. a systematic coverage of the design space. Thereof 270 variants fulfilled the inequality constraint on maximum block coefficient to be less than or equal to 0.88. For these 270 variants the CFD analyses were launched, using the FFW for process control. Six SHIPFLOW computations were needed for each variant to cover two speeds at three drafts (design, scantling and ballast). The speeds were chosen individually for each draft such that the lower speed would lie below the expected attainable speed while the higher speed would be a bit above the anticipated maximum.

Three response surfaces were finally built, one for every loading condition, assuming quadratic speed-power relationships. The attainable speeds were determined for fixed power installed of 13 560 kW. This value corresponds to a MAN 6S60MC-C at around 100 rpm as a representative engine for Aframax tankers. An engine output of 85% MCR and a sea margin of 10% were assumed.

Power delivered was computed from effective power and an individual estimate of propulsive efficiency. This was done using a wake quality index, called the SVA criterion as discussed in *Fahrbach (2004)*, multiplied with the ideal propeller

Fig.8: Superposition of surface panels and parts of the volume grid as used for potential (XPAN) and viscous flow simulations (CHAPMAN), respectively

efficiency as proposed by *Tillig (2010)*. Thus, the power delivered was dependent on the total resistance and the wake quality. Therewith the attained speed on all loading conditions could be determined for all variants created during the global optimization. (The approach's validity was checked and confirmed by means of separate numerical resistance and propulsion tests in SHIPFLOW to establish wake fractions and thrust deduction factors. A Wageningen optimal propeller could then be selected which showed that the obtained speed estimates were conservative.)

The response surfaces were produced employing a Kriging approach with anisotropic variograms, *Tillig (2010)* and *Harries (2010)*. The Kriging algorithm ensures that sample points are interpolated while oscillations of the RSM are avoided. Interpolation values are computed using a weighted sum of all samples on the basis of the variograms. Here a variogram for each variable direction was produced and the total variogram value of the interpolation point was obtained as a weighted sum of all directional variograms. Thus the influences of the different variables on the function value of interest were captured. The RSM was realized as a *Scilab* application for variogram creation and as a *Python* script for the function value estimation - which was later called from the FRIENDSHIP-Framework during the optimization.

Utilizing the three response surfaces it was possible to estimate the attainable speeds at ballast, design and scantling draft directly for a specified power installed, instead of performing an iterative CFD based search. Each RSM analysis thus took about one minute per variant instead of one to two days of full CFD simulation.

4.3 Stability and accidental oil outflow

Compliance with the regulatory requirements for stability and oil outflow was determined within NAPA on the basis of actual tank shapes and hull forms as provided by the FRIENDSHIP-Framework. The hull form is transferred to NAPA using a standard iges format representation. A set of parameters is taken as input to recreate the exact geometry of the inner hull and watertight subdivision. Suitable NAPA macros were developed, facilitating the calculation of the mean oil outflow index as well as the assessment of intact and damage stability requirements and the regulatory and operational trim and draft constraints in the various loading conditions.

Resolution MEPC.117(52) was taken as the regulatory basis for the evaluation of design variants. Regulations 18, 19, 23, 27 and 28 set the requirements for the segregated ballast tanks capacity, the double hull arrangement, accidental oil outflow and transverse stability in intact and damaged condition. For example, for crude oil tankers of 20 000 tons DWT, Regulation 18 calls for sufficient capacity of segregated ballast tanks (SBT), so that the ship may operate safely on ballast voyages without recourse to cargo tanks for water ballast. The capacity of SBT shall be at least such that, in any ballast condition at any part of the voyage, including the conditions consisting of lightweight plus segregated ballast only, the ship's drafts and trim can meet the following three constraints: Molded draft amidships $\geq 2.0+0.02$ L, trim by the stern ≤ 0.015 L and draft aft (Taft) always yields full immersion of the propeller(s). Additional requirements come in via Regulation 19 for ballast tanks (or spaces other than tanks carrying oil), effectively protecting the cargo space with various minimum dimensions.

The accidental oil outflow performance of oil tankers of 5 000 tons DWT and above, delivered on or after the 1st of January 2010, is to be evaluated according to Regulation 23, based on the so-called non-dimensional oil outflow parameter or, shorter, oil outflow index (OOI). The upper limit of the mean oil outflow depends on the total volume of cargo oil tanks of the ship. In particular, for ships with a total volume of cargo oil tanks at 98% filling less than 200 000 m3, as is the case for Aframax tankers, an OOI value not exceeding 0.015 is required. In other words, statistically no more than 1.5% of the total volume of the oil tanks shall be lost.

Quantity	Equation / Symbol
Oil outflow index (mean outflow)	$OOI = (0.4\,O_{MS} + 0.6\,O_{MB})/C$
Mean outflow for side damage in m^3	$O_{MS} = C_3 \sum_1^n P_{Si}\, O_{Si}$
Mean outflow for bottom damage in m^3	$O_{MB} = 0.7\,O_{MB(0)} + 0.3\,O_{MB(2.5)}$ $O_{MB} = \sum_{i=1}^{n} P_{Bi} O_{Bi}\, C_{DBi}$
Total volume of cargo oil tanks (incl. slop tanks and fuel tanks located within the cargo block length) at 98% filling in m^3	C
Corresponding outflow, assumed equal to the volume in cargo tank *i* at 98% filling, unless proven that significant cargo volume will be retained	O_{Si}
Probability of breaching a compartment in case of side damages (analogous procedure applies for the probability of breaching a compartment in case of bottom damage)	$P_S = P_{SL} \cdot P_{SV} \cdot P_{ST}$ $P_S = (1 - P_{Sf} - P_{Sa})(1 - P_{Su} - P_{Sl})(1 - P_{Sy})$
Probabilities of damage extending into the longitudinal, vertical and transverse limits of the tank, respectively	P_{SL}, P_{SV}, P_{ST}
Probabilities of damage lying entirely forward, aft, above or below or entirely outboard of each tank	P_{Sf}, P_{Sa}, P_{Su}, P_{Sl}, P_{Sy}
Mean outflow for bottom damage at zero tide condition and at 2.5 m tide condition	$O_{MB(0)}$ $O_{MB(2.5)}$
Factor accounting for the partial capturing of oil flowing out from a tank in the double bottom	$C_{DBi} = 0.6$ for tanks bounded below by non-oil compartments and $C_{DBi} = 1.0$ for tanks bounded by the bottom shell

Table III: Quantities needed for computing the oil outflow index

The oil outflow is calculated independently for side and bottom damages and then combined in non-dimensional form. The calculations of the mean outflows for side and bottom damage are based on a probabilistic approach, Table III, and takes probability distributions for side and bottom damage cases as input. Finally, Regulation 27 sets the intact stability criteria when at sea in the same form that is applicable to most types of ships. In addition a minimum meta-centric height (GM) of 0.15 m after correction for free surface effects is required at port to ensure minimum stability while loading or unloading. The maximum damage extent for side and bottom damage, along with the corresponding stability requirements in damaged condition are defined in Regulation 28. All these regulations were accounted for in a batch mode execution of NAPA, making them part of the simulations within the optimization.

5. SELECTED RESULTS

5.1 Exploration

During the course of the design work approximately 2500 variants were generated and assessed. To start with a Design-of-Experiment (DoE) for the exploration of the global design space was performed, yielding a database with all relevant simulation outputs and the key measures of merit, namely RFR, OOI and EEDI. A conventional Aframax tanker served as a reference (baseline) for comparison and normalization, Table IV. For identifying the tankers with attractive economic performance for instance, the design variants were ranked according to RFR, Fig. 9. Naturally, any other preference of the decision makers can be considered and the two best designs for OOI and EEDI, respectively, are marked in Fig. 9, too. The diagram shows that the cost of transport (normalized RFR) falls with rising deadweight (DWT) until a certain minimum is reached. Cost of transport

could be reduced by about 4%. The performance of the heaviest tankers is slightly less attractive with regard to RFR but the tanker with lowest EEDI is found among them. The best tanker with lowest OOI turns out to be among the smaller designs with a slight penalty in RFR of ~2%.

Normalization was done with the baseline's data to gain a certain independence from current price levels and their volatility. The RFRs were determined via a roundtrip model for the Caribbean trade on the basis of contemporary cost levels. (Capital costs were based on a newbuilding price of 65 Million $, 25 years of lifetime and an interest rate of 8%. Fuel costs were computed with HFO at 500 $/t and MGO at 800 $/t for the transfer within the ECA. Other operating costs were approximated with 3 Million $/year and presumed to be independent of the variations.)

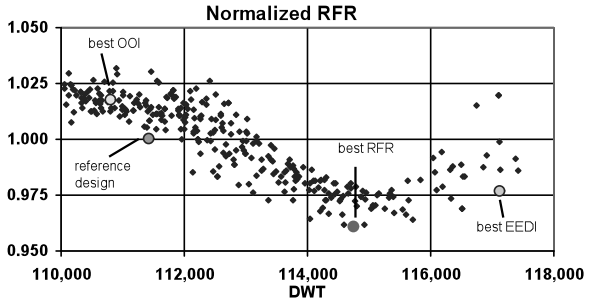

Fig.9: Designs established by means of the integrated CAE approach

5.2 Refinements

Since quite a few designs produced during the DoE offered nearly the same RFR, see Fig.9, the variant with the best OOI among them was selected for further refinements. A local hydrodynamic optimization, utilizing a deterministic search strategy, was undertaken for the aftbody, focusing on the quality of the wake field as an objective. The aftbody was allowed to change such that the impact on the cargo tanks previously established in the global optimization was negligible. The fine-tuning of the hydrodynamics yielded a further increase in speeds V such that the tanker would be expected to attain 15.6 kn at design draft and 16.8 kn at ballast draft with a level of confidence of ±1.3% V. The main characteristics of this favored design are summarized in Table IV and compared to the reference design. The associated hull form is presented in Fig.10. The lines stem from the parametric model and were realized within the FFW without further interactive work, i.e. they are a direct outcome from the optimizations.

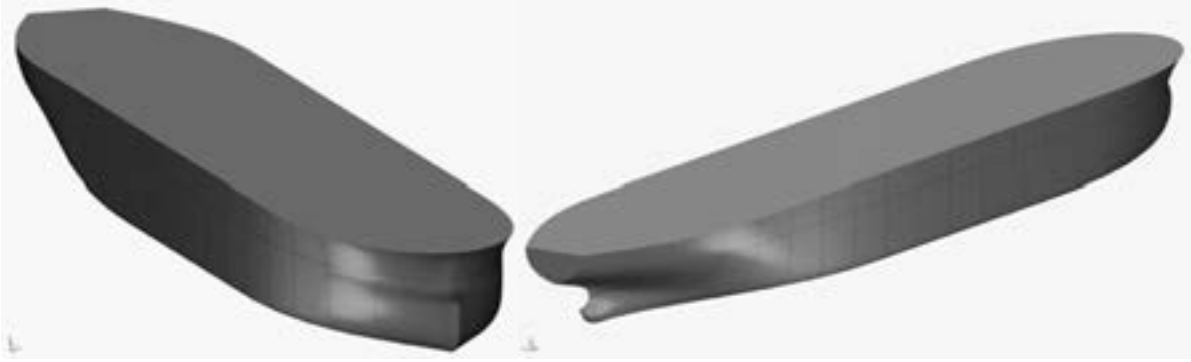

Fig.10: Hull form of favored design

Parameter	Reference design	Favored design
Length over all	250 m	250 m
Beam	44 m	44 m
Depth	21.0 m	21.5 m
Design draft	13.7 m	13.7 m
Block coefficient	0.83	0.85
Inner bottom height COT 2-6 (S+P)	2.50 m	2.10 m
Inner bottom height COT 1 (S+P)	2.50 m	2.75 m
Side shell width	2.50 m	2.65 m
Angle of hopper plate	50°	37°
Width of hopper plate	5.25 m	5.20 m
Frame spacing	3.780 m	4.400 m
Shift of bulkheads	0 m	0 m
DWT	111 436 t	114 923 t
Maximum cargo volume	124 230 m^3	129 644 m^3
OOI	0.0138	0.0142
Speed at design draft	15.1 kn	15.6 kn
Speed at ballast draft	15.9 kn	16.8 kn
EEDI	3.541 g CO_2 / (t nm)	3.281 g CO_2 / (t nm)

Table IV: Main particulars of reference and favored design

5.3 Sensitivities

In order to understand the robustness of the established design with regard to small modifications a separate DoE was performed. About 150 additional variants were generated whose free variables changed within ±1% of the corresponding parameters of the favored design. Fig.11 presents a selection of sensitivities, with changes in RFR displayed in the upper row and changes in OOI and EEDI in the middle and lower row, respectively. The favored design can be regarded as a (local) optimum for RFR while in its vicinity only few variants perform slightly better with regard to OOI and EEDI. In general, the sensitivity is quite small. This indicates that the favored design does not represent an extreme breed for just one purpose.

5.4 RFR-OOI study

The relationship between RFR and OOI was further investigated, again utilizing the integrated CAE approach. The tank geometry was systematically varied within the bounds summarized in Table V while freezing all other variables at the values of the best RFR design. Fig.12 opens a view on the compromise between economy (ordinate) and safety (abscissa). The smaller the accidental oil outflow the higher the cost of transport. This is not unexpected but the diagram quantifies how much an operator needs to pay for a safety margin beyond the regulatory limit set by MARPOL. Relaxing the normalized RFR from 0.961 to 0.966, i.e. taking just 3.4% gains instead of 3.9% in comparison to the reference tanker, leads to a further reduction of OOI from 0.015 to 0.012. In Fig.12 the design called best RFR is highlighted. It is evident that this design is a good solution for both economic performance and environmental safety. Fig.13 offers a synthesized impression of the resulting ship.

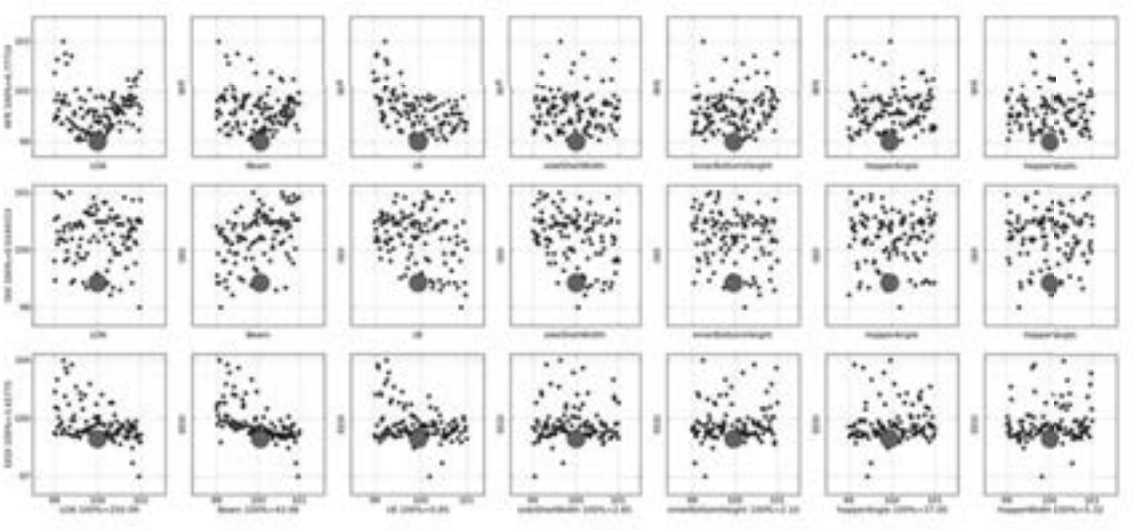

Fig.11: Sensitivity of best RFR design (marked by red bullets, band width of abscissas ±1%)

Free variable	Lower bound	Upper bound	Primary influence
Inner bottom height of cargo oil tanks 2 to 6 (S+P)	2.1 m	3.0 m	Tank geometry
Lifting of inner bottom of cargo oil tank 1 (S+P)	0.2 m	2.0 m	Tank geometry
Side shell width	2.1 m	3.0 m	Tank geometry
Angle of hopper plate	30°	60°	Tank geometry
Width of hopper plate	4.0 m	6.0 m	Tank geometry

Table V: Free variables and their bounds for RFR-OOI study

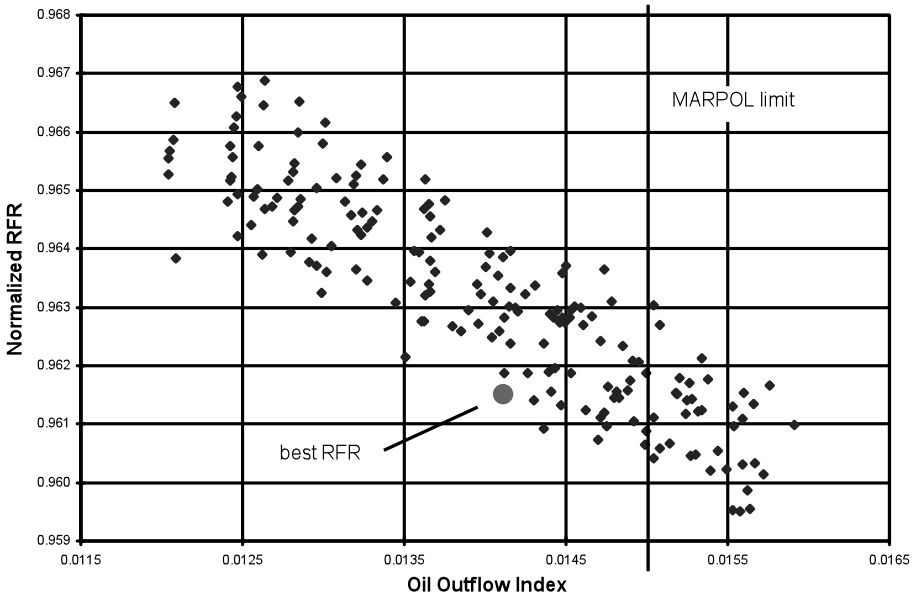

Fig.12: Economics vs. safety in Aframax tanker design

Fig.13: Resulting design including the wave field and pressure distribution from CFD
(side shell and deck removed to show tanks and inner structure)

6. CONCLUSIONS

An integrated approach was developed that simultaneously covered all relevant aspects of early ship design: main dimensions, hull form, hydrodynamics and powering; structures, strength and weight estimates; safety including intact and damage stability; economics; and regulatory requirements. An example application was presented for an Aframax tanker with the aim of realizing better safety (lower OOI), efficiency (lower EEDI) and economics (lower RFR). Formal explorations and exploitations were combined to investigate the design space and, subsequently, advance competing design proposals into certain directions. About 2500 variants were realized, each instance having its individual hull form (outer shell), tank compartmentation and an inner steel structural system.

The integrated system brings together sophisticated software systems for analysis and simulation. Challenging issues, like CFD simulations, can be replaced by systematic numerical series and suitable meta-models (RSM). This not only speeds up the time needed for investigations by several orders of magnitude but it also reduces the complexity associated with CFD analyses and, hence, allows to already utilize them early in the process when gains are potentially the highest.

The presented example showed that once a (quasi-randomly created) database of variants is available it is quick and easy to search for the preferred combination of measures of merit. One may then choose a more conservative design, being a balanced all-rounder, or deliberately decide to favor a more extreme solution, featuring excellent performance in one measure of merit. Additional investigations can be done easily once the CAE environment is established, for instance to gain an appreciation of the relationship between costs and safety or to check the robustness of the favored design.

Setting up an integrated approach still requires quite some effort at this point in time. Nevertheless, the necessary software is available and the presented project proved feasibility. Major prerequisites are parametric models which allow automation. Significant design improvement can then be realized even for moderate deviations from established design practice.

ACKNOWLEDGEMENT

The authors would like to warmly thank their colleagues directly involved in the project, most importantly Evangelos Boulougouris, Mattia Brenner, Kevin Coyne, Michael Haasis, Peter Horn, Apostolos Papanikolaou, Henner Eisen and Pierre Sames.

REFERENCES

1. Abt, C.; Harries, S. (2007), *Hull variation and improvement using the generalised Lackenby method of the FRIENDSHIP-FRAMEWORK*, The Naval Architect, September
2. ABT, C.; HARRIES, S.; WUNDERLICH, S.; ZEITZ, B. (2009), *Flexible tool integration for simulation-driven design using XML, generic and COM interfaces*, 8th COMPIT, Budapest
3. ABT, C.; HARRIES, S. (2007), *A new approach to integration of CAD and CFD for naval architects*, 6th COMPIT, Cortona
4. BRENNER, M.; ABT, C.; Harries, S. (2009), *Feature modelling and simulation-driven design for faster processes and greener products*, ICCAS, Shanghai
5. FAHRBACH, M. (2004), *Bewertung der Güte von Nachstromfeldern*, Diploma Thesis (in German), TU Hamburg-Harburg
6. HARRIES, S. (2010), *Investigating Multi-dimensional Design Spaces Using First Principle Methods*, 7th Int. Conf. High-Performance Marine Vehicles (HIPER), Melbourne
7. HARRIES, S.; ABT, C.; HEIMANN, J.; HOCHKIRCH, K. (2006), *advanced hydrodynamic design of container carriers for improved transport efficiency*, RINA Conf. Design & Operation of Container Ships, London
8. MEPC (2003), Resolution MEPC.110(49) - *Revised Interim Guidelines for the Approval of Alternative Methods of Design and Construction of Oil Tankers Under Regulation 13F(5) of Annex I of MARPOL 73/78*, MEPC, International Maritime Organization, London
9. MEPC (2004), *Resolution MEPC.122(52) - Explanatory Notes on Matters Related to the Accidental Oil Outflow Performance Under Regulation 23 of the Revised MARPOL Annex I*, MEPC International Maritime Organization, London
10. MEPC (2008), *MEPC 58/17/2- Formal Safety Assessment – Crude Oil Tanker*, International Maritime Organization, London
11. MEPC (2009), *MEPC.1/Circ.681 - Interim Guidelines on the Method of Calculation of the Energy Efficiency Design Index for New Ships*, MEPC, International Maritime Organization, London
12. Papanikolaou, A.; Zaraphonitis, G.; Boulougouris, E.; Langbecker, U.; Matho, S.; Sames, P. (2010), *Optimization of an AFRAMAX oil tanker design*, J. Marine Science and Technology
13. TILLIG, F. (2010), *Parametric Modeling and Hydrodynamic Analysis of Twin-Skeg Vessels*, Diploma thesis, TU Berlin

Stefan Harries
FRIENDSHIP SYSTEMS
Potsdam/Germany
harries@friendship-systems.com

Fabian Tillig
FRIENDSHIP SYSTEMS
Potsdam/Germany
tillig@friendship-systems.com

Marc Wilken
Germanischer Lloyd
Hamburg/Germany
marc.wilken@gl-group.com

George Zaraphonitis
National Tech. Univ. of Athens
Athens/Greece
zar@deslab.ntua.gr

WANG Shengyin
PhD, M. Eng, B. Eng

Matthew QUAH Chin Kau
PhD, CEng, CMarEng, FIMarEST

CFD Simulation of Water Oscillations in the Moonpool of a Drillship

ABSTRACT

In this work, the advanced Computational Fluid Dynamics (CFD) simulation approach, together with High Performance Computing (HPC) techniques, was applied to simulate water oscillations in the moonpool of a drillship. The effect of water oscillations on resistance and propulsion performance of the drillship were investigated in detail. The added resistance due to a moonpool may reduce the drillship forward speed in transit significantly. This resistance can be reduced effectively by adopting an appropriate moonpool design to suppress water oscillations. The CFD simulation results correlate well with the MARIN model test data. It is suggested that the CFD simulation approach be used as a reliable conceptual design tool to obtain more efficient moonpool configurations so as to suppress moonpool water oscillations and reduce the added resistance of a moonpool.

ACKNOWLEDGEMENT

This work was partially supported by Deepwater Technology Group (DTG), Keppel FELS Pte Ltd. We are grateful to Edwin Nah Hock Choon of DTG for sharing his insights and expertise in deepwater technologies. We would also like to express our sincere gratitude to CFD expert, Peter Ewing, director of CD-adapco Australia, for his technical support and guidance.

INTRODUCTION

A drillship is a marine vessel fitted with drilling apparatus and designed to carry drilling platforms out to deep-sea locations worldwide. According to the ABS guide for building and classing drillships [1], a drillship belongs to a ship type and is a displacement hull offshore drilling unit. It can be regarded as an adaptation of a standard seagoing ship of mono-hull form, with an additional substructure for a distinctive moonpool from which the drilling operations may be carried out. A drilling moonpool is used to pass drilling equipment into the water from the drilling platform located on the deck of the drillship. In the early 1970s, a drillship was equipped with two moonpools [2]. In a current drillship, the relatively small Remotely Operated Vehicle (ROV) moonpool was abandoned and only the rectangular-shaped moonpool is left to lengthen and allow dual operation in one single moonpool [2].

A drillship's transition speed is important since the transition between different oil fields worldwide may take considerable time. It is much more desirable to reduce the resistance of a drillship in transit to increase its forward speed or to reduce its energy consumption [2-4]. However, the moonpool may cause a drastic increase in water resistance due to the moonpool water oscillation [5]. The phenomenon of moonpool water oscillation is quite complicated due to the strong coupling between vessel and moonpool motions [5]. Both vertical oscillation (or piston motion) and horizontal oscillation (or sloshing motion) of the water in a moonpool

may be involved, and the coupling between the heave and surge motions of the drillship and the moonpool water oscillations may yield a large-resistance increase. The challenging issues of how to accurately predict the added resistance of a moonpool and how to effectively reduce the added resistance have aroused the interest of many researchers, as discussed in the following literature review.

LITERATURE REVIEW

The problem of water oscillations in a moonpool when the ship is in forward motion in calm water is illustrated in Figure 1. The excitation mechanism of water oscillations in the moonpool under calm water conditions in transit is due to vortex shedding formed by flow separation at the leading bottom edge of the moonpool [5]. Vortex shedding introduces instabilities in the flow and initiates a transfer of energy from the flow to the disturbance, giving rise to flow fluctuations and added resistance. The vortex arising from the leading edge of the moonpool due to the abrupt velocity discontinuity would then contact with the trailing edge of the moonpool opening. The induced pressure fluctuation would spread over the surrounding flow field, leading to a dominant frequency with large energy, which is called the phase locking phenomenon [5]. Energy concentration may be found in the combination of phase locking, with the hysteresis effects associated with peaks in energy concentration at certain frequencies. The water oscillations may not only have a great impact on the moonpool structure but may also affect the vessel's motion. Due to the strong coupling effect between the vessel's motion and the water oscillations in a moonpool, large vessel motions as well as the large added resistance of a moonpool may be generated. It should be noted that water oscillations in a moonpool might also occur in waves under stationary conditions, which is outside the scope of the present study.

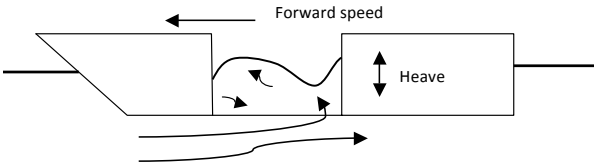

Figure 1. Water oscillations in a moonpool with a forward speed of the ship

In the literature [2-16], there are empirical, experimental and numerical methods used to predict the added resistance due to water oscillations in a moonpool when a ship is in forward motion in calm water. Furthermore, employing damping devices to reduce the excitation and decrease the motions has become the main method employed to lower added resistance [5]. The relevant study of liquid motion in an accelerating container has a long research history, as shown in the comprehensive literature review in [6].

Empirically based methods were popular in past ship design practice, in which the resistance curve prediction relied mainly on model tests in combination with experiences based on previous designs [2]. Accurate prediction of the added resistance of a moonpool in calm water was usually difficult due to the possible large variations in hull and moonpool designs and the limited availability of test data.

Experimental approaches in model tests have been widely accepted for the study of added resistance of a moonpool in a modern drillship [2,3,8] because of the past success of this method to predict the ship's hydrodynamic performance [7]. The model testing approach uses a scale model to experiment and extract the information, which can be scaled to the full-scale ship. However, a certain degree of empiricism is still necessary to enhance the prediction accuracy of the resistance of a full-scale ship. Moreover, the experimental approaches may be costly and time consuming with a limited number of data points and poor repeatability. To alleviate these drawbacks, it is not unusual for the organisation that operates a ship model basin to use the CFD software to numerically simulate the complicated flow around ships, though the CFD

calculations are not allowed to replace the model tests entirely.

Numerical prediction of the phenomenon of water oscillations in a moonpool excited by the forward motion of the ship is usually based on the potential flow theory [9-16]. Linear potential flow theory-based solutions are still popular because of their simplicity, ease of use and robustness. Further improvement may be needed since the hydrodynamic problem of moonpool water oscillations is quite non-linear in character. The 3D fully non-linear potential theory may represent a significant improvement over the linear theory. The non-linear effects in the free surface waves may limit the resonant response, which would be seriously over-predicted by the linear potential flow theory due to the relatively small linear potential flow damping [14]. However, the potential flow theory is not sufficient to address the complicated phenomenon of water oscillations in a moonpool because it cannot deal with the significant non-linear effects of flow separation and vortex shedding, which would play a significant role in the excitation mechanism [5] of water oscillations.

The use of complete CFD solutions has begun to emerge [17]. The fully non-linear CFD simulations have the potential to capture accurately the highly non-linear phenomenon of water oscillations in a moonpool. Furthermore, the CFD simulation approach may become less time consuming by applying HPC techniques [18] to distribute the parallel processes across multiple CPUs, and to speed up the iterative CFD computation. Hence, the CFD simulation approach has the potential to outperform the aforementioned experimental, empirical, or other numerical methods. However, only limited use of complete CFD solutions has been reported in the literature due to some technical barriers in the CFD software tools, lack of necessary high performance computing hardware and/or sound CFD experience. In Ref. [5], the first results obtained with CFD software ComFLOW were presented to reproduce model tests and moonpool behaviour observed during sea trials. The results showed a relatively good reproduction of flow separation. It appears that the CFD methods are able to model correctly the global physics underlying the moonpool behaviour [5]. However, some further developments should be made to include the coupling analysis of the drillship and moonpool motions. In Ref. [4], Son et al. used the CFD code FLUENT to investigate the water oscillations phenomenon inside a recess type moonpool. It was shown that a recess type moonpool might offer some improvements in water oscillations compared with a rectangular moonpool. Nevertheless, the complicated 3D effects on the moonpool behaviour were omitted [4]. In Ref. [14], Alsgaard used the open source code OpenFOAM to study the piston mode resonance phenomenon in a moonpool. The work showed some good quantitative agreements in the resonance frequency. However, some accuracy problems may exist due to the simplified 2D numerical simulations.

In the literature [2,5,19], many devices have been reported to suppress the moonpool water oscillations and reduce the added resistance of a moonpool with the forward motion of a ship. Generally, these devices can reduce either the cause of vortex creation or the consequence of large water oscillations [2,5]. Wedges are the classical solution to avoid excitation of water oscillations in the moonpool of a drillship in transit [5] without obstructing the moonpool opening. In Ref. [2], both wedges and cut-outs were proposed as the resistance mitigation devices. In Ref. [3], four moonpool configurations with wedges and cut-outs were tested. It was shown that the configuration with a triangular wedge at the leading edge and a cut-out at the trailing edge might significantly decrease the added resistance. Nevertheless, to date there is little known about designing the most efficient wedge and cut-out [2]. Other devices to reduce the cause of vortex creation include a grid of flaps, a large single flap mounted on a hinge, a vertical bulkhead and convergent openings [5]. Furthermore, viscous damping devices to reduce water oscillations have also been developed, including flanges, horizontal damping plates, floating lids or mats, baffles and damping chambers. However, most of the proposed devices may be difficult to manufacture and the devices with

moving parts may cause operational problems. In this study, only the relatively simple cut-out at the trailing edge of a moonpool was used to mitigate the moonpool water oscillations.

The objectives of this work are to apply state-of-the-art CFD methods and HPC techniques to predict the added resistance of a moonpool accurately and efficiently in order to investigate the effect of a cut-out at the trailing edge of the moonpool, and to provide reliable insight into the complicated phenomenon of water oscillations in the moonpool of a drillship to facilitate efficient moonpool design.

SIMULATION METHODS

The CFD Simulation Approach

The added resistance due to a moonpool is usually deduced from the total resistance of the ship with and without the moonpool, as done in the experimental approach in model tests [2]. In this study, the general-purpose CFD software tool STAR-CCM+ [18] was utilised to apply the CFD simulation approach. This CFD software tool includes modern software development technology, state-of-the-art computational continuum mechanics algorithms and excellent user-environment design. Furthermore, it maintains a four-month release cycle [18] to ensure that its users are constantly updated with the latest advances.

In the CFD simulation, a 3D computational domain surrounding the ship was pre-defined. To generate a high-quality volume mesh for the computational domain with an appropriate boundary layer resolution, STAR-CCM+'s advanced automatic meshing technology [18] was adopted and the trimmer meshing model, together with a prism layer mesher, was used. A dissipation zone with an extra active damping effect was defined to fulfil a wave reflection damping filter in the CFD solver of STAR-CCM+ [18], similar to, but more robust than, the filter scheme approach to achieving non-reflecting boundary conditions in [20]. The two-phase air and water flow in the computational domain was modelled by the Volume Of Fluid (VOF) method, which was first developed by Hirt and Nichols [21]. The Dynamic Fluid Body Interaction (DBFI) between the two-phase flow and the ship was tackled by STAR-CCM+'s DFBI module [18], and the induced rigid body motions of the ship may be efficiently simulated by its 6-DOF solver. The Reynolds-averaged Navier-Stokes (RANS) equations [18] were adopted to investigate the complicated flow dynamical behaviour around the ship. The implicit unsteady solver of STAR-CCM+ [18] was used to solve the RANS equations in a segregated manner. Furthermore, Menter's Shear Stress Transport (SST) K-Omega turbulence model [22] was adopted to capture the turbulent wake effects.

HPC Techniques

Due to the intensive computational work required to achieve a converged CFD solution, state-of-the-art HPC techniques were adopted to fulfil the parallel CFD computation to speed up the CFD computation. In this work, HPC techniques were implemented by the operating system Microsoft HPC Server 2008, together with the CFD software tool STAR-CCM+ [18].

The parallel computing operating system Microsoft HPC Server 2008 was used to manage a cluster of 64-bit machines comprising two HP Proliant Z6000 servers, with a total of four quad-core processors (16 cores) and 128 GB RAM, on both enterprise and private networks with a bandwidth of one Gigabits per second (Gbps). Under the Windows HPC Server 2008 environment, the Message Passing Interface (MPI)-based domain decomposition technique was used for efficient parallel computation. The CFD jobs were submitted from the CFD software tool STAR-CCM+ to the Windows job scheduler using MS-MPI either in batch mode or interactively [18]. Under the present configuration, the two HPC techniques of multiple cores and multiple machines were combined to execute jobs consisting of individual tasks to achieve an even more powerful HPC performance. It is important to scale the simulation size to be in line with the number of cluster nodes being used [18]. The optimal scaling is determined from a ratio of the time to compute and the time

taken to exchange data between cluster nodes. In this work, the minimum number of mesh cells placed on each cluster node is about 100,000.

RESULTS AND DISCUSSION

The present CFD simulation approach and HPC techniques were applied for the added resistance prediction of an ultra-deepwater drillship after their accuracy and efficiency were validated for a US navy combatant ship model. Further comparisons with the MARIN model test data for the drillship and discussion on efficient moonpool design were also provided.

CFD Validation for Resistance

In this study, the well-accepted surface combatant ship model David Taylor Model Basin (DTMB) 5415 [23,24] was chosen for the present CFD validation analysis. The ship model DTMB 5415 is a towing tank model representing a modern US naval combatant. The model geometry, which includes both a bulbous bow and a transom stern, as shown in Figure 2, has been adopted by International Towing Tank Conference (ITTC) as a recommended benchmark for CFD validation in resistance and propulsion [23].

Figure 2. Hull geometry of the ship model DTMB 5415

The principal particulars of this model are shown in Table 1. In the present CFD validation study, only the bare hull model of DTMB 5415, with a scale factor of 1:24.824 and a specified sinkage of -0.01041 m and a trim of -0.108 degree [24], was chosen, as used in the model tests carried out by Olivieri et al. in [25].

Figure 3 displays the computational domain for this problem. Due to the symmetry, only a half domain was used. Figure 4 shows the volume mesh generated by the trimmer meshing model of STAR-CCM+ [18]. Since the trimmed mesh was dominantly composed of hexahedral cells, the total number of unknowns would be reduced. Figure 5 is a local sectional view of the trimmed mesh at the symmetry plane (centreplane or x-z plane [26]). Local mesh refinement was implemented to capture the flow separation around the bare hull. Figure 6 shows the convergence history of the resistance components. The total resistance is dominated by the friction resistance since flow separation for the streamlined hull form can be insignificant. Table 2 shows a comparison of the measured and simulated resistance values. The CFD simulation discrepancy with respect to the measured data is quite small. Hence, the present CFD simulation approach is able to achieve an excellent correlation with the CFD simulation results and the model test data [24,25].

Particular	Full Scale	Model Scale
Length (m)	142	5.72
Breadth (m)	17.973	0.724
Draught (m)	6.15	0.248
Wetted Surface Area (m^2)	2972.6	4.861
Speed (m/s)	9.252	2.097
Reynolds Number	1.40E9	1.26E7
Froude Number	0.248	0.28

Table 1. Principal Particulars of the Ship Model DTMB 5415

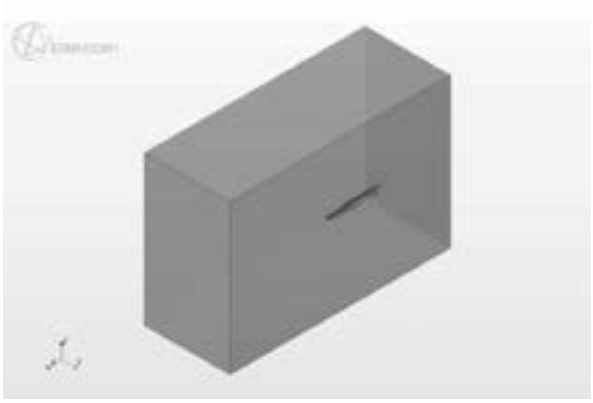

Figure 3. Computational domain for the ship model DTMB 5415

Figure 4. Volume mesh for the CFD simulation

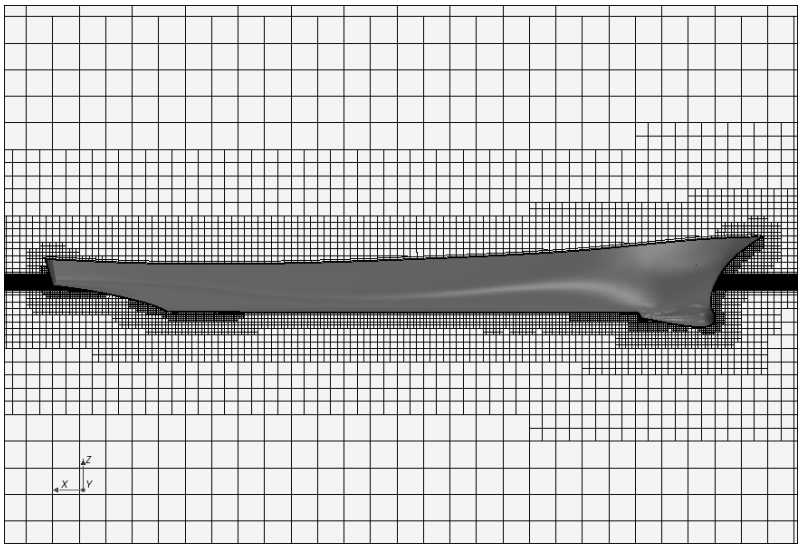

Figure 5. Local sectional view of the volume mesh around the DTMB 5415 hull

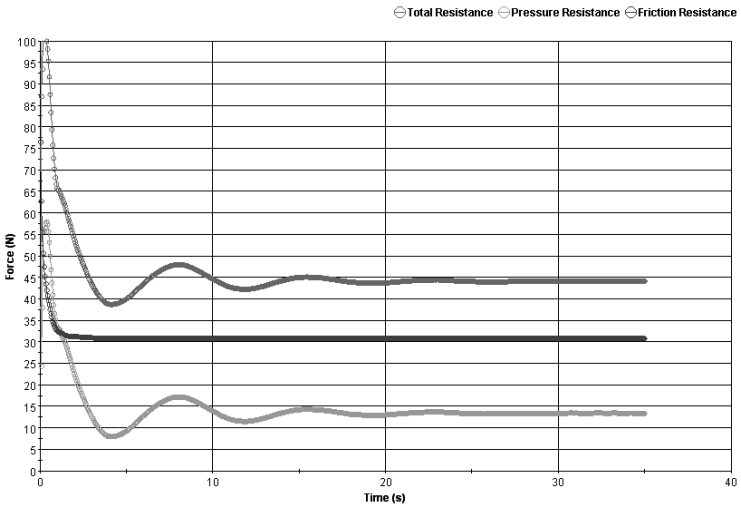

Figure 6. Convergence history of the resistance components of the DTMB 5415 model

Particular	Value
Experimental Result (N)	44.864
CFD Simulation Result (N)	44.106
Error	1.69%

Table 2. Resistance of the Ship Model DTMB 5415

Figures 7, 8 and 9 display a further comparison of the simulated and measured wave elevations at three different wave cuts [24,25]. The present CFD simulation results correlate well with the experimental data in Ref. [25]. Figure 10 shows the wave pattern simulated by the present CFD simulation approach. It is remarkably close to the theoretical Kelvin wave pattern [27] for an ideal ship with a single bow pressure point, which is characterised by a divergent wave system and a transverse wave system. Figure 11 shows a comparison of the simulated and measured wave patterns. The wave pattern simulated by the present CFD approach correlates quite well with the wave pattern measured by Olivieri et al. [25].

As a whole, the CFD simulation approach is able to achieve accurate simulation results for the DTMB 5415 model [25]. It has the potential to replace the actual ship model tests in the future.

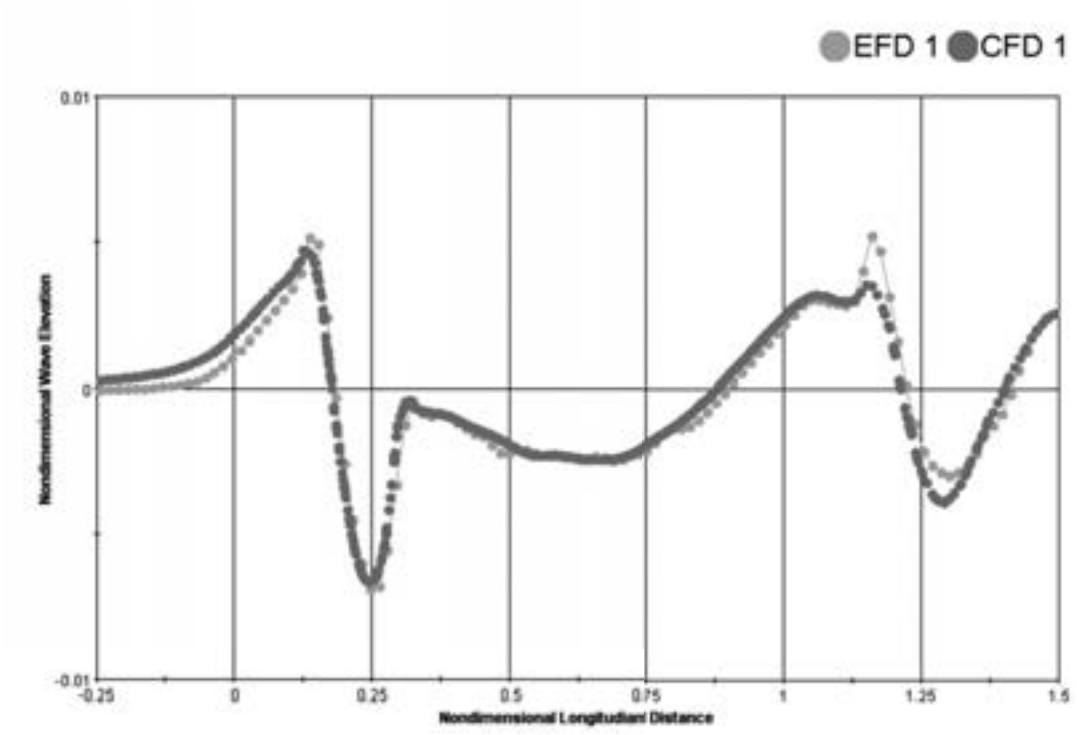

Figure 7. Comparison of the predicted and measured elevations along the cut at $yLpp$=0.0082

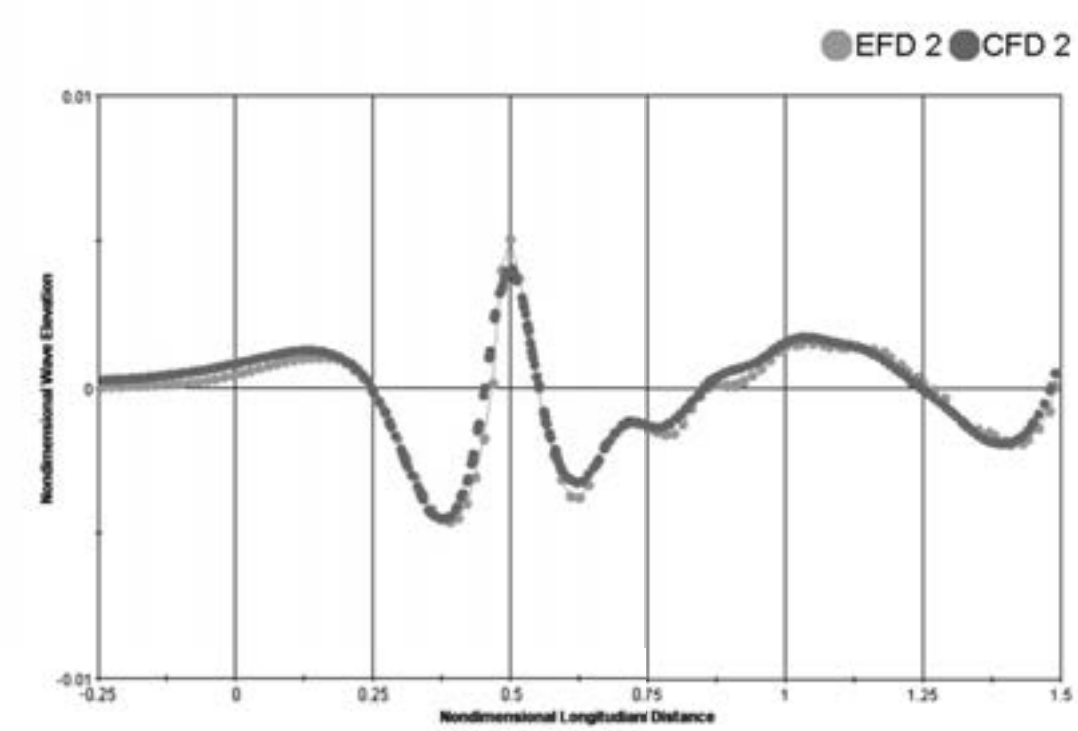

Figure 8. Comparison of the predicted and measured elevations along the cut at $yLpp$=0.172

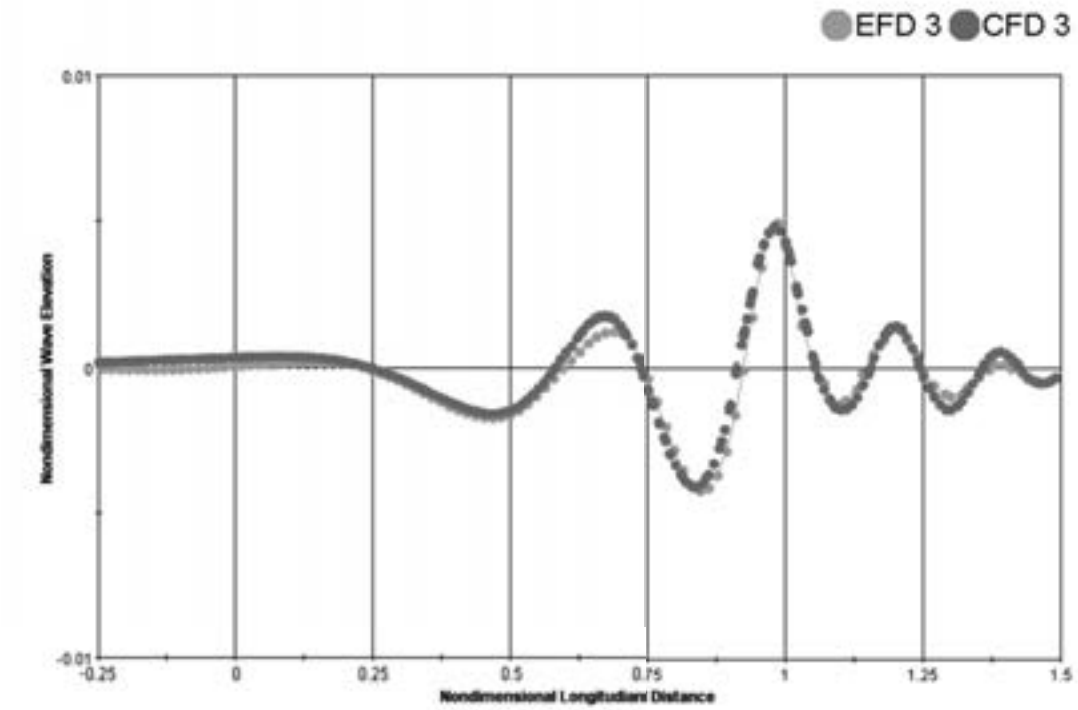

Figure 9. Comparison of the predicted and measured elevations along the cut at $yLpp$=0.301

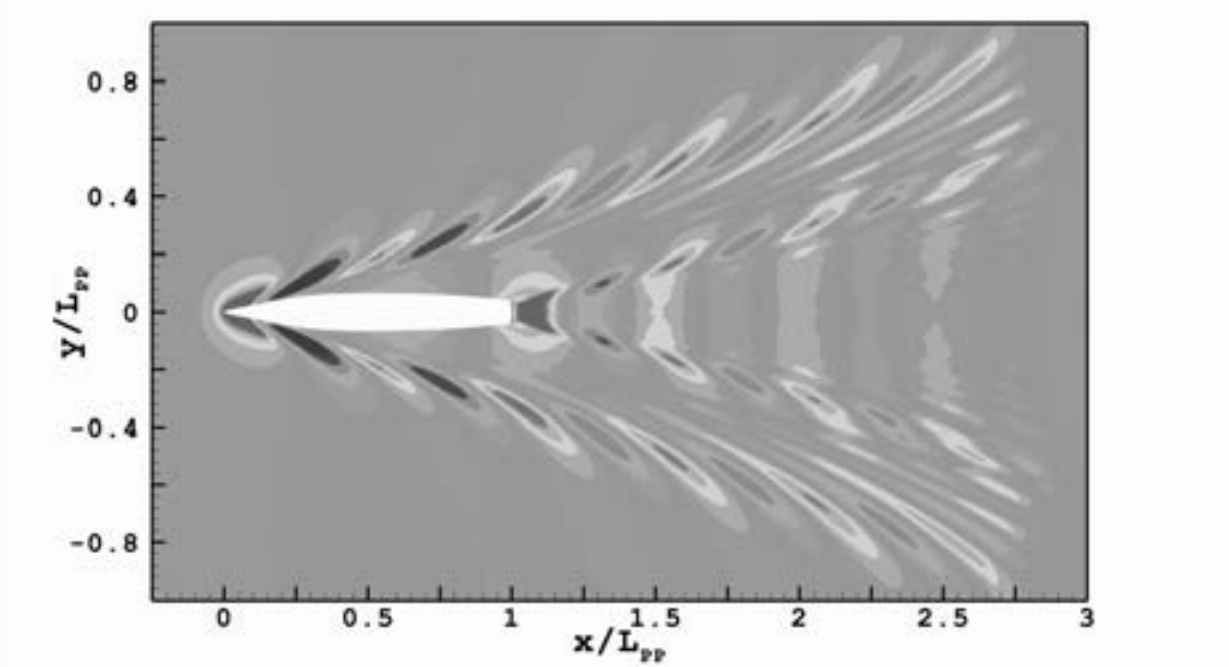

Figure 10. Predicted wave pattern generated by the ship model DTMB 5415

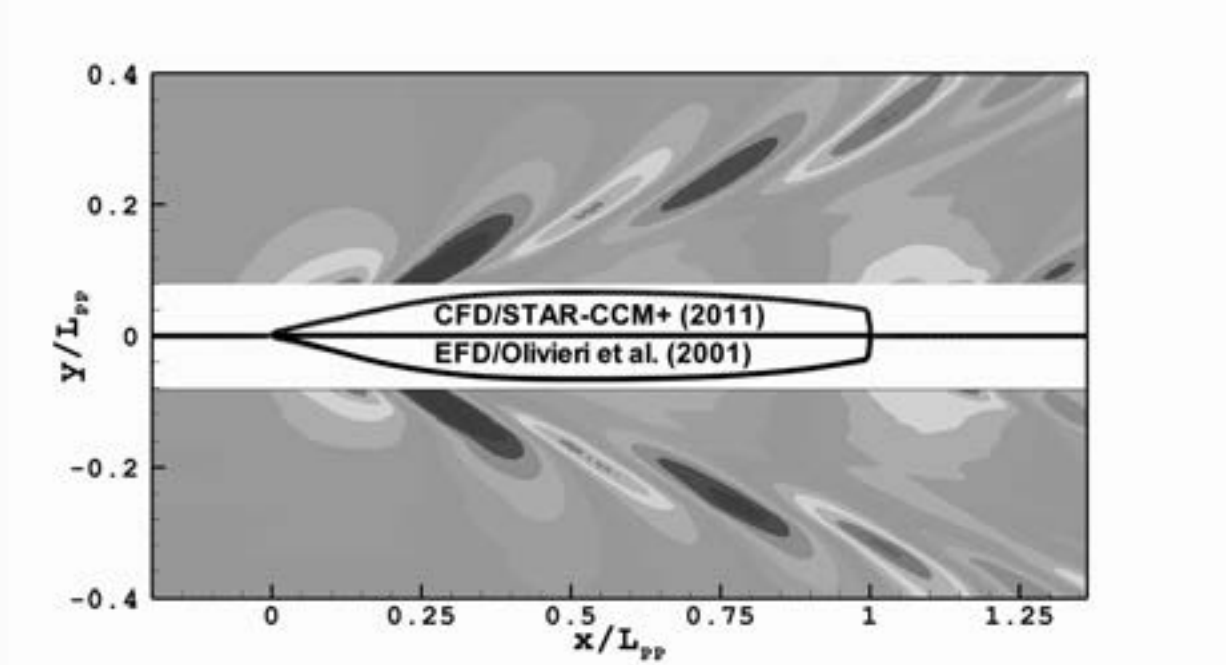

Figure 11. Comparison of the predicted and measured wave patterns generated by the model

CFD Simulations for a Drillship

CFD simulations were further performed for a drillship with different moonpool configurations. The drillship was developed by Keppel FELS Pte Ltd. and the corresponding model tests have been carried out by MARIN, as reported in [28]. The principal particulars of the drillship and the moonpool configurations are shown in Tables 3 and 4. The moonpool configurations of the drillship are shown in Figure 12, in which the drillship without a moonpool is also included as "Moonpool 0" to facilitate the present added resistance computation. The configuration Moonpool 1 is a standard rectangular moonpool. Moonpool 1A is shorter with a larger cut-out angle with respect to the vertical direction while Moonpool 1B is longer with a smaller cut-out angle. A comparison study was carried out to find the best performance of these configurations.

Particular	Value
Length between Perpendiculars (m)	198
Breadth (m)	35
Static Draught (m)	10
Thruster Motor Power (kW)	4500
Number of Thrusters	6

Table 3. Principal Particulars of the Drillship

Moonpool Configuration	Opening Length (m)	Opening Width (m)	Cut-out Angle (deg)
1	25.2	12.6	0
1A	25.2	12.6	30
1B	29.4	12.6	23.96

Table 4. Principal Particulars of the Moonpool Configurations

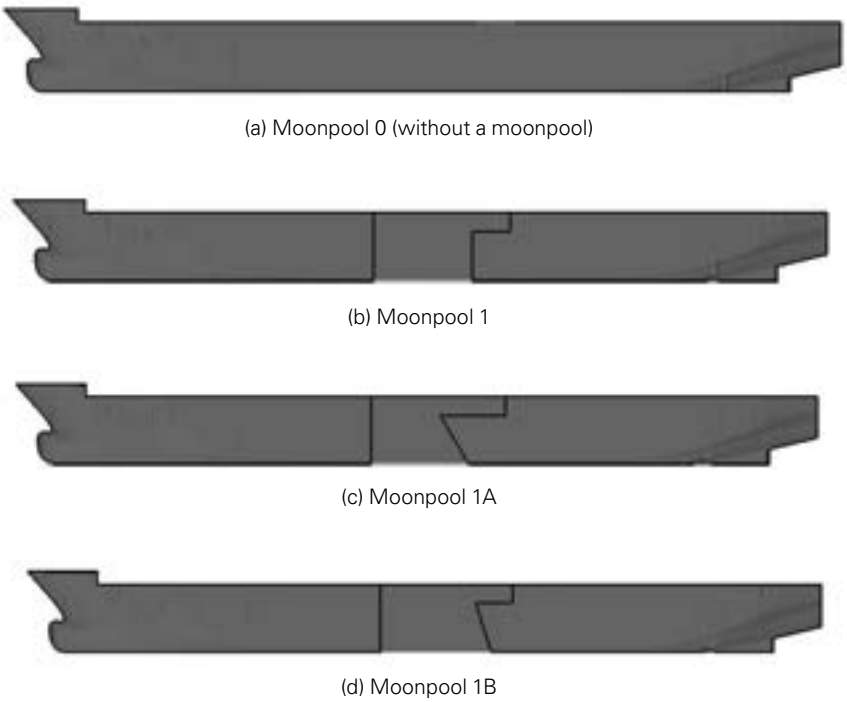

(a) Moonpool 0 (without a moonpool)

(b) Moonpool 1

(c) Moonpool 1A

(d) Moonpool 1B

Figure 12. Moonpool design configurations of the drillship

Figure 13 displays a local sectional view of the volume mesh generated by STAR-CCM+ for each moonpool configuration. Local mesh refinement was produced to capture the free surface and flow separation around the bow, stern and moonpool. Table 5 shows a comparison of the parameters of the drillship deduced from the given static draught (design draught moulded). The length on waterline (*LWL*), the length overall submerged (*LOS*) and volume displacement (∇) deduced by the CFD software correlate well with the data used in the model tests [28]. Since the maximum difference of 1.56% is quite small, it can be regarded that the CFD geometry representation is accurate enough.

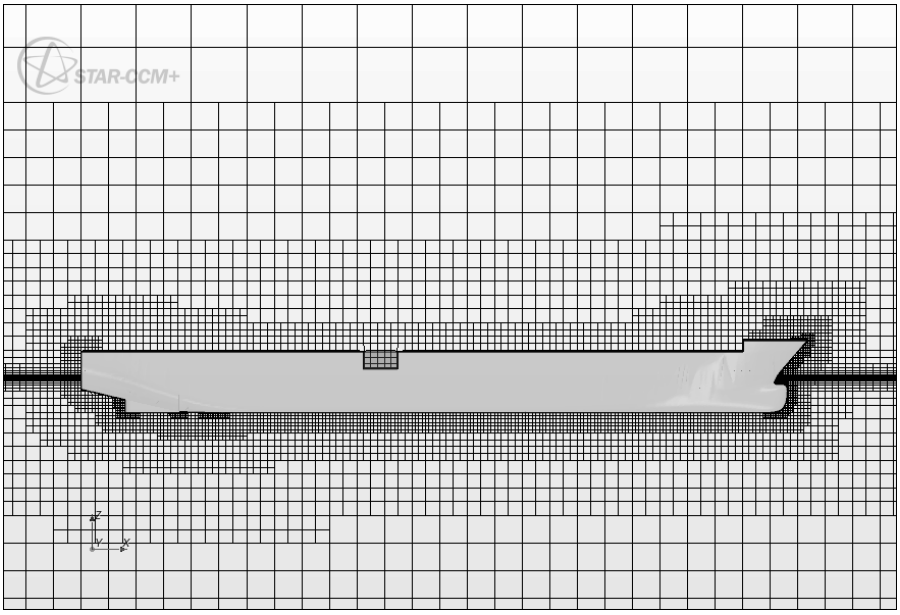

(a) Moonpool 0 (without a moonpool)

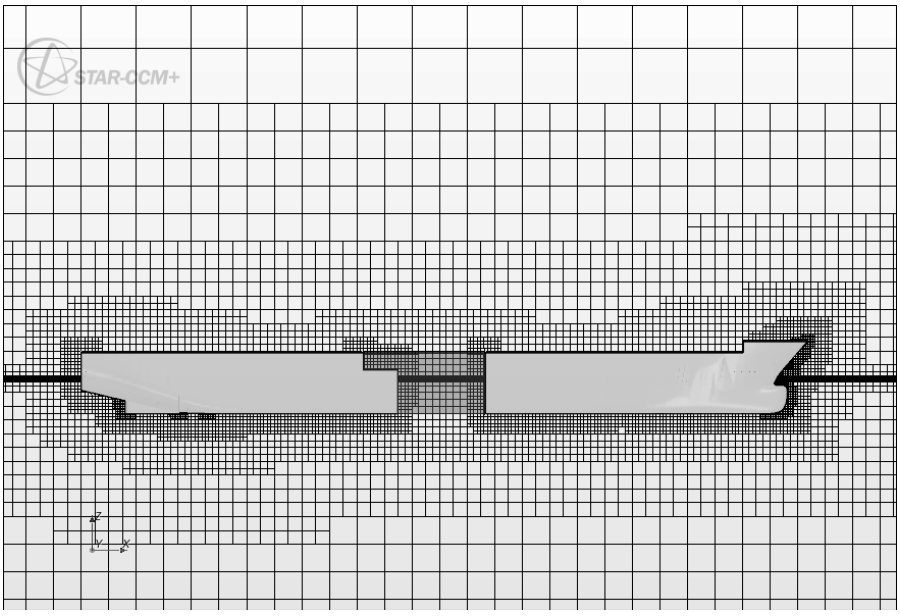

(b) Moonpool 1

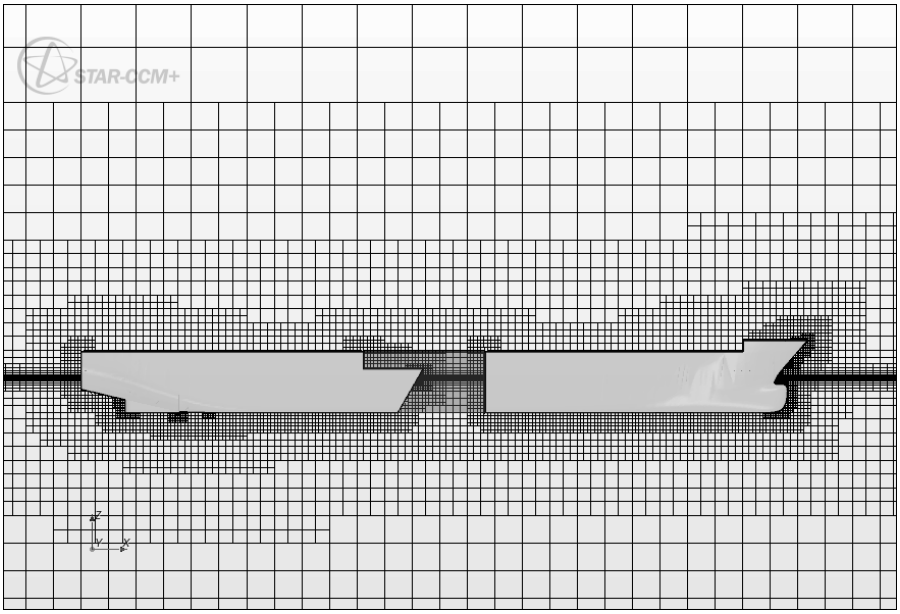

(c) Moonpool 1A

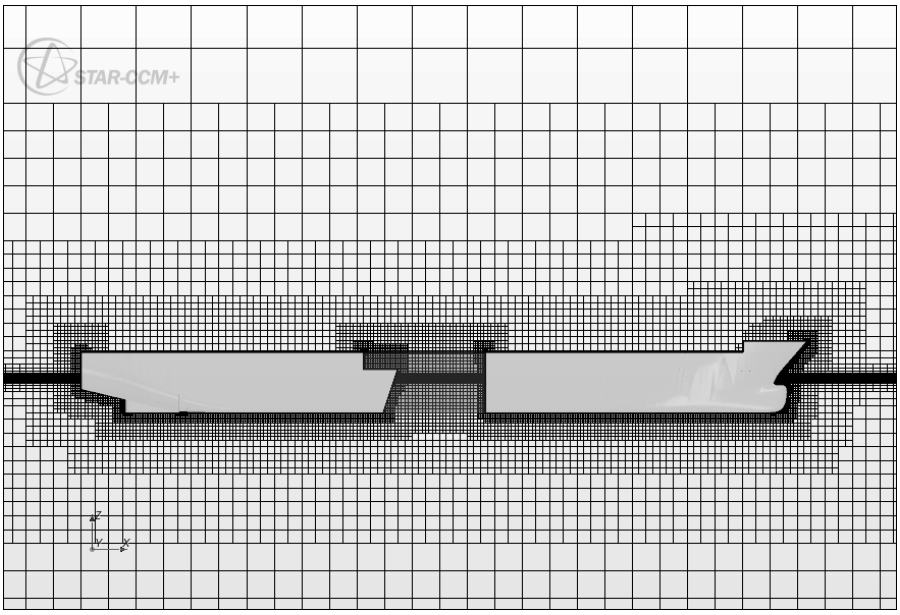

(d) Moonpool 1B

Figure 13. Sectional view of the mesh at the symmetry plane

Moonpool Configuration	Parameter	Experiment	CFD	Difference
1	(m)	200.05	199.79	-0.13%
	(m)	204.22	203.04	-0.58%
	(m^3)	56151.7	57088.0	1.04%
1A	(m)	200.05	199.85	-0.1%
	(m)	204.22	203.04	-0.58%
	(m^3)	56208.5	57088.0	1.56%
1B	(m)	200.05	199.87	-0.09%
	(m)	204.22	203.06	-0.57%
	(m^3)	55945.8	56416.0	0.84%

Table 5. Comparison of the Deduced Parameters of the Drillship

Table 6 shows the calm water resistance of a drillship with a forward speed of 10 knots predicted by the present CFD simulation approach. The percentage increases of the added resistance for moonpool configurations 1, 1A and 1B are 57.17%, 14.34% and 25.93%, respectively. The resistance increases can be consistent with the model test results by Veer and Tholen in Ref. [2], in which the added resistance of moonpools are in the order of 30% at low or moderate speed, and can be as large as 100% at high speed. As reported by MARIN [28], the added resistance of the present moonpool configurations is quite significant. Due to the lack of any resistance mitigation device, the added resistance of the drillship with the rectangular configuration Moonpool 1 is the largest. Configuration Moonpool 1A, with a shorter moonpool and a larger cut-out angle, would increase the resistance much less than configuration 1B with a longer moonpool and a smaller cut-out angle. The reason could be that the shorter moonpool would experience less water sloshing [2] and the larger cut-out angle would lessen the amount of water coming up from the trailing edge of the moonpool opening [5]. Table 7 shows a comparison of the forward speeds predicted by the model tests [28] and the present CFD simulations. It can be seen that the present CFD predictions correlate quite well with the experimental predictions. The largest discrepancy of 8.03% with respect to the experimental predictions for the configuration Moonpool 1 may be related to the less-than-normal measurement accuracy due to the strong sloshing, as reported in [28].

Moonpool Configuration	Total Resistance (kN)	Added Resistance due to a Moonpool (kN)	Percentage Increase
0	509	0	0.0%
1	800	291	57.17%
1A	582	73	14.34%
1B	641	132	25.93%

Table 6. Calm Water Resistance of the Drillship with a Forward Speed of 10 Knots

Moonpool Configuration	Number of Thrusters Used	Model Tests (kn)	CFD Simulations (kn)	Error
1	2	10.96	10.08	-8.03%
1A	2	11.91	11.64	-2.27%
1B	2	11.06	11.44	3.44%
1	6	15.07	14.37	-4.64%
1A	6	16.68	15.90	-4.68%
1B	6	15.26	15.76	3.28%

Table 7. Speed Prediction for the Drillship in Calm Water

Figure 14 displays the convergence history of the resistance components for each moonpool configuration. Due to the moonpool water oscillations excited in calm water by forward ship motion [5], there is a pressure fluctuation surrounding the moonpool. The resulting resistance fluctuation may be enlarged or reduced by the ship's motion because of the coupling effect between the moonpool water oscillations and the ship's motion [5]. As shown in Figure 14, moonpool configuration 1A would experience the least pressure fluctuation, while configuration 1B would cause the most significant pressure fluctuation.

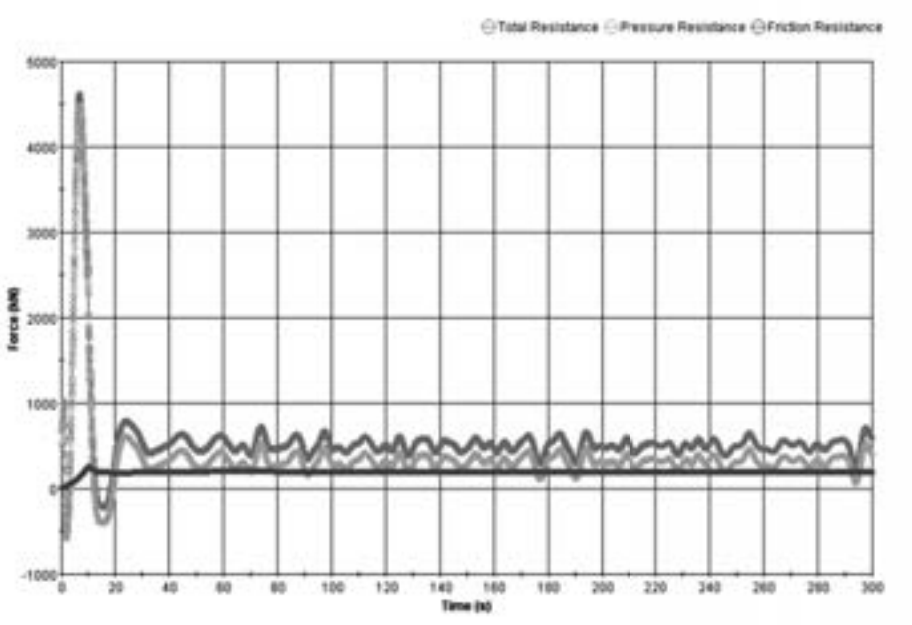

(a) Moonpool 0 (without a moonpool)

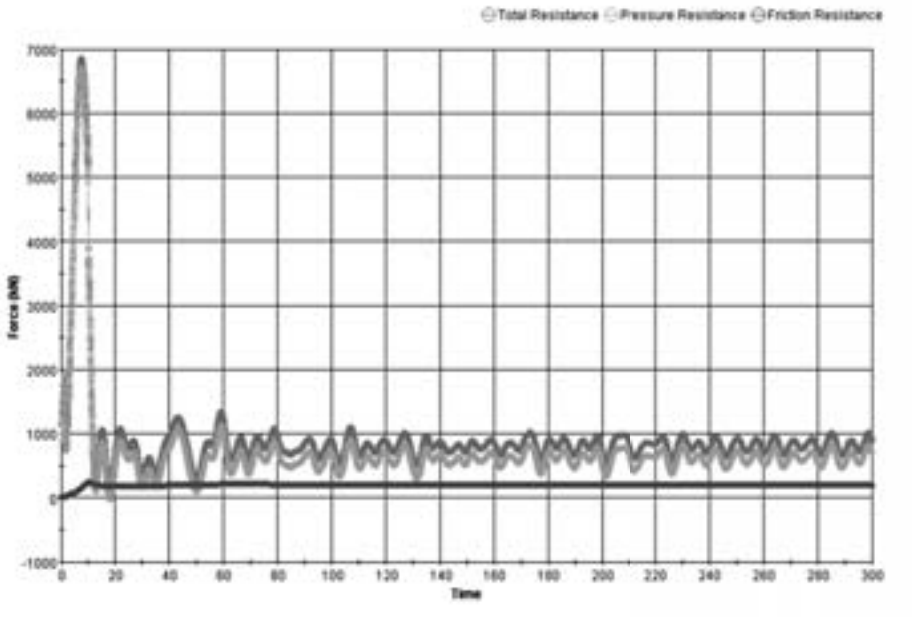

(b) Moonpool 1

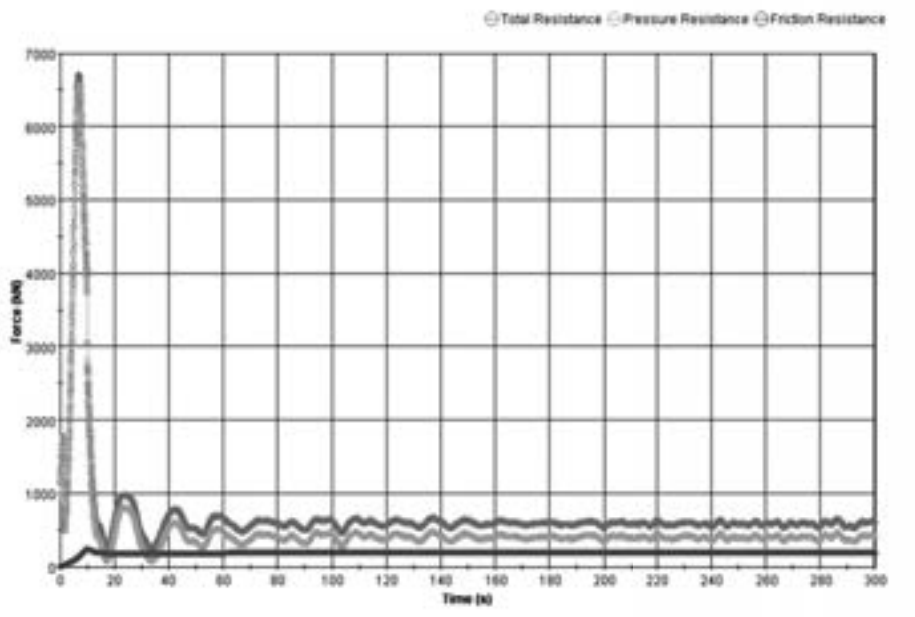

(c) Moonpool 1A

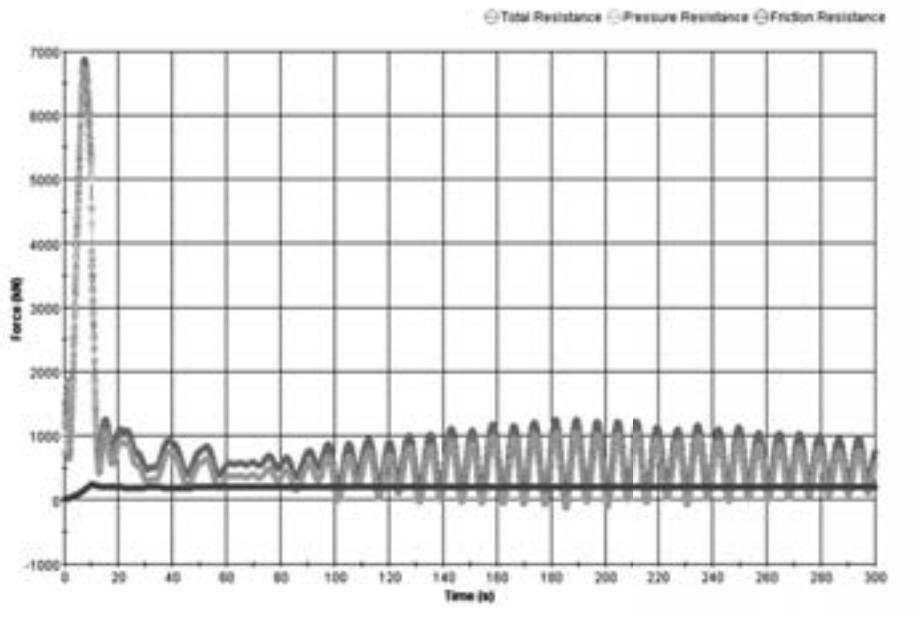

(d) Moonpool 1B

Figure 14. Convergence history of the resistance components

Figure 15 displays the wave patterns around the hull of a drillship in calm water with a forward speed of 10 knots simulated by the present CFD simulation approach. The wave patterns would become quite complicated due to flow separation and vortex shedding, which may destroy the transverse wave system in the wake [24]. The wave pattern for moonpool configuration 1 shows that the rectangular moonpool would greatly increase the height of the excited wave, leading to the larger resistance, as shown in Table 6.

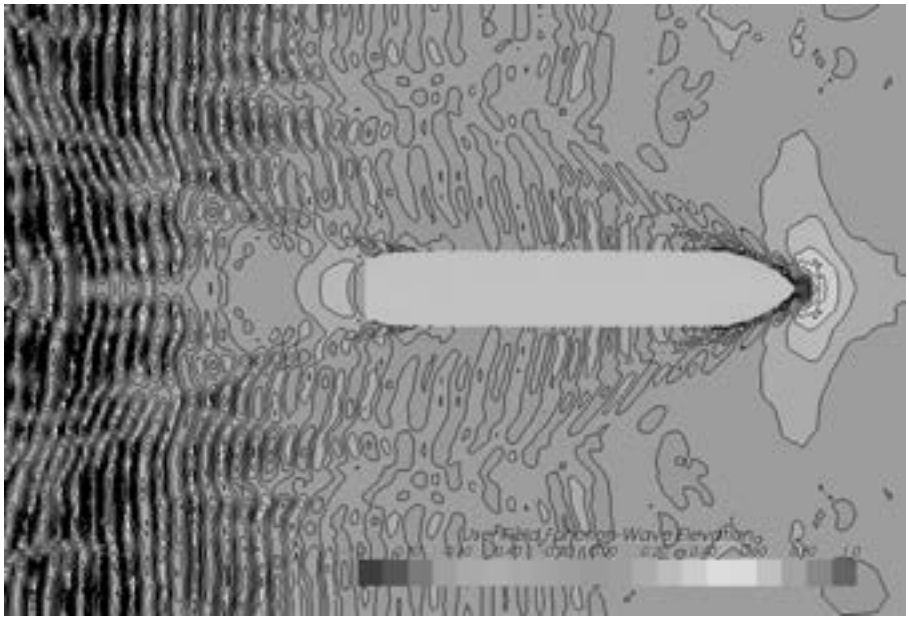

(a) Moonpool 0 (without a moonpool)

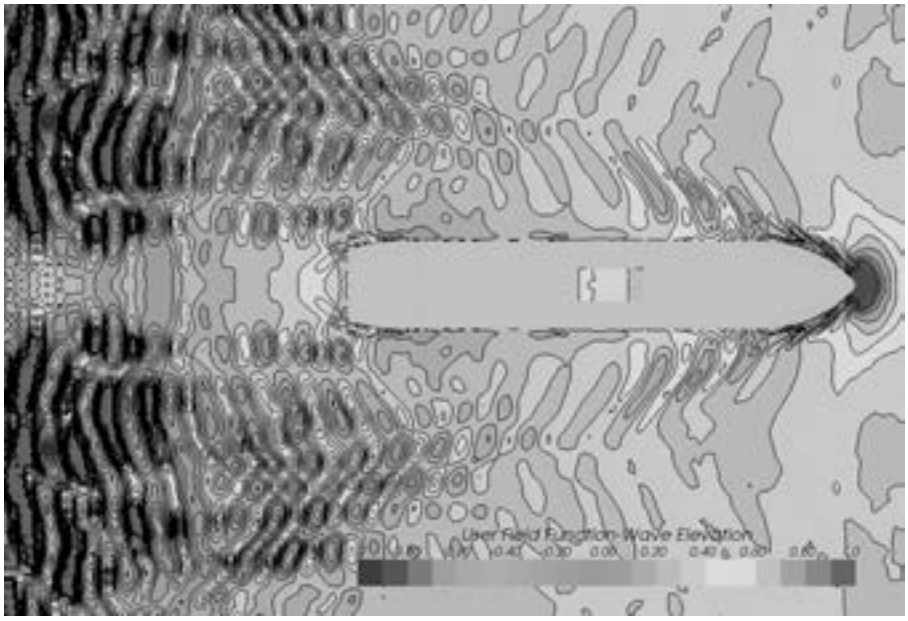

(b) Moonpool 1

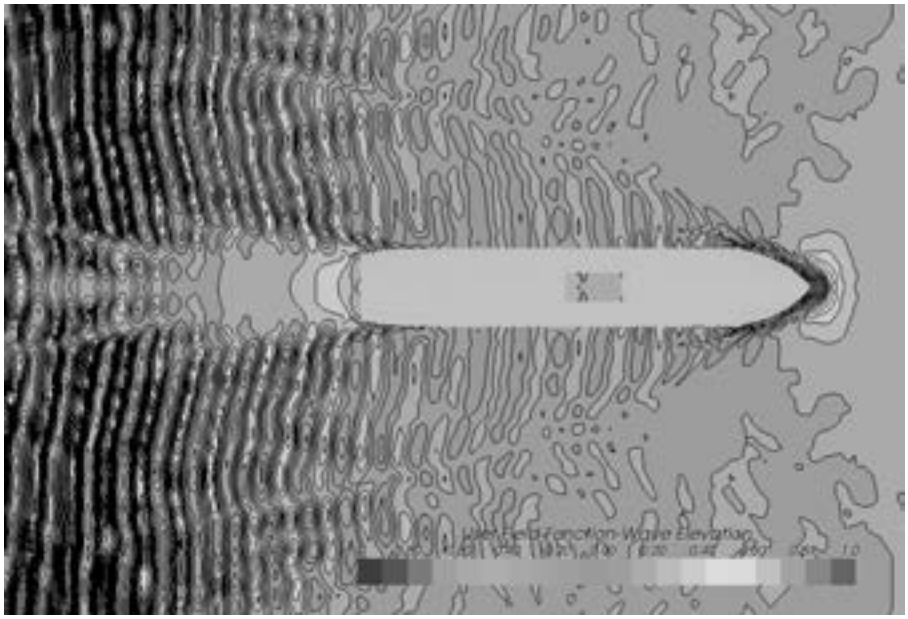

(c) Moonpool 1A

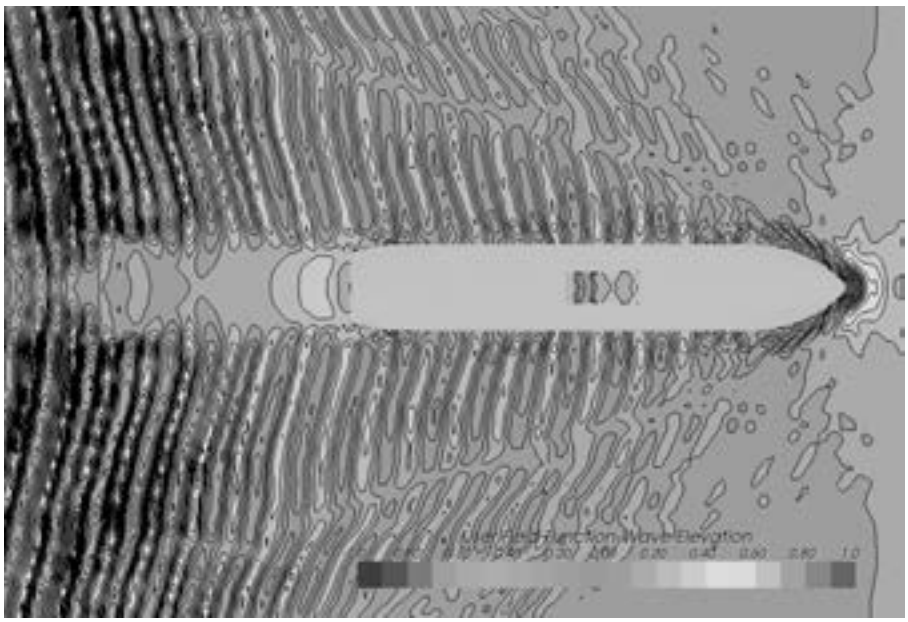

(d) Moonpool 1B

Figure 15. Comparison of the simulated wave patterns

Figure 16 shows a comparison of water oscillations for different moonpool configurations with a forward ship speed of 10 knots. It can be seen that the water oscillations in the moonpools are dominated by the sloshing mode (horizontal oscillation) and that the vertical oscillation is insignificant due to the relatively longer moonpools. According to Table 4, the length/width ratios of the present moonpool configurations are equal to or larger than two. In the drillship model tests in Ref. [2], it was shown that the dominant mode is the sloshing oscillation when the moonpool length/width ratio increases to two. The standard rectangular moonpool configuration Moonpool 1 would generate the largest vortex, the largest upward mass flux at the downstream wall of the moonpool, and the most significant horizontal oscillation inside the moonpool. The resulting added resistance would be the largest, as shown in the simulation results in Table 6. The relatively simple cut-outs at the trailing edge of the moonpool opening would mitigate the water oscillations and the resulting added resistance may thus become smaller. Moonpool configuration 1A is better than 1B in reducing the added resistance since the water horizontal oscillation inside the moonpool would become less energetic and the dominant water-sloshing behaviour would be less significant due to the shorter length of the moonpool opening and the larger cut-out angle.

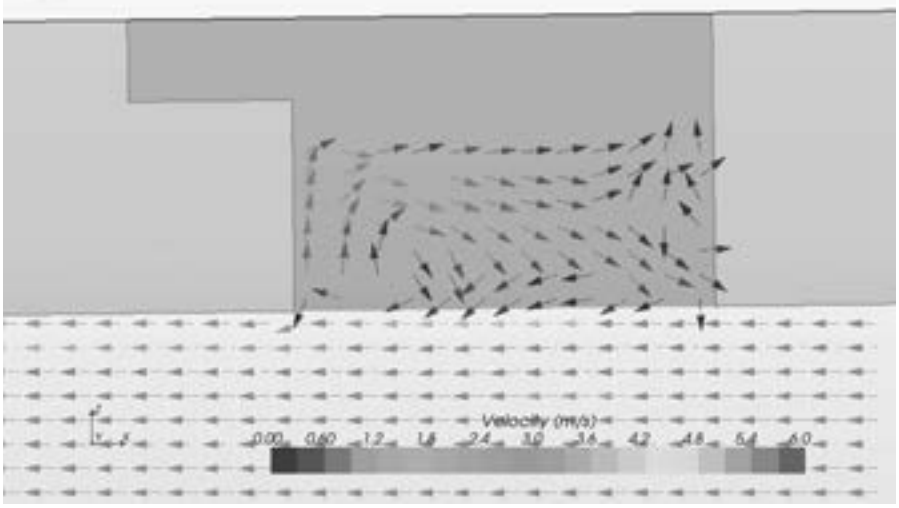

(a) Moonpool 1

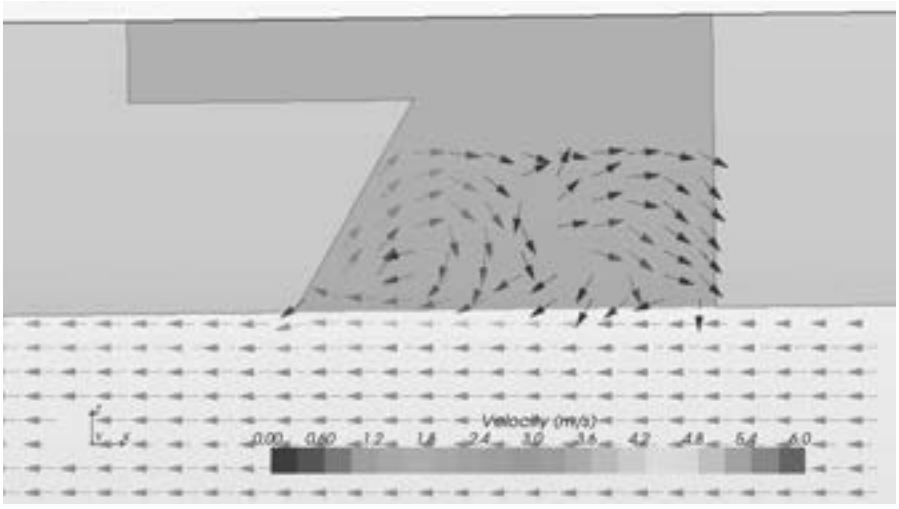

(b) Moonpool 1A

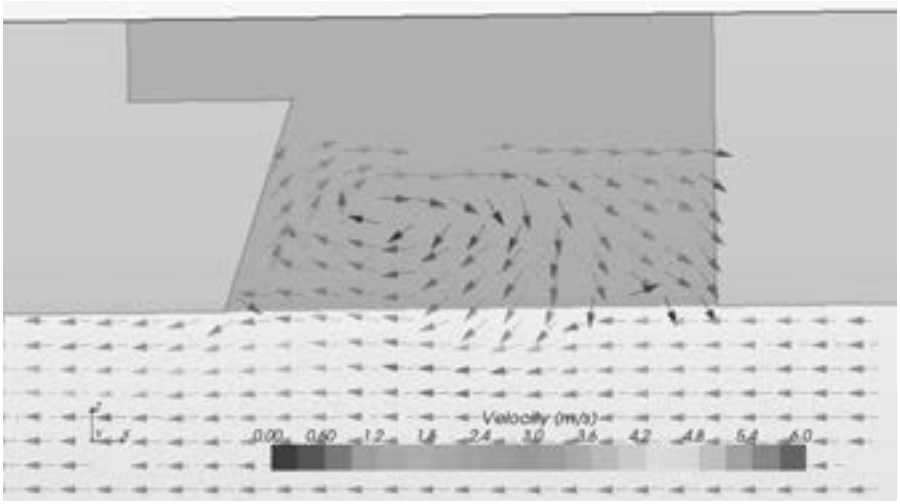

(c) Moonpool 1B

Figure 16. Comparison of the simulated water oscillations

CONCLUSIONS

The CFD simulation approach, together with the HPC techniques, has been applied to investigate the water oscillation phenomenon in the moonpool of a drillship in forward motion in calm water. In the validation analysis of a ship model, the resistance and wave elevations predicted by the present numerical method correlate well with the well-accepted model test results. In the CFD simulations of a drillship, different moonpool configurations were studied. The numerical results show that the complicated moonpool water oscillation phenomenon can be accurately simulated and the moonpool, with a shorter length and a larger cut-out angle, would reduce the added resistance significantly since the excitation of vortex shedding can be effectively reduced and the dominant sloshing motion can be significantly mitigated. The CFD simulation results correlate quite well with the available MARIN model test data. It is suggested that the CFD simulation approach, with the recent advances in computer hardware and CFD software as well as the well-honed expertise of skilled engineers, should have the potential to replace the actual model tests for future ship design.

REFERENCES

[1] "Guide for Building and Classing Drillships", American Bureau of Shipping (ABS), Houston, USA, 2011.

[2] R. van Veer and H. J. Tholen, "Added Resistance of Moonpools in Calm Water", Proceedings of the ASME 27th International Conference on Offshore Mechanics and Arctic Engineering, OMAE2008-57246, Estorial, Portugal, 2008.

[3] G. S. Virk, H. Chiu, D. R. Deter, C.v. d. Stoep, "Design of the Dynamic Positioning System for the Drillship Glomar C. R. Luigs", OTC 11954, Offshore Technology Conference, Houston, USA, 2000.

[4] H.-J. Son, S.-H. Choi, M.-W. Kim, and S.-M. Hwangbo, "Drag Reduction of Recess Type Moonpool under Vessel's Forward Speed", OMAE2008-57118, Proceedings of the ASME 27th International Conference on Offshore Mechanics and Arctic Engineering, OMAE2008, Estoril, Portugal, 2008.

[5] G. Gaillarde and A. Coteleer, "Water Motion in Moonpools - Empirical and Numerical Approach", ATMA - Association Technique Maritime et Aeronautique, Paris, France, 2004.

[6] H. N. Abramson, "Dynamic Behavior of Liquids in Moving Containers with Application to Space Vehicle Technology", NASA-SP-106, 1966.

[7] V. Bertram, "Practical Ship Hydrodynamics", Butterworth-Heinemann, Oxford, 2000.

[8] J. T. Madhani, "Sloshing Motion of Water in a Moonpool", Masters by Research thesis, University of Strathclyde, 1985.

[9] C. P. Pesce, E. A. Tannur, and L. Casetta, "The Lagrange Equations for Systems with Mass Varying Explicitly with Position: Some Applications to Offshore Engineering", Journal of Brasilian Society of Mechanical Science and Engineering, 28:4 (2006) pp. 496-504.

[10] O. M. Faltinsen, "Sea Loads on Ships and Offshore Structures", Cambridge University Press, Cambridge, UK, 1990.

[11] K. Fukuda, "Behaviour of Water in Vertical Well with Bottom Opening of Ship, and Its Effect on Ship Motions", Journal of the Society of Naval Architects of Japan, 151 (1977) pp. 107-122.

[12] B. Molin, "On the Piston and Sloshing Modes in Moonpools", Journal of Fluid Mechanics, Cambridge University Press, 430 (2001) pp. 27-50.

[13] Y. Wei, J. Yang, G. Chen, and Z. Hu, "The Research of Moonpool Size Effect on the Hydrodynamic Performance of FDPSO", Proceedings of the ASME 2011 30th International Conference on Ocean, Offshore and Arctic Engineering, OMAE1011-49586, Rotterdam, Netherlands, 2011.

[14] J. A. Alsgaard, "Numerical Investigations of Piston Mode Resonance in a Moonpool Using OpenFOAM", M.Sc. thesis, Norwegian University of Science and Technology, 2010.

[15] C. Maisondieu and P. Ferrant, "Evaluation of the 3D Flow Dynamics in a Moonpool", Proceedings of the Thirteenth International Offshore and Polar Engineering Conference, Hawaii, USA, pp. 493-500, 2003.

[16] P. Ferrant, "Fully Non-Linear Interactions of Long-Crested Wave Packets with a Three-Dimensional Body", Proceedings of 22nd ONR Symposium on Naval Hydrodynamics, Washington, USA, pp 403-415, 1998.

[17] ISSC, "Report of Technical Committee I.2: Loads", Proceedings of the 17th International Ship and Offshore Structures Congress, Seoul, Korea, 1 (2009) pp. 127-210.

[18] "User Guide: STAR-CCM+ Version 6.02.009", CD-adapco, 2011.

[19] R. A. Ibrahim, "Liquid Sloshing Dynamics: Theory and Applications", Cambridge University Press, 2005.

[20] K. M. T. Kleefsman, "Water Impact Loading on Offshore Structures - A Numerical Study", Dissertation, University of Groningen, Netherlands, 2005.

[21] C. W. Hirt, and B. D. Nichols, "Volume of Fluid (VOF) Method for the Dynamics of Free Boundaries", Journal of Computational Physics, 39 (1981) pp. 201–225.

[22] F. R. Menter, "Two Equation Eddy Viscosity Turbulence Models for Engineering Applications," AIAA Journal, 32:8 (1994) pp. 1598-1605.

[23] "Benchmark Database for CFD Validation for Resistance and Propulsion", ITTC QM 7.5-03-02-02, 22nd International Towing Tank Conference, 1999.

[24] L. Larsson, F. Stern, and V. Bertram, "Benchmarking of Computational Fluid Mechanics for Ship Flows: The Gothenburg 2000 Workshop", Journal of Ship Research, 47:1 (2003) pp. 63-81.

[25] A. Olivieri, F. Pistani, A. Avanzini, F. Stern, and R. Penna, "Towing Tank Experiments of Resistance, Sinkage and Trim, Boundary Layer, Wake, and Free Surface Flow Around a Naval Combatant INSEAN 2340 Model," Iowa Institute of Hydraulic Research, The University of Iowa, IIHR Report No. 421, 2001.

[26] "Dictionary of Ship Hydrodynamics", ITTC, 2011.

[27] W. Bascom, "Waves and Beaches: The Dynamics of the Ocean Surface," Anchor Press, New York, 1983.

[28] J. H. Allema, and G. Radstaat, "Drillship DS 12000: Calm Water Powering Tests", Report No. 23816-1-DT, MARIN, The Netherlands, 2010.

[29] J. Liang, J. Y. Cao, and C. H. Tan, "CFD for Prediction of Current Load on Drillship", KOMtech Technology Review (2010). Pg 69 – 74.

Asbjorn Mortensen
Dr. Ing.

Saswat Mohanty
MSc.

Installing Offshore Wind Turbines in Harsh Environments

Figure 1: Basic WTI layout, with its fixed handling and racking equipment

SUMMARY

This paper outlines how wind turbine blades may be handled on a large 4- legged Jack- Up Wind Turbine Installer (WTI) vessel, from the staging area in the harbour, to be installed safely and efficiently on the offshore location, by use of the *Principle of Horizontal Guiding* for all lifting operations. The vessel's two cranes can work in parallel, in order to minimize the offshore time, such that tower sections are installed by the large crane, while the rotors are assembled in a lower elevation by the smaller Knuckle Boom Crane (KBC). The KBC is equipped with a conventional blade gripper consisting of two canvas belts, and is a central component for the layout of fixed topside equipment for this vessel. Specifically, it is shown an elevated racking system to store multiple blades, which fits the blade frames commonly in use for transporting the blades from factory to installation site. This racking system is adapted to a quayside ramp, in order to minimize harbour loading time. Blades are assembled at the

offshore site to become a rotor, in a horizontal or vertical shaft orientation by use of a hub turning device. The complete rotor is hoisted to the top of the Wind Turbine tower. Three alternative means of handling the rotor is shown, all fitting the same vessel layout with blade rack and KBC. The fixture used to temporarily support the rotor during its assembly, has various embodiments depending on the design weather conditions, and the installation technology offered by the WT supplier.

INTRODUCTION

The offshore wind industry is based on the same ***Wind Turbine (WT)*** as widely used in onshore applications. The most common assembly method in use follows a sequential procedure, starting with one or two vertical ***Tower*** sections bolted to a grounded ***Foundation***. Then follows the ***Nacelle*** housing the generator and a drivetrain, located on top of the tower. At last follows the ***Rotor***, which consists of a ***Hub*** and three ***Blades***. See picture 2.

A number of very innovative assembly methods for offshore WT have been proposed, in order to make its assembly more cost efficient and having less downtime due to weather conditions. The methods are strongly dependent on the chosen vessel configuration. This paper describes the use of a large Dynamic Positioned (DP) 4- legged Jack- Up (JU), in order to create a stable platform for shallow water installation, with capacity to carry 5-10 WT's for each harbour visit. The described assembly method in this paper is conservative in that most WT's are assembled from individual parts having lifting points certified for crane lift, and with an existing lifting technology using spreader beams, yokes, grippers, fixtures/ cradles, and special assembly tools as hub tilting/ turning tool.

Rotors are typically assembled in two ways for an onshore WT:

1. Elevated assembly, horizontal blade/ hub turning method: The nacelle has a hub turning motor, enabling the hub to be slowly turned 120 degrees before the next blade is bolted into the hub. A crane with a blade gripper lifts the blade from the ground to the top of the WT, always in horizontal orientation. The blade gripper may have integrated blade pitching features, and typically using two wide canvas belts to strap the blade from above.

2. Ground assembly, horizontal rotor method: The 3 blades are bolted to the hub sitting on a turning fixture on the ground, then one or two cranes lift the assembled rotor to the top of the WT, using a hub tilting lifting device, and bolts it into the nacelle shaft

The purpose of this paper is to describe an efficient way of safely storing a number of offshore WT in individual parts, on a large ocean going JU, as well as to describe vessel topside equipment to create a safe and efficient method to assemble the WT in a shallow water up to 65m deep offshore environment with minimum downtime for weather.

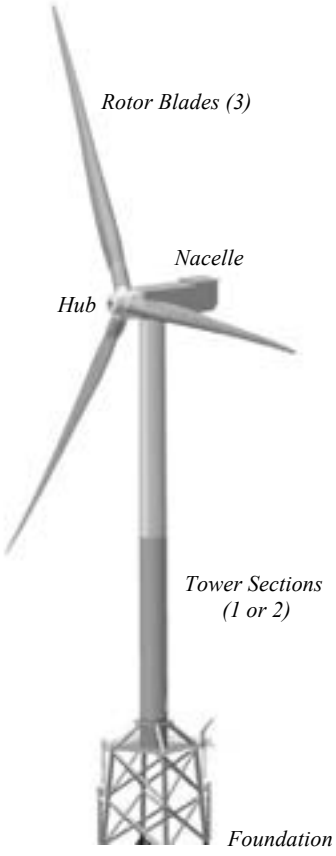

Figure 2: WT parts

This paper also describes a method to prepare storage of a multitude of blades in the harbour, and an efficient transfer of this magazine to a JU vessel. The rotor is assembled on the offshore location, in a lower elevation than the top of the WT tower, by using either of the above two ways of assembly.

Although a number of other assembly methods exists, like the "bunny ear" method, harbour assembly and erect/ slanted transportation for offshore installation, the two above described ways are the dominant, and proven. At the same time, it is a growing perception in the industry, that it must be higher focus on safe lifting operations, to improve the accident track record of the industry. As the industry grows with increasing WT sizes, it is important to develop generally accepted methods. Handling of empty blade frames and other fixtures, weighing several tons and with the potential to kill people if they trip over, must also be planned properly.

HANDLING OF BLADES IN ROOT AND TIP END FRAMES

Blades are supported by a root end frame, and a tip end frame, during transportation from the blade casting factory and to the staging harbour site, and further on to the offshore wind park. These frames are part of a WT supplier's inventory system, and must be returned to the casting factory after use. As these frames each weigh a few tons, care must be taken for the safe handling of them on the JU. The frames must fit into the JU's racking system, by an adapter or similar. Assuming blades are stored on top of each other, the tip end frames must be removed for each pick, in order to access the next layer of blade. Root end frames can stay in the rack, if so is preferred. See figure 3.

Note that the racking magazine has ladders and walkways available to all areas of human access, i.e. those points where the blades are bolted or suspended into the root and tip end frames. See figure 5.

Figure 3: Blades supported by root end and tip end frames

KNUCKLE BOOM CRANE AND BLADE GRIPPER USED FOR ROTOR ASSEMBLY

Blades are relatively lightweight compared to nacelles and tower sections. They have a high wind catching area/ weight ratio, due to their intended use, meaning even low wind speeds will cause large side forces causing the blade to swing if freely suspended from a crane. An established blade lifting method, is to use a gripper with two soft V-shaped grooves and two wide canvas belts, and two horizontal tag lines attached to tugger winches for pulling the blade up against the wind, as well as rotate the blade. The tugger winches are integrated in the gripper's frame or on the crane, and wireless operated from the crane cabin.

Use of a Knuckle Boom Crane (KBC) reduces the length of hoist rope from the crane tip to the blade gripper, and will limit swinging motion in severe weather. The limitation of the KBC crane is that it cannot reach the top of the WT tower, without becoming excessively large and costly. This limitation is solved by introducing a rotor fixture at a lower elevation, which can turn the hub during blade assembly. Such a crane will enable operation in more severe weather compared to normal lattice boom cranes . KBC cranes are widely used in marine applications and offshore oil drilling operations, because of the ability to pick loads from a deck with the tip of the crane near the deck. The key is to avoid using a standard lattice boom crane with hook suspended high up and far from the gripper, as this creates swinging motion of the blade.

The blade gripper from the WT supplier typically comes with a canvas belt tension control so the blade pitch angle can be fine- tuned prior to inserting the blade into its hub location. The blade rotation can be controlled by managing the two tag line tugger winches. Dependent on the nacelle and hub technology, and availability of power during the installation process, the hub rotation and blade pitch may also be controlled from the nacelle's electrical equipment, when matching the blade bolt pattern and the hub end flange.

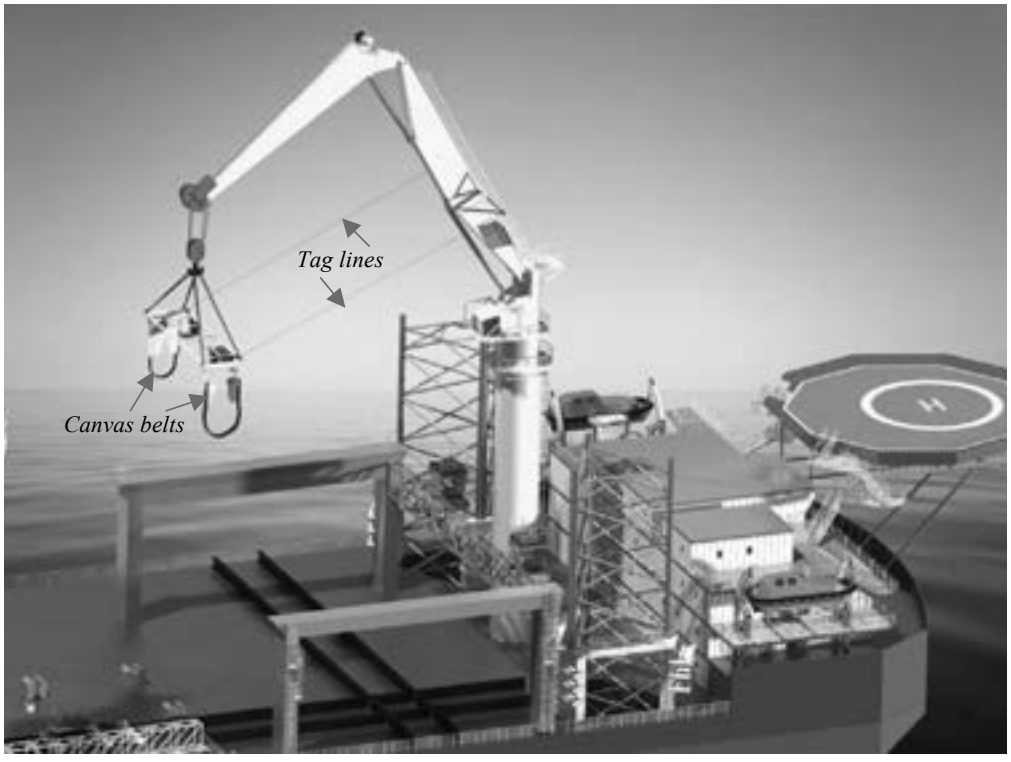

Figure 4: Knuckle Boom Crane with tag- line stabilized canvas gripper

BLADE RACKING ON THE VESSEL

A WT rotor occupies a large volume if stored in the assembled mode on a vessel. Furthermore, due to its large diameter 150- 180 m for 7-10 MW turbines, meaning 70-80m long blades, it is difficult to sail such rotors out of most harbours on a vessel, even as a collection of individual blades. There is an economic upper limit for the vessel length, and a harbour limit for the vessel width. In order to make efficient use of the vessel's main deck, the tip end of the blade will often extend outside of the vessel, making it necessary to elevate the blades to avoid them hitting the sea in rough wave conditions. Special transportation solutions may be developed, but such vessels often lack the flexibility to be used for other offshore operations, and are therefore a commercial risk for the owners.

When blades are stored aside each other, aligned in parallel, they occupy far less total volume, compared to when assembled as rotors. This paper shows an elevated racking solution with blades stored athwart the vessel, see picture 5. The functional idea is to design a racking and crane solution with minimal distance between blade storage position and assembly position for the rotor, and to guide horizontally all hanging, swinging loads so high uptime for wind can be achieved. The practical application of this idea must include easy human access to all points of operation and maintenance, so high safety and efficiency is achieved.

Figure 5: Blades stored elevated and athwart the vessel, with scissor lifts for blade gripper access

BLADE RACKING AND TRANSFER IN THE HARBOUR

Dayrate for a large Wind Turbine Installer (WTI) including the cost of its crew and tools, is typically in the higher end of 100,000 USD ++. It is therefore of high importance to reduce the loading time of WT components in the harbour to a minimum, in the same way as we minimize the offshore WT assembly time. Assuming the harbour is the staging area for several 1000's of WT for a remote offshore field, as the Doggerbank site planned offshore UK, and with offshore installations going on for 3- 5 years or more, there is economy of scale to pay down specialized loading ramps as shown above. The advantage is also less use of cranes, and therefore higher safety. The downtime due to high wind speed in the ocean- facing harbour, is also reduced.

The nacelles are bolted to a skid base, and located on a double track, with push-pull tractors for skidding. The track is extended so it matches a similar track across the JU. A harbour based "tractor" and a similar vessel based "tractor" is using its hydraulic cylinders for the task. This tractor technology is in use for moving BOPs and subsea modules in the offshore oil and gas industry today, as an alternative to crane operations.

See figure 6: Elevated above the nacelle track, is another extendable track for the blade magazine. The entire blade magazine, typically weighing several hundred tons, is pulled over the tracks acting as a bridge, to the JU. This approach does also minimize unwanted forces into the blades from a yoke during lifting of the blades, since blades can more easily slide in their loosely mounted frames during the skidding operation.

Figure 6: Triple harbour activity, to simultaneously load towers, nacelles and blades

NACELLE STORAGE ON AN XY SKIDDING TRACK

Due to the functional requirement to elevate the blade rack, as explained earlier, it is available deck space under the blade rack. Skidding tracks are welded on top of the vessel's main deck, in a XY pattern, such that the nacelles can be pulled outside and moved to a pick-up position. Skidding tractors, with a local power supply system, may be used to pull or push the nacelles bolted to its skidbases to the outside of the rack, available for crane access.

Nacelles can be skidded directly into this deck space from a nearby ramp.

During offshore assembly of turbines, one and one nacelle is pulled out by use of the two tractors. The tracks are elevated from the main deck, so these profiles can be moved, and width can be adjusted when rearranging for another vendor's nacelle.

Figure 7: Nacelles stored under the blade rack, on skidbases on an XY skidding track.

HUB TURNING AND HUB LOCATION FOR TEMPORARY ROTOR SUPPORT

The central idea of the harsh weather WTI is the assembly of individual blades to become a rotor in a low elevation, by use of a KBC giving horizontal support to the blades during handling in tight areas. These wind critical operations are the handling of blades when being lifted out of its root and tip frames in the blade rack, and during the assembly when the blade is bolted to the hub.

Three issues must be solved for the offshore rotor assembly:

1. Hub rotation by a local device
2. Mechanical support of the hub in a suitable height for the KBC, during the assembly of blades
3. Final handling of the assembled rotor to the top of the WT tower.

Hub rotation by use of a nacelle integrated hub turning device is offered by some WT suppliers. Otherwise, a special fixture enabling such local rotation of the hub may be necessary to enable the offshore assembly of the rotor.

Issue 3 above, the final handling of the hub to the WT top, may be achieved by a dedicated mast. Figure 8 shows an advanced solution using a cantilevered mast, having local winches and a track for horizontal support of the nacelle or hub, during the final lifting operation.

The mast has one or two locations for support of the nacelle and hub, by use of extending forks for supporting the rotor against wind forces, and allowing manual access to the hub. The nacelle's skidbase has a geometry fitting the forks. A spreader frame is suited to the nacelle or hub by a combination of lifting slings. The spreader frame is lifted by two synchronized winches.

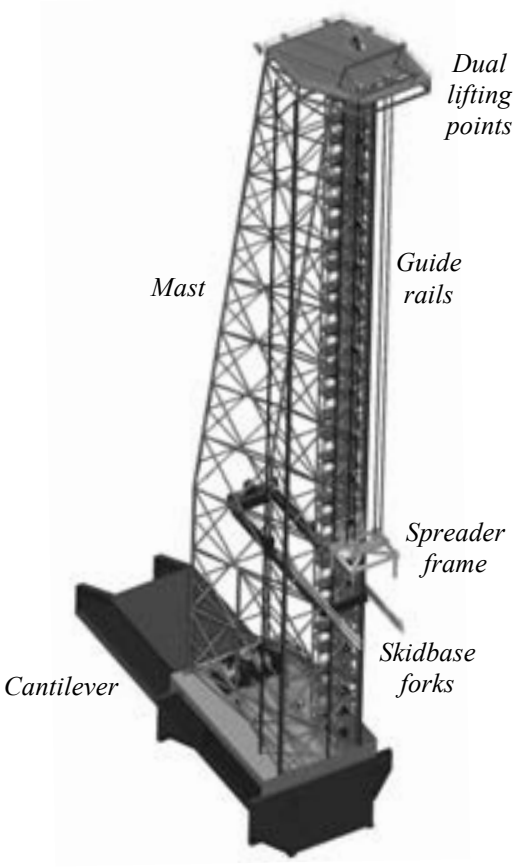

Figure 8: Mast and cantilever for assisted installation of rotor

METHOD 1: HORIZONTAL ROTOR ASSEMBLY BY USE OF A HUB TURNING TOOL

The rotor may be assembled in the horizontal plane, with the blades sweeping outside the JU's main deck. This is similar as often used for onshore WT rotor assembly, with the hub resting on a fixture with its "nose" facing up, such that its rotation axis is vertical. The KBC picks blades from the blade rack, and brings them to the same position three times, for horizontal blade assembly. The hub is bolted temporarily to a hydraulic torque device which turns the hub 120 degree for each new blade, and such that the rotor is elevated higher than the JU legs. See figures 9, 10.

When the rotor is totally assembled, the large lattice boom crane picks the rotor by use of a hub tilting device, and brings it to the nacelle which is already installed at the tower top by the same boom crane. Horizontal tugger winches will control the rotor tips according to established practice.

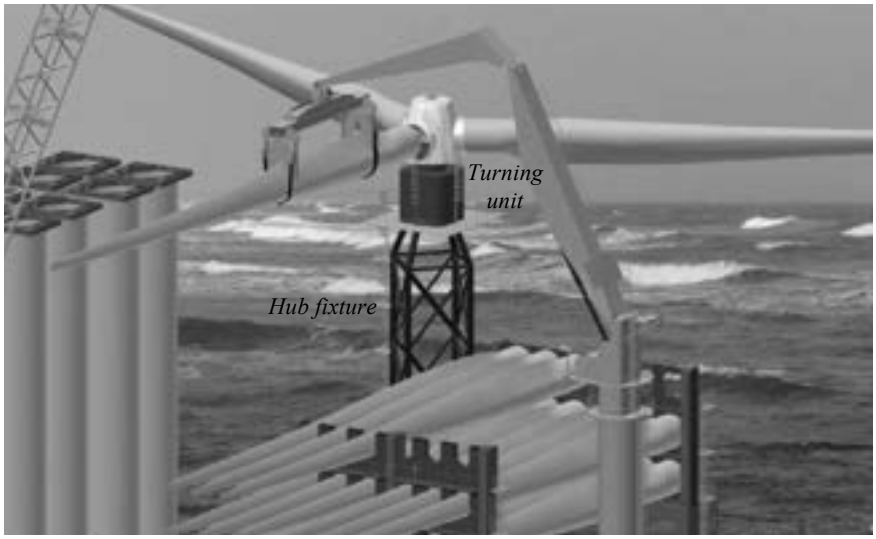

Figure 9: Horizontal rotor assembly, by use of a hub fixture and turning unit

Figure 10: Installation of rotor by large crane and hub tilting device

METHOD 2: VERTICAL ROTOR ASSEMBLY BY USE OF A HUB TURNING TOOL

This WT assembly method is based on the same vessel configuration as method 1, using a blade gripper and a KBC crane located near the blade racking system. In addition, a cantilever and mast is added to the main deck, in order to support an elevated hub turning station within reach for the KBC.

This KBC picks blade by blade out of its rack, see figure 11, and brings it to the same horizontal position each time for bolting onto the hub. The hub is connected to a hub turning device, which is temporarily supported by a platform in the mast, in order to give safe access for humans to the hub. When all three blades are properly attached to the hub, rotating 120degree each time so it becomes a full rotor, the entire system is elevated such that the rotor can be rotated another 30degree. This is the proper pick-up position of a full rotor with one blade facing down, such that the hub can be disconnected from the hub turning device and brought to the nacelle on top of the WT tower sections. See figure 12.

For this method 2, the rotor is horizontally guided by dollies and tracks in the tower, and lifted from above by winches via sheaves located on the top of the tower. This method is suitable for harsher weather conditions, compared to method 1 where the rotor is guided only by tugger winches during the final assembly.

Note that for any WT assembly method, weather limitations are mainly governed by design considerations as determined by the WT supplier. The assembly methods proposed in this paper, require the WT supplier to certify and size existing lifting points on the WT components, so its handling is suitable for harsh weather.

Figure 11: Assembly of horizontal blades, to a hub with a torque tool for rotor turning

Figure 12: Guided installation of rotor by use of cantilevered mast, and hub turning motor temporarily elevated out of way

METHOD 3: ROTOR ASSEMBLY BY USE OF NACELLE INTEGRATED HUB TURNING

This harsh weather WT assembly method 3 is based on the same vessel configuration as method 1 and 2, i.e. in addition to the same crane configuration and blade rack, it is also included a cantilever and mast for guided installation of the rotor. The variation from method 2, is that the nacelle now has an integrated hub turning device, such that an external hub turning device is no longer necessary.

Figure 13 shows how the nacelle and hub is temporarily supported by a retractable fixture inside the mast, such that the KBC can reach the hub for installation of horizontal blades. The mast has a guided track consisting of two rails. A dolly with wheels is running inside the track, and supports the nacelle during hoisting operations.

The nacelle comes with lifting points on its inside, certified for single lifts and combined lifts including hub and rotor. A spreader frame supported by the mast's two hooks is used for the lifting operations. When the rotor is assembled, the nacelle's Center Of Gravity is shifted. The spreader frame is equipped with various sets of wire slings, for each lifting configuration. When lifting off the nacelle from its rotor assembly fixation point, the change of COG is managed by various sets of slings.

To summarize: When using a cantilevered mast to install the rotor, providing XY position control above the WT foundation, it is used a dolly running up and down in a track bolted to the vertical mast. This dolly supports against swinging from horizontal wind forces affecting the nacelle and rotor under installation, at the same time as the assembly is lifted from above. This ensures minimum downtime during installation in windy weather.

Figure 13: Vertical rotor assembly in low elevation, using KBC and nacelle with hub turning device

Figure 14: Final stage of installing nacelle and rotor to top of the tower having xy motion

CONCLUSION

It is shown how offshore wind turbines can be installed in high wind speeds, by using the *Principle of Horizontal Guiding* during all lifting operations. The vessel's topside equipment is designed for safe use by human operators, to all areas requiring access. Due to the high commercial risk for an owner of a WTI vessel, it has chosen a basic crane configuration that is flexible and is fitting for various offshore assembly techniques, as well as fitting other offshore applications.

The main enabler of the horizontal guiding principle is to use a Knuckle Boom Crane to lift blades, and a blade gripper with integrated tag lines, to provide horizontal guiding by the crane. This small crane's limited reach envelope in turn leads to the use of an elevated rack for storing single blades, so blades can be assembled to rotors in a lower elevation than the top of the wind turbine. The final enabler for the last step of the installation process, in order to close the circle and always follow the principle of horizontal guiding, is to use a powered cantilever and mast when bringing the nacelle with the rotor on top of the WT tower aside the JU vessel. This cantilever is an optional and loose device that can be skid off the vessel, so the vessel's large main deck is accessible for other use.

It is shown how a ramp in the harbour can be used to hold nacelles and blades, such that the transfer time to load the vessel is minimized. This is called triple harbour loading activity.

It is shown three alternative WTI layouts fitting the same blade rack and crane layout, depending on how windy the final wind park destination is, and depending on the rotor tilting and nacelle hub turning technology available from the turbine supplier. For the benign installation weather case, method 1, a simple rotor turning device can be used, using a lattice boom crane for the final rotor handling to the top of the tower. For the more windy weather locations, it is shown how a cantilever with a transverse skidding mast and a track with a guide dolly, can be used to guide the combined nacelle and rotor (method 3), or the hub/ rotor alone (method 2).

It is recommended to plan future large wind parks using such installation techniques. For the wind park owner, prior to the ordering of new turbines, it should be planned vessel and assembly method, so the turbine's lifting points including blade frame interfaces, and hub turning technology, can be planned in detail. This is necessary in order to minimize downtime due to weather during the installation period, and accurately predict overall installation cost.

REFERENCES

1. Foo Kok Seng, Mortensen Asbjorn, Wong Toh Tung, King Yeong Jin: "Offshore Wind Turbine Installer", *KOMtech Technology Review 2010*, pp 5-17.
2. Mortensen Asbjorn and Vincent Sudhan: "Safe Working Environment when Loading and Installing Offshore Wind Turbines from a large JU Vessel", EWEA2011, Nov. 2011, Amsterdam.

Department of Drilling Equipment
Keppel Offshore & Marine Technology Centre
Pte Ltd, 31 Shipyard Road, Singapore 628130
Telephone: (+65) 6591 5450
Fax: (+65) 6265 9513
E-mails: asbjorn.mortensen@komtech.com.sg,
saswat.mohanty@komtech.com.sg

Håvard Brandt
Business Development Manager
DNV - Deepwater Technology Centre, Singapore

Successful Risk Management of Deepwater Well Operations

ABSTRACT

The Oil & Gas industry continues to move into new and more challenging operating environments encountering risks and technical challenges not encountered in more conventional shallow water development and operations. Further, the Macondo blowout in the Gulf of Mexico has dramatically increased the attention and the aware of the risk exposure represented by drilling and well operations. The pressure from the public opinion, as well as the regulatory authorities has changed significantly as a result of this incident.

In this context, quantitative blowout risk analyses have become increasingly more common throughout the industry as a tool to address these risks. These blowout risk analyses are however based on traditional risk methodology, with a strong focus and attention to the consequence modeling; addressing gas dispersion, ignition sources and the safety risk exposure on the platform and rig as a result of an uncontrolled release. Similar sophisticated modeling tools are available to assess hydrocarbon dispersion in sea and the environmental consequence of an oil spill. These analyses are however all based on historical data to generate the main input to the model, i.e. the blowout probabilities and likelihood for different blowout scenarios. Industry databases have been generated from historical blowout events; however this data is generic with limited consideration for the specific well characteristics and challenges related to a particular well operation.

To address this shortcoming, DNV has together with the industry developed a new methodology for assessing the specific blowout risks related to a particular drilling or well operation, with the objective to provide a more realistic risk picture which also can be used to manage the risks. A multidisciplinary team-based workshop is applied during the risk assessment process, with the objective to evaluate the drilling or well operations according to a set of predefined criteria or risk factors. This analysis is used to assess the probability of a hydrocarbon release or a blowout for a specific drilling or well operation.

This new method considers the field specific and reservoir specific challenges, the best available technology and best operational practices used in order to generate a more field and operation specific risk exposure of the drilling or well operation. The results are more accurate risk predictions which also can be actively used to reduce the risk and take risk mitigating actions.

INTRODUCTION

Offshore oil and gas activities involve a number of risks which could expose life, property and the environment. Blowouts represent one of the main risks related to the exploration and development of offshore fields. History shows that such events can have catastrophic consequences, and can potentially occur to any exploration or development project. Recent events have increased public attention on blowout risks. In addition, oil and gas projects

explore more and more challenging territories, both in terms of operations and when considering the response in case of accidental events. There is therefore increasing focus on potential risks from oil and gas drilling and well activities, and consequently an increasing need to better understand and systematically manage these risks.

Risk analyses such as Quantitative Risk Assessments (QRA) or Environmental Risk Analyses (ERA) allow assessing risk levels for projects or existing installations, and are used as a basis for decision making. In certain parts of the world, e.g. The Norwegian Petroleum Safety Authority, there has been a drive towards specific requirements on the operators to conduct blowout and environmental consequence analysis to demonstrate the risk exposure associated with their oil and gas operations and activities.

As described by Holand (1997), the quality of the input data is an essential aspect required to ensure a satisfactory quality of a risk analysis. Good input data quality ensures a realistic risk picture, which is critical for the value of the risk analysis and for its use as a basis for decision making. Focusing on the blowout characteristics, three parameters are among the most influent for the environmental and safety risks level: the blowout probability, its duration, and the quantity of hydrocarbons which potentially could be released. The blowout probability has a direct impact on the risk level, since risk is defined as the combination of the probability of occurrence of harm and the severity of that harm; reference Standard Norway (2010). The blowout duration and quantity of hydrocarbons released will therefore influence the event severity.

Use of historical data

As for many other types of risks, historical data and statistics are the most common sources of information used for assessing blowout risks.

SINTEF records blowout occurring all around the world in their Offshore Blowout Database, reference SINTEF (2012). The database documents numerous information on each event, such as its location, the well characteristics, the type of operation underway when the event occurred, the causes for the incident, characteristics of the blowout, and finally other relevant information such as the control method applied or the data quality. Each year statistics from the database are provided as a report issued by SINTEF. The database and annual report are confidential and only accessible for the project sponsors.

The SINTEF data is currently the most common source of information for the characterization of potential blowout scenarios as input to Environmental Risk Analyses (ERA) and Quantitative Risk Assessments (QRA).

Specific risk analyses

Each well has a unique risk level, due to specific reservoir and underground conditions, operational characteristics and constrains. The blowout statistics are grouped into well categories, e.g. development or exploration drilling, but give very limited consideration to well risk factors. As an illustration, two HPHT exploration wells with different operating margins, i.e. the window between the pore pressure and fracture gradient, would not present equal risks. A lower operating margin would increase the risks related to losing the primary barrier (drilling fluid column) during the drilling operation. Using historical blowout frequencies for these two wells would not reflect the two different risk levels. A more realistic characterization of the blowout risk picture would require taking into account the well and operations specific risk factors.

The well-specific blowout risk assessment methodology has been developed based on the need and request to provide better input data to the ERA and QRA to reflect a more realistic and well specific risk level. This is even more relevant for those projects that could be subject to scrutiny due, for instance their sensitive location, or application of new technology. The methodology should be as objective as possible, and the process and results should be documented.

METHOD

The methodology addresses the three main parameters influencing the environmental and safety risks level related to blowouts: its probability, the potential hydrocarbon flow rates, and its duration.

Well-specific blowout probability

The methodology is based on an adjustment of generic blowout probabilities based on a detailed assessment of the characteristics related to a specific drilling or well operation. A list of factors which contribute to a potential blowout is systematically reviewed and evaluated by a multidisciplinary team familiar with the drilling rig, the rig equipment, the reservoir and well characteristic and the detailed well program and operation to be conducted. Risks are weighted and a well and operations specific risk score is calculated. This score is compared to a benchmark, and a blowout probability is generated based on these benchmark frequencies.

Picture of the Deepwater Horizon (Macondo) blowout in the Gulf of Mexico (picture from the US Chemical Safety Board)

Well barriers

The Norwegian standard NORSOK Z-013 requires the continuous presence of two tested and independent well barriers at all times during conventional drilling of offshore oil and gas wells. Each barrier is in itself intended to prevent uncontrolled flow of reservoir fluid to the surrounding environment. A blowout may only occur when both well barriers fail, i.e. both the primary barrier represented by the drilling fluid column and the secondary barriers represented by the blowout preventer (BOP), wellhead, cement and surface casings.

Risk factors

The probability for failure of the well barriers, and consequently the probability of a blowout, is influenced by a number of risk factors. These risk factors can be organized into three categories, whether they are related to the reservoir and underground conditions at the well location, to the rig, riser and well, or to operational aspects.
Twelve risk factors related to the reservoir and underground conditions have been identified when establishing this methodology. Among these risk factors are the operating margin, the pore pressure, stability of the formations, or the seismic quality and uncertainties. As an illustration, a smaller operating margin increases the risk of losing the primary well barrier through insufficient hydrostatic pressure, or through the loss of drilling mud to the formation (fracturing). Poor seismic quality and high uncertainties can lead to improper well design, and therefore increase the risk of a blowout during the drilling operation.

Risk factors related to the rig, riser and well cover issues like the drilling crew experience and the water depth. Crew preparation and experience is critical to ensure that proper decisions are made during the drilling operations. Operation related risk factors also have an influence on the blowout risks. Such factors include the number of trips related to the well operation, i.e. coring, or the number of logging runs. Tripping tools out of the hole can unbalance the pressure in the well, which can result in a kick due to swabbing. A higher number of trips would therefore tend to increase the risk for a blowout to occur.

Risk review

The well and operation specific risk factors are systematically reviewed and evaluated during a qualitative risk identification workshop. The session

typically includes drilling experts, geologists and HSE representatives. A risk ranking methodology is applied, and each factor is attributed a score e.g. from 1 to 9, reflecting the relevant risk level. This risk ranking is based on available information on reservoir and underground conditions, the well design, the project, and on the team experience and best engineering judgment. Criteria are provided for each risk factor, to help guide the team during the assessment process. The criteria were developed based on a detailed review of historical data, scientific publications and other revenant experience. The methodology is adjustable, and additional risk factors may be added if relevant for the specific well being assessed. At the end of the review the team is provided with an overview of the main risk factors and a clear and common understanding of the main risk factors which may include the risk of a blowout.

Probability adjustment

Different risk factors may have a different influence on the blowout probability. For instance the pore pressure is expected to have a more significant influence on the risk level than the anticipated number of trips. Therefore the risk factors are given a defined weight. The weigh is intended to reflect the influence of each risk factor, regardless of the well and operational characteristics. Risk factors scores are weighted and averaged for each category, which gives a score for each impact factor category, i.e. reservoir and underground conditions, rig, riser, well design and operational aspects.

The three categories again also have different influence on the blowout frequency; therefore the categories are also given a weight. Based on detailed analysis of the blowout statistics, it has been evaluated that risk factors related to reservoir and underground conditions (e.g. unexpected overpressures, narrow pressure margin) contribute to more than 60% of the blowout risk. The contribution from operational aspects (e.g. tripping) is estimated to be approximately 8%, and issues related to rig, riser and well amount to 32% (e.g. issues with cementing, crew experience, equipment failure).

A well score is calculated based on each category score and the weighting between them. The well score is intended to reflect the well specific risk level. Figure 1 illustrates the process from risk factors to the well score.

Benchmark" scores have been attributed to the risk level of an HPHT well and of a "regular" well. The SINTEF statistics provide blowout frequencies for both of these wells. By comparing the well and operations specific risk score to the benchmark, it is possible to calculate a blowout probability, through an interpolation.

Figure 2 presents an example of a case with a well specific score of 4.5. A "regular" well is scored 3 on the benchmark and the corresponding blowout frequency is 1.1 x 10^{-4} per drilling operation. A "typical" HPHT well is given the value 7, and the blowout frequency for such a well is 6.9 x 10^{-4} per

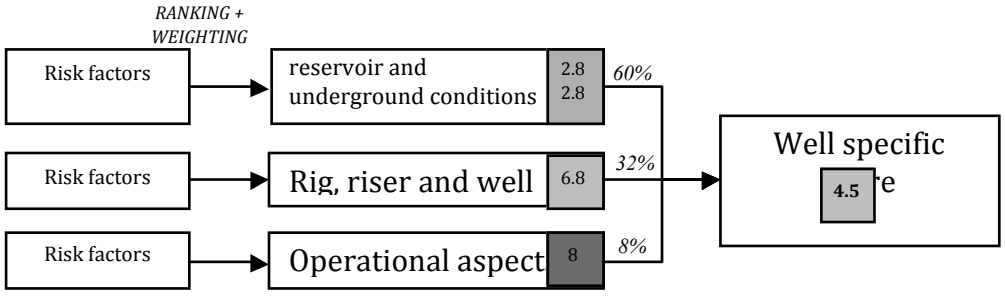

Figure 1 – schematic view of the well score methodology

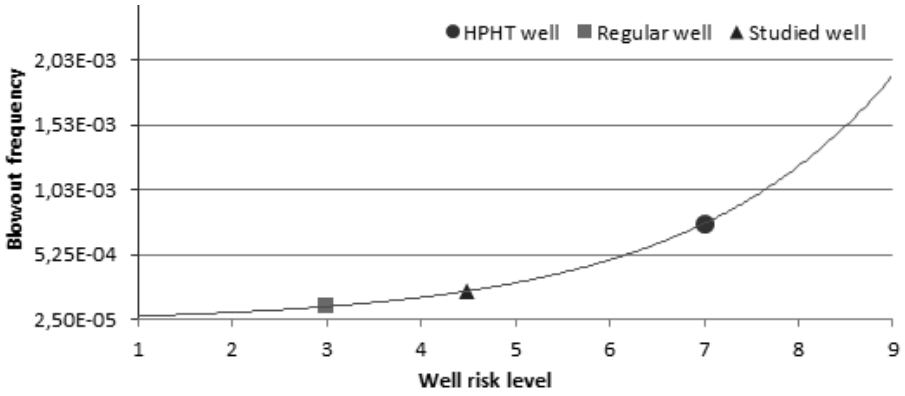

Figure 2 - Schematic view of the probability adjustment curve

drilling operation. Interpolation between the two benchmarks with the well specific score gives a well specific blowout probability of 2.2×10^{-4}.

The interpolation curve used for the blowout probability is exponential. This allows limiting the calculated probabilities for wells with very low risk scores. Using a linear curve for the calculation of the blowout probability would lead to a result equal or inferior to 0 for wells with risk scores below 2.3. The exponential curve also provides conservative results for wells with high risk scores.

Depending on the results from the well risk review, the well-specific score may range from 1 (low risk) to 9 (high risk). The corresponding blowout probabilities for an exploration well range from 4.5×10^{-5} to 1.7×10^{-3}, respectively. The lowest probability is still about two times higher than the blowout frequency for a development well. The main difference between a development drilling operation and an exploration drilling operation is that there is significantly more information available when drilling a development well.

WELL-SPECIFIC BLOWOUT SCENARIOS

A single blowout can lead to a range of potential hydrocarbon release scenarios or blowout scenarios which all have a different flow rate potential and duration. The term "blowout scenario" here refers to the different potential origins and flow paths and scenario resulting in the blowout.

By identifying the different blowout scenarios which are credible, and by implementing flow models, it is possible to obtain the range of potential hydrocarbon flow rates and release scenarios related to a particular well operation. This will be essential information when implemented into the detailed oil drift and response calculations in an Environmental Risk Analyses (ERA) or in a gas dispersion model in a Quantitative Risk Assessments (QRA). Assigning specific probabilities to each scenario allows for a well specific assessment of the blowout risk.

Scenario parameters

In the well specific blowout scenario assessment, the following key elements related to the well operation are systematically evaluated:

- The formation – There may be several reservoirs to be targeted by the drilling operation all with different flow and hydrocarbon potentials
- The operation – The drilling operation and the casing program will have an impact on the potential blowout scenario
- Open hole section – The flow potential from a formation will be dependent on the length of the open hole section drilled.
- Flow path – The flow potential will be dependent on the flow path, i.e. annulus flow would be different that an open hole flow scenario
- BOP restriction – The BOP may fail totally, fully open, or fail to seal. The restriction at the BOP could significantly impact the flow potential

For a well targeting several reservoirs, the blowing formation or combination of formations would have an impact on the resulting hydrocarbon flow rates. Based on the formation properties and the specific information and uncertainty related to the specific formation, it is possible to attribute a specific blowout probability related to each of the zones drilled. The purpose is to illustrate which of the formations are the most likely to cause a blowout. Typically formations with higher pressure, smaller operating margin, and higher uncertainties, would represent the highest risk for a blowout.

For exploration wells a pilot hole may be drilled, particularly when there is a significant uncertainty related to a particular formation. The information obtained when drilling the pilot hole may then be used to adjust the operation to the relevant well factors and significantly reduce the risk of a blowout when drilling the larger hole section. Thus, this operational adjustment of drilling a pilot hole may significantly reduce the risk exposure, as the uncertainty, i.e. well kicks, most likely will be taken when drilling the smaller dimension pilot hole, which has a significantly lower flow potential. Similarly, there are a number of other operational adjustments which will impact both the probability and potential flow rate related to a potential blowout.

The length of the open hole section in the formation could significantly impact the flow potential. In general, there is a relatively high probability of taking a kick relatively quickly after entering a new formation due to unexpected pressure from that particular zone. This will obviously also depend on the uncertainty of the reservoir information for the particular well being drilled. In principal a blowout could occur at any time during the drilling operation, but experience indicate that kicks tend to occur either relatively quickly after entering a new zone, or when pulling out due to swabbing effects. When pulling out often the entire hole section could be exposed. To cover all possible scenarios three cases are typically considered in this risk evaluation; the first represents a release after drilling a few meters into the zone, the second represents the full penetration of the zone and last scenario considers

Picture of a bird caught in an oil spill
(picture from the Green Living Earth)

the zone half drilled (to cover any kicks which could occur anytime during the drilling operation). The probability distribution is assessed on a case by case basis, taking into account historical data, the uncertainties related to the specific formation being studied and expert input generated during the risk workshop.

Depending on the BOP status and on the position of the drill pipe, the hydrocarbon released during a potential blowout has multiple flow paths. A blowout occurring when the drill pipe is tripped out of the hole would lead to an open-hole flow, which typically results in higher flow rates. If the drill pipe is in the hole when the blowout occurs, the flow would generally occur through the annulus between the well casing and the drill pipe. Should the pipe ram be closed, the flow path could be through the drill pipe itself. Historical data and assessment of the equipment provide is used to provide the probability splits for the different scenarios.

The BOP failure mode is the last parameter assessed when evaluating the possible blowout scenarios. A partly closed BOP could have a significant influence on the potential blowout flow rates. The flow of hydrocarbons could be restricted depending on the degree of opening of the BOP in case of a blowout. In the case of a total failure with a BOP in full open position, the flow will not be restricted at all. Two degrees of opening are typically selected: fully open or restricted flow. Historical data and assessment of the specific equipment is used to provide probabilities for the two alternative failure scenarios.

Scenario probabilities

By combining the parameters described above, it is possible to obtain a range of possible blowout scenarios reflecting a spread of flow rates and release scenarios all relevant to the specific drilling operation being considered. Depending on the assumptions made and the probabilities attributed to each of the main parameters, there will be a series of possible blowout scenarios each with a unique probability which represent the possible blowout scenarios relevant to that particular drilling operation. By modifying some of the steps in the drilling or well operations, e.g. applying different technologies, the assumptions and probabilities will change resulting in a set of different blowout scenarios and associated probabilities. Consequently, the model can be used directly to evaluate the risk impact of modifying the equipment, applying different methods, and/or making changes to the planned well operation.

As an example, by making the decision to drill a pilot hole prior to drilling the main hole section in an exploration well with significant uncertainty, there will typically be a significant shift from potentially large release scenarios to much smaller release scenarios as the uncertainty and risk is shifted to the pilot hole operation. Similarly, a log may reduce the uncertainty related to a step in the drilling operation and result in a reduced probability of a blowout from that section.

THE RISK ANALYSIS

Based on the possible blowout scenarios identified and relevant probabilities, more realistic Environmental Risk Analysis (ERA) can be conducted. This implies implementing and taking the blowout scenarios defined above, and conducting:

1) Oil drift modeling
2) Dispersion analysis
3) Environmental impact assessments

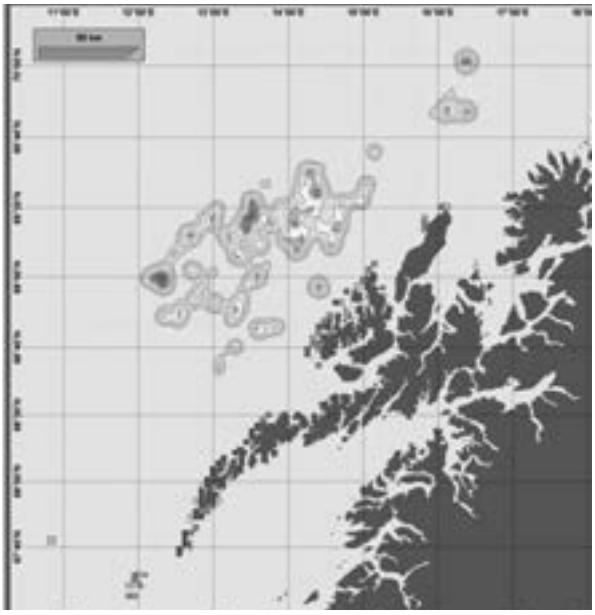

Figure 3 – Illustration of an oil release

Sophisticated tools are available to provide an overview of the areas affected by the oil release, and the impact area can be plotted directly in a map as illustrated in Figure 3. This plot provides an overview of the areas impacted by the oil release considering the oil drift and dispersion calculations based on relevant environmental data for the particular area considered.

The environmental modeling tool further calculates the impact on fish and seabirds based on relevant information from the particular area being affected. Thus, biological data is implemented considering the number of fish and sea mammals in the particular area, the age, the breathing period and resistance to such an oil spill. Consequently, the blowout scenarios can be directly linked to an environment consequence, i.e. the estimated number of fish and sea mammals being killed as a result of the release.

By having the direct link to the technical assumptions related to the planned drilling or well operation, the operator can now evaluate alternatives and modifications and directly assess how this will impact the risk picture. In Figure 4, this is illustrated for a planned drilling operation in a particular environmental sensitive area. In the base

case a the drilling operations was planned using conventional methods, while the alterative case illustrate the significant risk reduction which could be achieved by adopting a number of risk reducing methods, i.e. extensive use of Measurement While Drilling (MWD) and Logging While Drilling (LWD) technologies, drilling certain sections with an initial pilot hole and assuring safe and reliable setting points for the casing, i.e. assuring that the production casing was set a safe distance from the reservoir. As illustrated the potential risk reduction was significant.

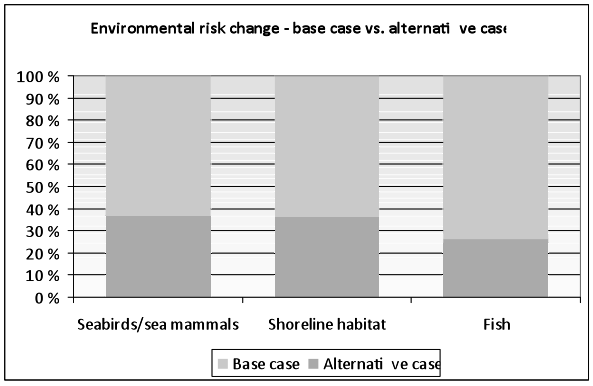

Figure 4 – Illustration of how modifications to the drilling operation can significantly alter the risk picture.

CONCLUSIONS

The well-specific blowout risk assessment methodology allows for better understanding of blowout risks and provides a more specific risk picture related to a specific drilling or well operation. Conventional blowout studies purely based on historical data may provide an unrealistic risk picture and would typically not reflect and identify the actual risks related to the particular well operation. Consequently, it does not provide a tool to manage the well specific risks.

The systematic risk factor based methodology and expert based parameter adjustments provides a process which will identify the most critical risks related to the specific well operation being assessed while also taking into account factors which may contribute to lower blowout probability. The methodology and team based process is systematic and objective, and will provide valuable support in the well design and planning process. Experience has also proven that the well risk review provides an excellent opportunity to gather different disciplines within a project team and put focus on the risk identification of blowout related risks and risk reduction measures. The entire process is documented and the results are properly justified.
The blowout probability adjustment retains experience from blowout statistics while at the same time taking into account the project specific risks. The well risk score allows better understanding of the risk level specific to the particular project. By also adjusting the blowout scenarios (flow rates), this methodology also significantly improves the quality of Environmental Risk Analysis (ERA) and Quantitative Risk Analysis (QRA) addressing blowouts assuring more realistic results.

REFERENCES

1. Holand, 1997. Offshore blowouts: causes and control. Houston, Texas: Gulf Publishing Company.
2. SINTEF, 2012. SINTEF Offshore Blowout database, web version. Available for members at http://blowout2011.exprosoft.net/ Accessed 25-06-2012
3. Standard Norway, 2010. NORSOK Standard Z-013, Risk and emergency preparedness assessment, Edition 3. Available at http://www.standard.no/en/Sectors/Petroleum/NORSOK-Standard-Categories/Z-Risk-analyses/Z-0132/ Accessed 14-06-2012

Håvard Brandt has during the last years been working with business development in DNV with a responsibility for Risk Management services. He has recently taken on a business development role with the new DNV Deep Technology Centre in Singapore.

Areas of Expertise: Risk management including qualitative and quantitative risk assessments with a strong focus on technical and economical evaluations and application of risk assessment for subsea systems, drilling and well operations.

He has more than sixteen years of experience in the oil and gas industry, and has worked on a number of project assignments throughout the world. For more

than six years Håvard was based in DNV's offices in Houston, where he was the Deputy Manager for the asset risk team with responsibility for a large portfolio of offshore development projects.

Career: Stavanger (1996-2000), Houston (2000-2006), Høvik (2006-2012), Singapore (2012-present)

Education: M.Sc from Norwegian Institute of Technology, with final Master Thesis from Technical University in Delft, the Netherlands

Liu Ming, Chong Wen Sin, Nirmal Raman Gurunthalingam and Jens Wallevik

Wet Scrubbing Process for Marine Emission Control

ABSTRACT

More stringent regulations on gaseous pollutant emissions from ocean going vessels are being legislated in recent years. As compliance approaches, various technologies and processes are being developed and implemented to reduce the pollutant emitting to atmosphere. Outlined in this paper, wet scrubbing processes with the emphasis on SO_x (*sulfur oxides*) removal are reviewed. A process (Optima) developed by Keppel Offshore & Marine Technology Centre (KOMtech) is shown to be consistent in SO_x removal without adverse environmental impact.

1. INTRODUCTION

1.1 Marine Emission

As a result of fuel burning for propulsion and power generation, ocean going vessels produce pollutants containing exhaust gas including sulfur oxides (SO_x), nitrogen oxides (NO_x) and particulate matters (PM). These pollutants have several potential adverse impacts on the environment, including global warming, ozone depletion and acid rain.

1.2 Marine Emission Regulations

The focus of the current discussion is wet scrubbing processes to remove SO_x from marine exhaust gas, which has been widely adopted method among the industry. The following discussion on regulations if not specified, is focused on the discussion of SO_x emission only.

Ships operating in designated sea regions called ECA (Emission Control Area) face regulations on emission. Emissions from marine vessels are currently controlled by several international, regional and local regulations. At the international level, atmospheric emissions from marine vessels are regulated under Annex VI of International Convention for the Prevention of Pollution from Ship (MARPOL 73/78) set by International Maritime Organization (IMO). At regional level, there are rules set by European Union Commission Directive (EU Directive), the United States Environmental Protection Agency (EPA) and California Air Resources Board (CARB).

ECA geographic scope in Europe includes the Baltic Sea, North Sea and English Channel. In North America it extends approximately 200 nautical miles offshore. Potentially the ECA scope may include all coastal areas of the world, and the geographical areas outside of ECA zones are subjected to world-wide sulfur emission cap set by IMO. The current and upcoming ECA regulations on SO_x emission are listed in table 1.

REGULATION	YEAR																
	2005	2006	2007	2008	2009	2010	2011	2012	2013	2014	2015	2016	2017	2018	2019	2020	2025
MARPOL Annex VI	Entered into force																
- SO_x																	
a) Global		S<4.5%						S<3.5%								S< 0.5 %	Alternative date**
b) ECA*		S<1.5%				S<1.0%					S<0.1%						
EU																	
- SO_x																	
a) General		S<1.5%				S<1.0%					S<0.1%						
b) Port		S<1.5%				S<0.1%											
USEPA					Join IMO												
- SO_x								S<1.0%			S<0.1%						
CARB (California)																	
- SO_x					S<0.5% (MDO), S<1.5% (MGO)			S<0.1%									

* Emission Control Area (ECA): Baltic Sea and North Sea for SO_x and North America (including most of the U.S and Canadian Coast) for SO_x and NO_x.
** Subject to the feasibility review of fuel availability completed by 2018.

Table 1 Global and Regional Emission Regulation on SO_x emission (Current and Upcoming).

2. FORMATION AND REMOVAL OF SO_X AND PM FROM MARINE EXHAUST GAS

2.1 Overview of Control Strategies:

In principle, there are two types of strategies for SO_x emission control, "throw-away process" and "regenerative process". The throw away process capture SO_x from exhaust gas and convert it into a more stable and harmless form before it is discharged to environment. During in the regenerative process, SO_x is captured, concentrated and recovered as a resource for other value added processes, which requires additional setup, storage and reception facilities both onboard and at port. Hence, it has not seen trial installation on shipboard so far. The dominating systems designated for SO_x removal onboard today belong to "discard process".

2.2 SO_x Formation and Removal Mechanisms

SO_x emission from marine vessel is the result of fuel combustion that contains either organic or inorganic bond sulfur. The majority of sulfur is oxidized into SO_2 with small amount SO_3 coexisting due to thermodynamic limitation. SO_x is the general terms of the combination. A minute amount of inorganic sulfur is converted into sulfate particulate that contributes to an increased emission of particulate matter (PM).

As an acidic component from exhaust gas, the most straightforward way to remove SO_x is to use acid-base neutralization, which can be carried out conveniently in any well designed reactor or process. There are well developed land based desulfurization processes making use of lime stone operated either in dry or wet state. Gypsum is produced as the

neutralization product and is sold as a raw material to make wallboard and recover a fraction of the operating cost. There are also magnesium hydroxide based desulfurization processes (more popular in Japan) which claim to be less prone to scaling and more efficient than the lime based processes. For offshore exhaust gas cleaning system (EGCS), the alkalinity from sea water is a free and readily available source for SO_x neutralization. Therefore most EGCS proposed onboard are established on sea water wet scrubbing principle. The natural alkalinity from sea water neutralizes SO_x and convert it into bisulfite and sulfite form, after which they undergo further oxidation and become stable sulfate form as part of the natural component of sea water.

$$SO_2 + HCO_3^- = CO_2 + HSO_3^-$$
$$HSO_3^- + HCO_3^- = H_2O + CO_2 + SO_3^{2-}$$
$$2SO_3^{2-} + O_2 = 2SO_4^{2-}$$

According to chemistry stoichiometry, one unit of alkalinity from sea water is able to capture equal unit of SO_2 from exhaust gas, after which it requires additional equal amount of sea water to make the discharge neutral as required by regulations. For example, along with every 1 MWh brake power generated from a typical low speed marine engine powered by HFO (3% sulfur), 147 m^3 of sea water with average alkalinity (2,300 µmol/kg) has to be consumed to capture and stabilize the SO_x emission from exhaust gas. As the natural alkalinity of sea water may drop drastically in enclosed shallow water region where dilution plays significant role by surrounding fresh water estuaries, the sea water scrubbing process may require enormous amount of sea water and become impractical.

2.3 Particulate Matter (PM) (Formation, Effects, Removal method)

Along with SO_x emission, particulate matter (PM) is another pollutant of concern. It is the result of combustion of HFO (heavy fuel oil) which tends to have a high sulfur and metals content. Incomplete combustion, high impurity (sulfur and metal) concentration give rise to the amount of PM generated. Due to the fact that HFO quality varies from supplies, it is difficult to establish precise relationship between the fuel sulfur content and PM emission however higher amount of PM emission is anticipated when sulfur concentration of HFO increases [1].

In a wet scrubbing process, PM is removed mainly by impact and diffusion. Particles greater than 1 micron cannot follow the streamlines around liquid droplets as the particle's inertia causes it to deviate from the streamlines and to hit the droplet. For very small particles (< 0.1 micron) moving randomly as a result of gas molecules' continuous bombardment, the motion is diffusion in nature and the particle is collected by random colliding with liquid droplet in a confined space.

Although PM emitting from marine engine into atmosphere is not specified at the moment by IMO, its entering into liquid phase during wet scrubbing process does affect the discharge water specifications which is regulated by IMO guideline (MEPC 184/59) in terms of PAH (polycyclic aromatic hydrocarbon) and turbidity change. Any sea water scrubbing process has to take into account the PM trapped in liquid phase carefully before it is implemented.

3. REVIEW OF CURRENT TECHNOLOGIES OF WET SCRUBBING PROCESS FOR MARINE EMISSION CONTROL

3.1 Open Loop System

The open loop system relies exclusively on the natural alkalinity of sea water to scrub sulfur oxides from exhaust gas as 100% of scrubbing water is drawn from sea and subsequently discharged back after it passes through the system. In particular, sulfur dioxide removal takes place in a scrubber designed to accept maximum sea water flow, catering for the minimum possible alkalinity and maximum engine load. The internals of the scrubber are usually designed for the exhaust gas and scrubbing water to have maximum contacting surface to enhance the adsorption. Several types

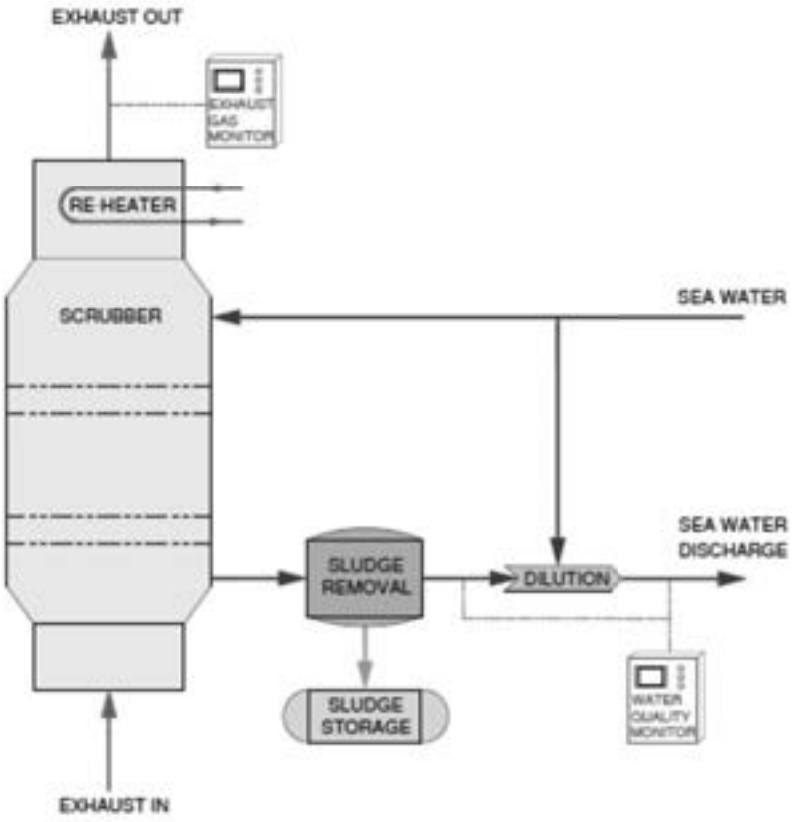

Figure 1 Open loop sea water scrubbing system

of scrubbers such as spraying, bubble batch, plate tower, packing column (structural and random packing) types or their combinations are generally used.

The spent sea water (wash water) passing through scrubber is loaded with acidic species, captured particulate matter from exhaust gas and silt from ambient sea water. The wash water has to be treated before being discharged back to the sea. It is either pumped or drained to a hydrocyclone separator that induces centrifugal separation of heavy suspended particulates from the water. At the end of the process, solids collected from the bottom of the hydrocyclone separator are stored in a sludge tank.

The wash water depleted of suspended solids is now mixed with equal amount of sea water that brings pH back to neutral (>6.5), as is required by IMO for overboard discharge.

Advantages:

- The system uses only free natural sea water as scrubbing agent, there is no concern on storage of additive chemicals on board.
- Fewer components are needed compared to other systems.
- Easier for crew to operate and familiarize.

Disadvantages:

- Operating in brackish or fresh water area will make the system underperform or fail due to the insufficient supply of natural alkalinity.
- Pumping cost remains high due to large amount of sea water is required as scrubbing and diluting agent.
- Overall acidifying effect to surrounding water, discharge may be restricted in some regions (such as at berth) where there are more stringent local regulations.

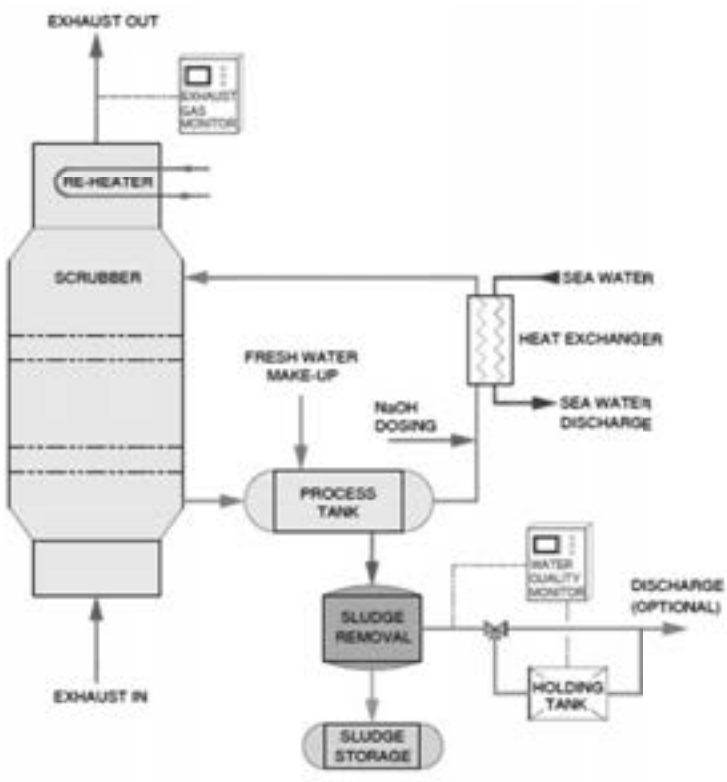

Figure 2 Closed loop scrubbing system

3.2 Closed Loop System

The principle of closed loop scrubbing system is to use re-circulated scrubbing media with chemical addition (NaOH) to maintain its alkalinity to achieve consistent SO_x removal. Fresh water instead of sea water is used in order to avoid potential scale accumulating in pipelines and scrubber internals. The scrubbing agent is contained in a closed scrubbing loop with inline process tank to accept chemical dosing and fresh water replenishment.

Evaporation loss of scrubbing liquid as a result of heat exchanging between hot exhaust gas and scrubbing water has to be minimized, which requires that the re-circulation loop be heat-exchanged with a sea water cooling line. At the same time, small amount of make-up water is added continuously to maintain the water level in process tank. The "bleed-off" flow is centrifuged to take away heavy particulates and is discharged when it is applicable. Alternatively, it can be stored in a holding tank and offloaded to reception facilities when ship arrives at port.

Advantages:

- The process relies on self carried alkaline and performs consistently.
- Pumping cost can be lower than open loop system by using more concentrated scrubbing agent.
- More efficient separation of solid contaminants from wash water can be achieved.
- All waste effluent can be stored onboard to achieve zero-discharge.
- Zero acidifying effect to surrounding marine environment.

Disadvantages:

- Supply and store NaOH onboard increases operating cost and requires special handling.
- Continuous fresh water supply and storage is required.
- The system has more components than an open loop system.
- Requires more training and equipment familiarization for the crew

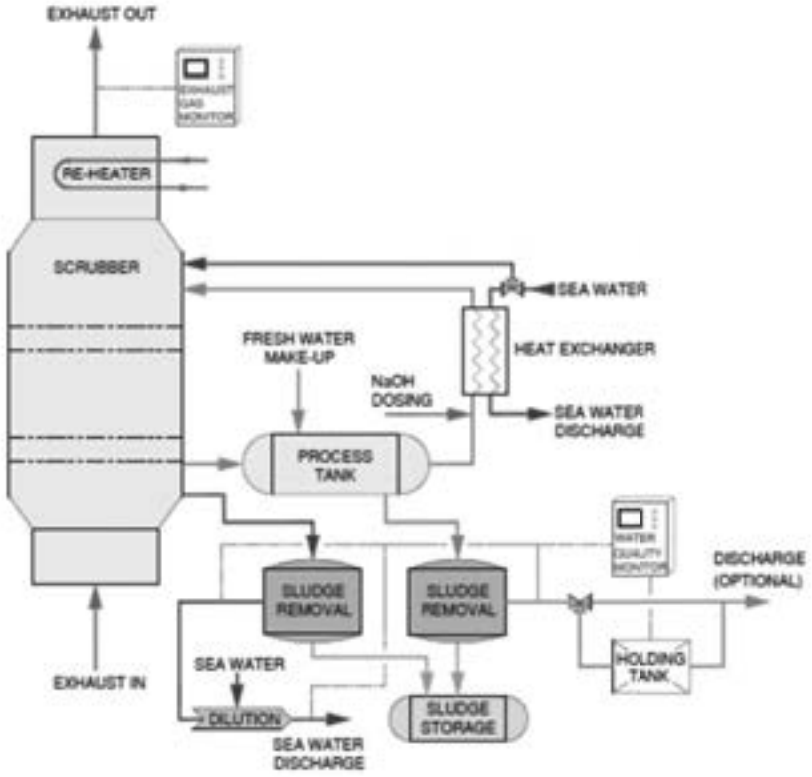

Figure 3 The hybrid scrubbing system

3.3 Hybrid System

A hybrid system combines the open loop and closed loop process. It resembles a closed loop system but incorporates additional components to enable it to operate as either an open or closed loop configuration. At open sea the system operates in open loop mode to avoid chemical consumption; at port it functions in closed loop mode to avoid issues associated with port discharge regulations.

The hybrid system has all of the same components that are present in the closed loop system however two wash water treatment devices are installed because the open loop mode of operation requires 100% of the water to undergo centrifugal separation while in closed loop mode the burden is much lesser. Switching from the closed loop mode to the open loop mode requires a change in the functions of certain components. The seawater pump used to provide cooling water to the heat exchanger in closed loop mode becomes the supplier of dilution water in the open loop mode. The heat exchanger is bypassed in open loop mode. The pump used to circulate fresh water in closed loop mode becomes the source of seawater for the scrubber in open loop mode. The mode change also requires change-over from the small volume centrifuge to the large volume cyclone separator.

The advantage and disadvantage of the hybrid system can be summarized as follows:

Advantages:

- Combines the advantages of open loop and closed loop systems to achieve consistent performance and specified regulatory compliance.

Disadvantages

- Requires the most components and extensive training for crew to be familiarized.

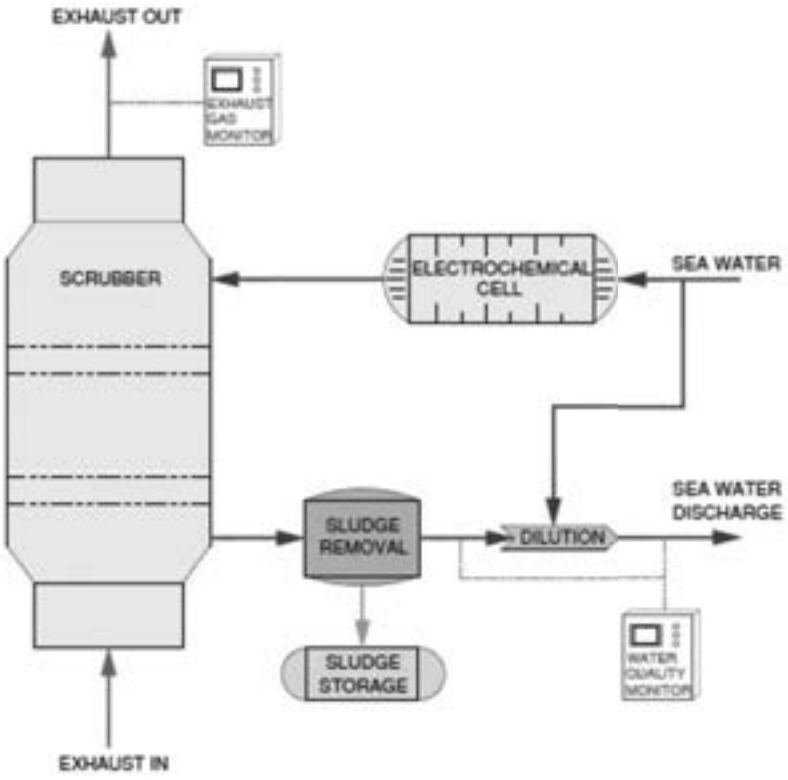

Figure 4 The electrochemical process

3.4 Electrochemical Process

The electrochemical process is established on the hypothesis that the adsorption characteristics of sea water can be enhanced by either electrolysis or electromagnetic treatment. Passing a DC current through a electrochemical cell is known to produce alkaline hydroxide species at the surface of a cathode, which has exhibits the potential to enhance the SO_x adsorption capacity of sea water. In addition to SO_x removal, the electrochemical process also claims simultaneous CO_2 and NO_x reduction from exhaust gas, with its removal mechanism pending to be clarified. More full scale tests are anticipated to prove the process is implementable.

Advantages

- No chemical is carried onboard because alkalinity is self generated from sea water by electrolysis.
- Consistent performance regardless of variation in sea water alkalinity

Disadvantages

- Electrolysis process is energy intensive.
  - Deteriorating of performance over time will happen due to scale deposition on membrane and electrode.
- By-products (chlorine and hydrogen) require special handling, storage and post-treatment.

4. EXHAUST GAS DESULFURIZATION PROCESS DEVELOPMENT IN KOMTECH

A high performance and cost effective wet scrubbing system relies on consistent input of scrubbing media, proper scrubber design and responsive control. KOMtech has developed a hybrid sea water exhaust gas desulfurization process named "Optima". It operates similar to a hybrid system with the flexibility to run in either open loop or closed loop mode. However with proper engineering and process control, supplying of fresh water makeup in

Sea Route	Optima	Open loop system	Closed loop system
Rotterdam to St. Petersburg (2015)[a]	**1.0**	1.6	1.9
New York to Rotterdam (2015)[b]	**4.4**	6.4	8.4
New York to Rotterdam (2020)[c]	**0.7**	1.0	1.3

(a) entire trip in ECA (Sulfur limit 0.1%); (b) partial trip in ECA (Global sulfur limit is 3.5% and 0.1% in ECA);
(c) entire trip in ECA (Global sulfur limit is 0.5% and 0.1% in ECA)

Table 2 Case study on the estimated payback period (years) of the Optima system
(main engine: 16.3 MW; auxiliary engine: 3.6 MW)

closed loop operation as what hybrid system does is no longer required, and the scale formation arising from sea water hardness can be avoided.

Lab tests have been carried out to demonstrate the effectiveness of KOMtech's "Optima" system. With a lab scale scrubber setup and control, the sea water alkalinity can be boosted significantly without side effect such as scaling and clogging. Given the fact that the required scrubbing water flow rate is determined by its alkalinity, the Optima system requires significantly less pumping flow as compared to a conventional sea water scrubber. In our lab scale setup test using simulated exhaust gas equivalent to burning HFO with 3.5 and 2.8wt% sulfur, we are able to reduce the sea water flow rate to 1/3 of that using untreated natural sea water. Starting from the preliminary data, a demonstration plant with exhaust gas scrubbing capacity of 200 Nm^3/hr has been built and fully commissioned.

The eco-toxicity study of the Optima process has been carried out by Det Norske Veritas (DNV) and received approval-in-principle in 2012, the process is found to have no identified environmental concern from the discharging of wash water into surrounding marine environment.

In order to estimate the payback period of the Optima system, we have done calculations on three scenarios chosen for two sea routes in ECA: New York to Rotterdam, and Rotterdam to Saint Petersburg. As compared to fuel switching and other open loop and closed loop process, the Optima system shows the least payback period under all scenarios (Table 2).

5. CONCLUSION

Current wet scrubbing processes designed for marine exhaust gas desulfurization are established on neutralization principles that utilize either the natural alkalinity from sea water or the added alkaline substance into fresh water as carrier. Alkalinity of the scrubbing media plays important role in system sizing and operation.

A wet scrubbing process (Optima) is has been developed by KOMtech for exhaust gas desulfurization. With consistent SO_x removal at reduced flow rate of scrubbing media, the Optima process has the potential to give reduced payback period as compared to fuel switching and other wet scrubbing processes (open loop or closed loop).

6. REFERENCES

[1] "A critical review of ocean-going vessel particulate matter emission factors", Todd Sax, Andrew Alexis, California Air Resources Board, 11/09/2007

Liu Ming

Nirmal Raman Gurunthalingam

Chong Wen Sin

Jens Wallevik

Nominal Roll

IN MEMORY

Chua Chor Teck

BOARD OF HONORARY MEMBERS

Lui Tuck Yew
Lim Boon Heng
Choo Chiau Beng

FELLOWS

Au Yeong Kin Ho
Banerjee Gurudas
Chen Chin Kwang
Cheng Huang Leng
Chew Yong Seng, Fabian
Chia Hock Chye, Michael
Chin Kong Weng, Francis
Chin Soon Siong, David
Choo Hock Cheng
Choo Yoo Sang (Professor)
Daruvala Dorab Dadabhoy
Das Gupta Mihir Kumar
Dev Arun Kr (Dr.)
Foo Chee Lee, Charles
Heng Chee Song, Peter
Hoe Eng Hock
Kee Ah Bah, Kenneth
Kinrade George David
Kirton Christopher
Leo Meng Si
Leow Ban Tat
Mallick Sandip Kumar
Merchant Aziz Amirali
Mukerji Subir
Ng Kean Seng
Ng Sing Chan
Ong Poh Kwee
Quah Teck Huat
Quek Tee Dhye
Raju Kurumbailmadham Manikkam
Rajwani Chandru Sirumal
Ray Amit
Richardson Anthony
Saha Makaraksha
Song Pang Lim
Tan Hee Ser, James
Tan Kim Pong
Tanubrata Wanasurya
Teo Soon Hock
Tham Yeng Fai
Wong Bheet Huan
Wong Meng Hoe
Wu Conan

MEMBERS

Ang Ee Beng
Ang Ban Gee
Ang Ban Hooi
Ang Eng Cheow
Aw Chin Meng
Awe Yun Nam
Ang Yan Siang
Balasubramaniam Prakash
Bhandari Rajan
Boey Thim Ming
Celarek Piotr
Chan Mun Lye
Chan See Yin
Chang Weng Kwai
Cheah Aun Aun
Chee Han Fui
Chee Soon Heng, John
Cheng Chao
Chen JieJing
Chen Joo Sin
Cheong Yew Chung, Gerry
Chern Meng Huat
Chew Khai Chong, Eddy
Chong Kar Ngian, Wesley
Chong Ked Poon
Chong Thian Sian
Chong Wen Sin
Chow Kam Chuen
Chua Chin Huei
Chua Soo Khoon
Chua Yian Hong
Chung Chee Kit
Cong YuJie
Davidse Jandirk Cornelis
Foo Hoe Ming
Foo Nan Cho
Foo Sek Peow
Galistan Selwyn Gerard
Gan Hock Huat David
Ganta Venkata Sudarshana Rao
Goh Boon Guan
Goh Chung Hun
Goh Eng Hock
Goh Han Tiong, Tony (Capt.)
Gopalan Somarajan
Ham Wan Ling
Heng Kian Hong
Hon Chee Wah
Hor Siew Weng
Hossain Mahmud
Jaafar Irwan
Joarder Golam Mahfuz
John Lionel
Kan Hoi Yuen
Karim Sazid Bin
Kee Kevin
Koh Nigel
Koh Shu Yong
Kuet Ee Yoon
Kuik Simon

Kumaran Rajkrish
Kuss Olaf
Kwek Winson
Lam Yen Chin
Lazar Sunu
Lee Chong, Andrew
Lee Ee Win
Lee Tai Kau, Lucas
Leong Kok Weng
Li Xun
Lim Jit Hap, Wellman
Lim Lian Nang
Liu Yu Han
Loke Yuen Piew
Low Chen Hee
Low Jin Kiat
Low Kok Chiang
Low Kuah Khia, Eugene
Lu Shang Yuan
Lui Nai Fatt, David
Lum Kin Wah
Mahfuzur Rahman
Mattar Sheikh Khaled
MD Shafiquzzaman
Menezes Denis L. (Capt.)
Mookerjea Sridev
Neo Tiong Tian, Nicholas
Ng Chai Ju
Ng Chun Wee
Ng Poh Yong, Paul
Ng Yi Han
Oei Chooi Leng, Dennis
Pang Daniel
Pang Kwee Sing
Prabowo Adie
Radukanovic Dimitrije
Rashid Md Harun AR
Ratnam Gopinath
Samynathan Asothan
Seah Ah Kuan
See Chee Wei
Seet Lee Kwang, Tony
Seow David
Shankar Prem
Sharma Vishnu Parmanand
Sheri Lelchand Kishinchand
Sit Kok Lee
Sondron Ganesan
Song Chee Weng, Sean
Song Keng Yong, Kevin
Stoytchev Stanev Ivan
Tan Chee Hock
Tan Keng Hock, Kelvin
Tan Tai Kia, Alvin
Tan Te Tong, Tony
Tan Wai Sing, Vincent
Tan Xiaoming
Tay Kim Seng, David Bernard
Tay Kwee Sim, Patrick
Thong Weng Choy
Toh Choon Phuang
Wang Yang Feng
Wee Cheng Chua, Edwin
Wong Bor Shing
Wong Choong Fee, Alvin
Wong Fee Min, Alfred
Wong Fook Seng
Wong Kong Meng
Wong Len Poh
Wong Peng Soon, Edwin (Capt.)
Yeap James
Yee Yew Seng
Yeo Teck Chye
Yong Tui Kong
Zhang Jinfeng

ASSOCIATE MEMBERS

Cheong Seng Kok, Gerry
Cheruparambil Chandran Sandeep
Chia Moi Poh
Chong Sharon S
Chong Yew Chee, Roy
Chow Lin Yi
Kang Toh Seong
Khoo Yong Kiang, Kelvin
Koh Kenneth
Kok Chong Weng
Law Puay Huan, Marilyn
Lim Ka-Wui, Gabriel
Mok Yu Ling
Muhamed Amin Baharom
Ng Cheng Thiam, Norman
Ng Yuan Xing
Ramasamy Ramesh
Shanmugasundar Windersalam
Sinayah Segaran
Soh Wikki
Tan Gerry
Tan Meng Hock, Patrick
Tang Kiam Seng, Francis
Tay Jason
Tin Suen Yee, Ric
Wong Yan Jing, Crystal
Yeo Boon Hock, Lawrence
Yeow Xian Ching
Zay Yar Tun

AFFILIATE

Ang Kwang Yong
Chan Chiang Joo, Nicholas
Khoh Beng Teck, Clarence
Lek Yi Ling Roxanne

JUNIOR

Chin Han, Eusebius
Foo Ji Ting
Goh Choon Wei, Benjamin
Goh Jie Jun, Marcus
Goh Zhi Kai
Goh, Ernest
Gui Zi Xiang
Haudy Yulianto
Khairy Muhammad
Lim Shiyi
Ng Ching Yee Fanny
Ong Hoon Tian
Ong Hui Hong
Onn Ying Hui
Safie Srinatikah
Seow Wei Qing
Sin Zi Xin, Samuel
Tan Qi Yuan, Nigel
Tan, Victor
Tarn Rui Seng, Willis
Teo Chang Meng
Yeo Rui Siang
Zhou Tongwen

Editor's Note

We're excited to mark the 40th Anniversary of the Society of Naval Architects and Marine Engineers Singapore (SNAMES) with the publication of the 34th SNAMES Annual Report, as part of the ongoing series of events to celebrate this proud milestone – 40 years of making friends and working together to promote the maritime industry.

This year, we've chosen the theme "New Frontiers" to encapsulate the spirit of new possibilities and ventures – beyond the current limits – in the industry.

We hope that through the various strategic and technical papers, covering leading-edge innovations and breakthroughs in the maritime industry, readers across the industry – business leaders, professionals and technologists – will be inspired to think and act beyond conventions.

"This year, we've chosen the theme 'New Frontiers' to encapsulate the spirit of new possibilities and ventures – beyond the current limits – in the industry."

In the process of preparing the Journal, we were very pleased to have received an array of substantive papers from accomplished authors and professionals. They ranged from offshore structures and technologies to deep well operations and environmental protection. Some seminal papers include:

1. Installing Offshore Wind Turbines in Harsh Environments By Asbjorn Mortensen Dr. Ing., Saswat Mohanty, MSc.

2. Successful Risk Management of Deepwater Well Operations By Håvard Brandt

3. Wet Scrubbing Process for Marine Emission Control By Liu Ming, Chong Wen Sin, Nirmal Raman Gurunthalingam, Jens Wallevik

These technical papers are published in the final part of this Journal. Meanwhile, reports of key events, such as the 27th Chua Chor Teck Memorial Lecture, technical talks, primer courses, etc have also been included. I hope you will find them informative and useful.

Indeed, this Journal would not have been possible without the enthusiasm of companies that have come alongside SNAMES; they have consistently extended their generous support to the Journal and SNAMES over the years via advertisement placements and event sponsorships. There is also a group of avid individuals coming together to lend

support to the Journal. We look forward to the continual strong support from our partners in the industry as well as our members in our activities.

Finally, I wish to acknowledge my publication team members who have contributed to the successful publication of this year's Journal. They are Ms Joan Chua, Executive Secretary of SNAMES, and our appointed Publisher, Tan ChinKar of JMatrix Consulting Pte Ltd, a publishing and communications firm.

In closing, together with my colleagues at SNAMES, I wish you and your organisation fair wind in the year ahead.

Sincerely

Ng Yi Han
Chairman
Publication Committee

Be Part of the SNAMES Community

Join Us Today to Expand Your Network

The Society was formed in 1981 after the Society of Naval Architects (SONAS) and senior Marine Engineers in Singapore agreed to collaborate to form the Society of Naval Architects & Marine Engineers Singapore (SNAMES).

As a leading maritime Society, SNAMES:

- ❖ Facilitates the exchange of ideas and information on the practical and scientific aspects of design, construction, operation, repairs and maintenance of marine machinery, structures, offshore and other vessels and related fields;
- ❖ Promotes the improvement of marine machinery, structures and vessels and all that specially appertains to them;
- ❖ Encourages school leavers to take up maritime studies leading to interesting, challenging and rewarding shipboard, shipyard and other shore-based jobs.

SNAMES organises a host of activities throughout the year to engage its members:

- ❖ Networking sessions to share practical and scientific experiences in the fields of design, construction, operation and repairs and maintenance of all marine machinery, structures, offshore and other vessels;
- ❖ Experiments and dialogues aimed at advancing knowledge in science, technology and management of shipbuilding, rig building and conversion, ship repairing, marine engineering, shipping and related fields;
- ❖ Panel discussions on scientific advancements, new inventions and materials applicable to marine technology;
- ❖ Collation and publications of relevant findings, new findings and state-of-art marine and naval architectural technology;
- ❖ Consultancy on matters pertinent to Naval Architects and Marine Engineers, such as career advancements, education and training;
- ❖ Industry nites, friendly golf networking, annual dinner, conferences and technical seminars, etc.

SOCIETY OF NAVAL ARCHITECTS AND MARINE ENGINEERS SINGAPORE

SNAMES

Society of Naval Architects and Marine Engineers Singapore
205 Henderson Road #02-01 Singapore 159549
Secretariat Contact: Ms Joan Chua
Tel: 6858-5846 | admin@snames.org.sg | snames.org.sg

Right people, Rigorous execution, Reputable partners, Robust technology – Keppel Offshore & Marine delivers superior solutions across 20 yards in 16 countries.

- Offshore rig design & construction
- Ship conversion & repair
- Specialised shipbuilding

Builder of distinction

Keppel Offshore & Marine

Keppel Offshore & Marine Ltd 50 Gul Road Singapore 629351 Tel: (65) 6863 7200 Email: marketing@keppelfels.com www.keppelom.com Co Reg No. 199900642R